


3-10-2010

Mission Analysis and Design for Space Based Inter-Satellite Laser Power Beaming

Nicholas M. Keller

Follow this and additional works at: <https://scholar.afit.edu/etd>

 Part of the [Astrodynamics Commons](#), and the [Plasma and Beam Physics Commons](#)

Recommended Citation

Keller, Nicholas M., "Mission Analysis and Design for Space Based Inter-Satellite Laser Power Beaming" (2010). *Theses and Dissertations*. 2065.

<https://scholar.afit.edu/etd/2065>

This Thesis is brought to you for free and open access by the Student Graduate Works at AFIT Scholar. It has been accepted for inclusion in Theses and Dissertations by an authorized administrator of AFIT Scholar. For more information, please contact richard.mansfield@afit.edu.



**MISSION ANALYSIS AND DESIGN FOR SPACE BASED
INTER-SATELLITE LASER POWER BEAMING**

THESIS

Nicholas M. Keller, Lieutenant, USN

AFIT/GA/ENY/10-M05

**DEPARTMENT OF THE AIR FORCE
AIR UNIVERSITY**

AIR FORCE INSTITUTE OF TECHNOLOGY

Wright-Patterson Air Force Base, Ohio

APPROVED FOR PUBLIC RELEASE; DISTRIBUTION UNLIMITED.

The views expressed in this thesis are those of the author and do not reflect the official policy or position of the United States Navy, the United States Air Force, the Department of Defense, or the United States Government. This material is declared a work of the U.S. Government and is not subject to copyright protection in the United States.

AFIT/GA/ENY/10-M05

MISSION ANALYSIS AND DESIGN FOR SPACE BASED
INTER-SATELLITE LASER POWER BEAMING

THESIS

Presented to the Faculty

Department of Aeronautics & Astronautics

Graduate School of Engineering and Management

Air Force Institute of Technology

Air University

Air Education and Training Command

In Partial Fulfillment of the Requirements for the
Degree of Master of Science in Astronautical Engineering

Nicholas M. Keller, BS

Lieutenant, USN

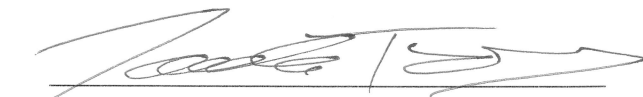
March 2010

APPROVED FOR PUBLIC RELEASE; DISTRIBUTION UNLIMITED.


MISSION ANALYSIS AND DESIGN FOR SPACE BASED
INTER-SATELLITE LASER POWER BEAMING

Nicholas M. Keller, BS
Lieutenant, USN


Approved:


Jonathan Black, PhD (Chairman)

16 MAR 2010
Date


Lt Col Douglas Decker, PhD (Member)

16 MAR 10
Date


Salvatore Cusumano, PhD (Member)

16 Mar 10
Date

Abstract

This research effort develops an interdisciplinary design tool to optimize an orbit for the purpose of wirelessly beaming power from the International Space Stations (ISS) Japanese Experimental Module Exposed Facility (JEM/EF) to a target satellite. For the purpose of this initiative, the target satellite will be referred to as FalconSAT6, a reference to the proposed follow-on satellite to the U.S. Air Force Academy's (USAFA) FalconSAT5 program. The USAFA FalconSAT program provides cadets an opportunity to design, analyze, build, test and operate small satellites to conduct Department of Defense (DoD) space missions. The tool developed for this research is designed to find an optimal solution balancing the need to maximize the amount of access time between the ISS and FalconSAT6 while minimizing the range between the spacecraft. This tool places mathematical rigor to the problem and determines realistic solutions using current technology. Using this tool allows mission planners to economically and accurately predict the outcome of a proposed wireless power beaming mission.

Acknowledgements

I'd like to first thank my awesome wife for all her love, support, and patience for the many hours spent working on this research. The time spent helping with proof-reading and editing is truly appreciated. Next, thanks to my thesis advisor and mentor Dr. Jon Black for his expert guidance and advice. I'm sure this thesis would have been monumentally harder if not for his down to earth attitude and constant willingness to help. Thanks to J. Simmons for being an outstanding friend, mentor, and sanity check. His expert knowledge of ModelCenter and L^AT_EX were indispensable in the completion of this research. Finally, thanks to Brendan Houlton of Analytical Graphics, Inc. for his time and valuable Satellite Tool Kit knowledge.

Nicholas M. Keller

Table of Contents

	Page
Abstract	iv
Acknowledgements	v
List of Figures	viii
List of Tables	xi
I. Problem Statement	1
II. Background	5
2.1 Chapter Overview	5
2.2 The Roots of Wireless Energy	5
2.3 Space-Based Lasers	7
2.4 ISS Attributes	11
2.4.1 ISS Body Frame	11
2.4.2 Japanese Experiment Module	11
III. Methodology	17
3.1 Chapter Overview	17
3.2 Orbital Propagators	17
3.2.1 J4Perturbation	17
3.2.2 SGP4	18
3.3 Hill's Equations	20
3.4 Software Used in the Construction of the Design Tool	21
3.4.1 Satellite Tool Kit v9.0.1	21
3.4.2 ModelCenter v8.0	21
3.5 Model Construction	24
3.5.1 Satellite Tool Kit Model	25
3.5.2 ModelCenter Simulation	39
3.5.3 Summary of Model Constraints, Assumptions, and Limitations	40
3.6 Model Verification and Validation	40
3.6.1 Model Initial Conditions	42
3.6.2 Orbital Elements	43
3.7 Summary	51

	Page
IV. Results and Discussion	52
4.1 Chapter Overview	52
4.2 Design of Experiments	52
4.3 Genetic Optimization	56
4.3.1 Darwin Results	62
4.4 Obscuration Analysis	68
4.5 Expanded Constraints	71
4.5.1 1MW Laser and 15sec Minimum Access Time	73
4.5.2 6kW Laser and 30sec Minimum Access Time	74
4.6 Summary	76
V. Conclusions	78
5.1 Overview of Research Effort	78
5.2 Conclusions	78
5.3 Recommendations for Future Work	79
Appendix A. Selected Screenshots of the STK and ModelCenter Graphical User Interface	81
Appendix B. Additional Multi-Dimensional Darwin Plots from ModelCenter .	86
Appendix C. STK Access Report for Optimized Orbit	89
Appendix D. Abridged STK AER Report for Optimized Orbit	92
Bibliography	105
Index	107

List of Figures

Figure	Page
1.1 NASA / Air Force Institute of Technology (AFIT) / USAFA Laser Power Beaming Concept	1
1.2 Photograph of the JEM/EF Onboard the ISS [3]	2
1.3 BHT-200 [1]	3
1.4 Construction of FalconSAT5 [5]	3
2.1 Drawing of Wireless Power Transfer in Nikola Tesla's 1891 U.S. Patent No. 454,622 [32]	6
2.2 The "City of Light" at the 1893 World Columbian Exposition in Chicago [32]	7
2.3 SELENE Concept [25]	8
2.4 A Functional Taxonomy for Lasers in Space [29]	10
2.5 Image of the Space Based Laser - Integrated Flight Experiment [9]	10
2.6 ISS Body Frame [8]	11
2.7 Diagram of the Japanese Experimental Module [7]	12
2.8 Kibo's Pressurized Module Under Construction [7]	13
2.9 Diagram of the Kibo Exposed Facility[6]	14
2.10 Kibo's Exposed Facility Under Construction [6]	15
3.1 PRN11 Almanac Comparison Statistics [24]	19
3.2 STK Main Window	21
3.3 ModelCenter Main Window	23
3.4 Pareto Front [27]	24
3.5 STK Analysis Period	25
3.6 ISS Orbit Definition in STK	27
3.7 Demonstration of the ISS and FalconSAT6 Co-located	28
3.8 ISS Model from the Space Test Program	29
3.9 STK Object Browser	30
3.10 Laser Dimensions	32
3.11 Laser Location on ISS	33
3.12 Laser Tracking Parameters	34
3.13 ISS to FalconSAT6 Access Assignment	36
3.14 LaserMountPoint Basic Constraints	37
3.15 FalconSAT6 Orbital Definition	38

	Page
3.16	USAFA's FalconSAT5 STK Model 39
3.17	ModelCenter Parametric Study Tool 42
3.18	Total Access Time as a Function of Semi-Major Axis 44
3.19	Mean Range as a Function of Semi-Major Axis 45
3.20	Total Access Time as a Function of Eccentricity 46
3.21	Mean Range as a Function of Eccentricity 46
3.22	Total Access Time as a Function of Inclination 47
3.23	Mean Range as a Function of Inclination 48
3.24	Total Access Time as a Function of Argument of Perigee 48
3.25	Mean Range as a Function of Argument of Perigee 49
3.26	Total Access Time as a Function of Right Ascension of Ascending Node 49
3.27	Mean Range as a Function of Right Ascension of Ascending Node 50
3.28	Total Access Time as a Function of Mean Anomaly 50
3.29	Mean Range as a Function of Mean Anomaly 51
4.1	Variable Influence Profile with respect to Total Access Time 53
4.2	Variable Influence Profile with respect to Mean Range 54
4.3	3-Dimensional Carpet Plot of Mean Range as a Function of Semi-Major Axis and Eccentricity 55
4.4	3-Dimensional Carpet Plot of Total Access Time as a Function of Semi-Major Axis and Eccentricity 56
4.5	2-Dimensional Plot of Total Access Time vs. Mean Range - All Solutions 58
4.6	5-Dimensional Plot of Eccentricity, Semi-Major Axis, Mean Anomaly, Mean Range, and Total Access Time 60
4.7	4-Dimensional Plots of Eccentricity, Semi-Major Axis, Mean Range, and Total Access Time 61
4.8	4-Dimensional Plots of Eccentricity, Semi-Major Axis, Total Access Time, and Mean Range 63
4.9	2-Dimensional Plot of Total Access Time vs. Mean Range with Pareto front, Infeasible Solutions, and Optimal Solution (Design 4083) Hi-lighted 64
4.10	Darwin Data Explorer Window Showing Optimized Results in Tabular Form 65
4.11	Detail View of Optimal Design 4083 66
4.12	Association of Optimized FalconSAT6 Orbit (in pink) and ISS Orbit (in blue) 67
4.13	Instantaneous Values for: Azimuth, Elevation, Range, Angular Rate, and Range Rate for Figure 4.12 68

	Page
4.14	STK's Access Obscuration Window 69
4.15	Graphical Obscuration Report 71
4.16	Bore Sight View of Laser at the 10 Feb 2010 12:10:30.000 Suspected Obscuration Time 72
4.17	Comparison of Feasible Orbits When Using a 3kW Laser and a 6kW Laser 77
A.1	ModelCenter's Design of Experiments Tool 82
A.2	ModelCenter's Carpet Plot Tool 82
A.3	ModelCenter's Genetic Optimization Tool 83
A.4	Darwin's Data Visualizer Configuration 84
A.5	STK's Access Obscuration Tool 85
B.1	5-Dimensional Plot of Right Ascension of Ascending Node, Argument of Perigee, Mean Anomaly, Mean Range, and Total Access Time - Feasible Solutions Hi-lighted 86
B.2	4-Dimensional Plots Showing the Relationship of Total Access Time and Mean Range to Inclination - Feasible Solutions Only 87
B.3	5-Dimensional Plot Showing Semi-Major Axis, Eccentricity, Inclina- tion, Total Access Time, and Mean Range - Feasible Solutions Only 88

List of Tables

Table	Page
2.1 Japanese Experiment Module - Exposed Facility Specifications	13
3.1 International Space Station Two Line Element Set at Epoch Time [10] . .	28
3.2 International Space Station and FalconSAT6 Orbital Elements at Epoch Time [10]	28
3.3 Summary of Model Constraints and Assumptions	41
3.4 FalconSAT6 Orbital Parameter Ranges Used in Parametric Studies	41
3.5 Global Statistics for STK Access Report with FalconSAT6 Co-located with the ISS	43
3.6 Global Statistics for STK AER Report with FalconSAT6 Co-located with the ISS	44
4.1 Global Statistics for STK Access Report with FalconSAT6 in Opti- mized Orbit	68
4.2 Global Statistics for STK AER Report with FalconSAT6 in Optimized Orbit	68
4.3 Suspected Obscured Times During Analysis Period	70
4.4 Differences in FalconSAT6's Optimized Orbital Elements from ISS's Orbital Elements	72
4.5 Optimal Orbit with Minimum Access Time of 15sec and Maximum Range of 32030km Using a 1MW Laser	73
4.6 Global Statistics for STK Access Report with FalconSat6 in Enhanced Orbit Using a 1MW Laser	73
4.7 Global Statistics for STK AER Report with FalconSat6 in Enhanced Orbit Using a 1MW Laser	74
4.8 Differences in FalconSAT6's Optimized Orbital Elements from ISS's Orbital Elements	74
4.9 Optimal Orbit with Minimum Access Time of 30sec and Maximum Range of 1170km Using a 6kW Laser	75
4.10 Global Statistics for STK Access Report with FalconSat6 in Enhanced Orbit Using a 6kW Laser	75
4.11 Global Statistics for STK AER Report with FalconSat6 in Enhanced Orbit Using a 6kW Laser	75
4.12 Differences in FalconSAT6's Optimized Orbital Elements from ISS's Orbital Elements	76

MISSION ANALYSIS AND DESIGN FOR SPACE BASED INTER-SATELLITE LASER POWER BEAMING

I. Problem Statement

For years various groups have been discussing using lasers to power satellites, other space vehicles, or beam power to the Earth's surface from orbit [29]. These concepts have included: Dr. Landis' 1991 proposal for an Earth based laser to power a satellite called Space Laser ENERGY (SELENE) [25] and recently Japan's Space solar power system (SSPS). Until now, there has been little to no mathematical or engineering rigor behind such ideas with the authors mostly "assuming" that such a system would be physically possible, if not entirely feasible. The National Aeronautics and Space Administration (NASA) however has considerable interest in such a system for its electric propulsion potential. Possible advantages include reduced fuel requirements over more traditional thrusters. This technology in turn can lower launch cost by reducing mass or allowing for a larger payload. Increasing the power available to an ion or electrical propulsion system can dramatically enhance the performance of such a system. Additionally, if fuel mass is left constant the lifetime of the satellite may increase.

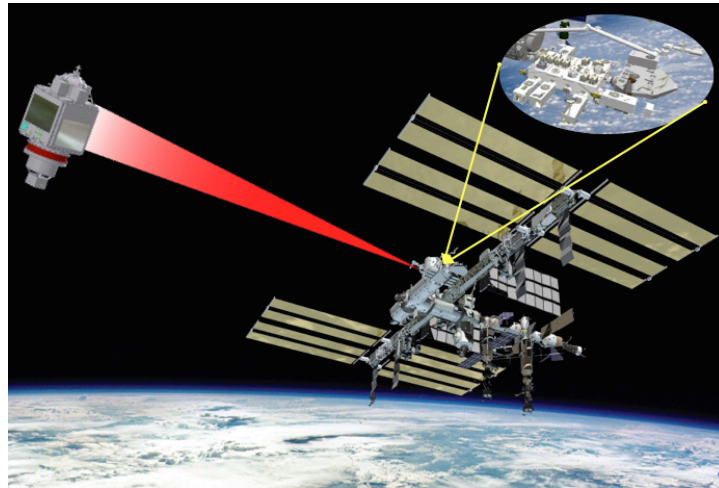


Figure 1.1: NASA / Air Force Institute of Technology (AFIT) / USAFA Laser Power Beaming Concept

As seen in Figure 1.1, the motivation for this research stems from the notion that one can power an orbiting spacecraft payload wirelessly via laser from another spaceborne platform. This research effort develops a multi-disciplinary design tool to optimize an orbit for the purpose of wirelessly beaming power from the International Space Station's (ISS) Japanese Experimental Module Exposed Facility (JEM/EF) seen in Figure 1.2 to a target satellite to power a BusekTM Hall-Effect Thruster (BHT) as seen in Figure 1.3. For the purpose of this initiative, the target satellite will be referred to as FalconSAT6, a reference to the proposed follow-on satellite to the U.S. Air Force Academy's (USAFA) FalconSAT5 seen in Figure 1.4. The USAFA FalconSAT program provides cadets an opportunity to design, analyze, build, test and operate small satellites to conduct Department of Defense (DoD) space missions. FalconSAT research is conducted within the Academy's Space Systems Research Center [11]. This tool analyzes all possible orbits and determines realistic solutions using current technology. Using this tool allows mission planners to economically and accurately predict the outcome of a proposed wireless power beaming mission.

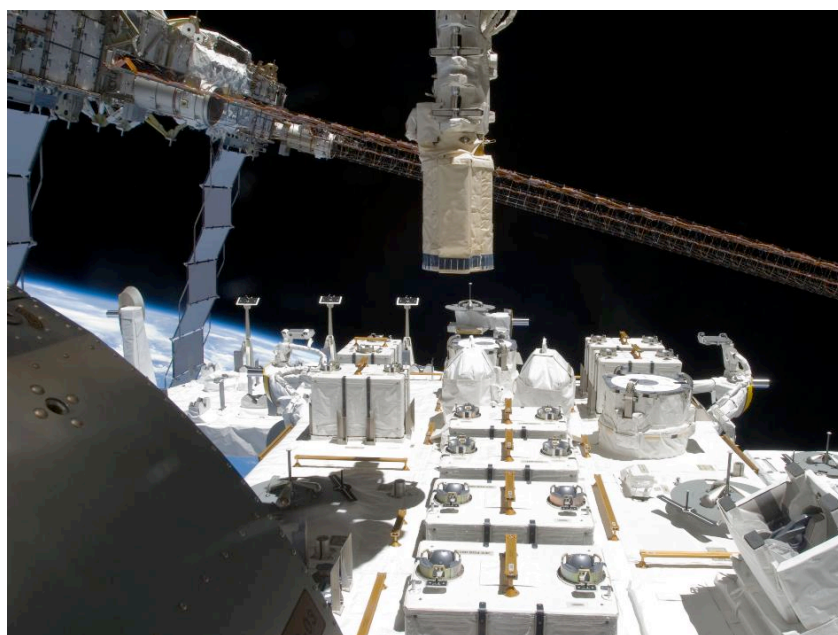


Figure 1.2: Photograph of the JEM/EF Onboard the ISS [3]

The goals of this research are to develop, test, validate, and exercise a computer based orbital model that, given the orbit of the ISS and various physical real world

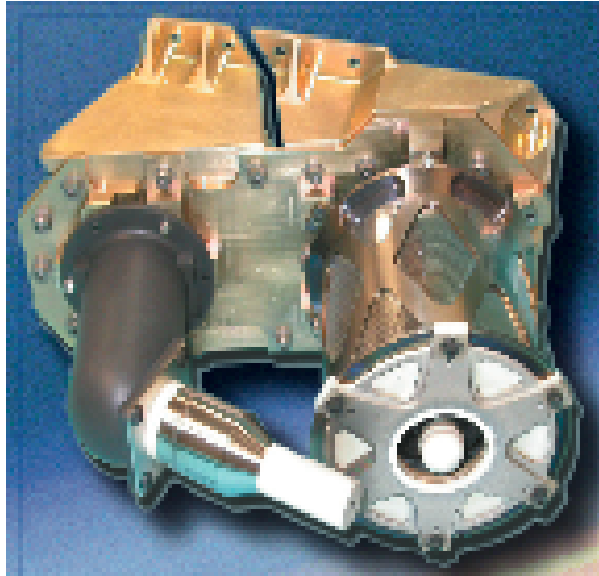


Figure 1.3: BHT-200 [1]

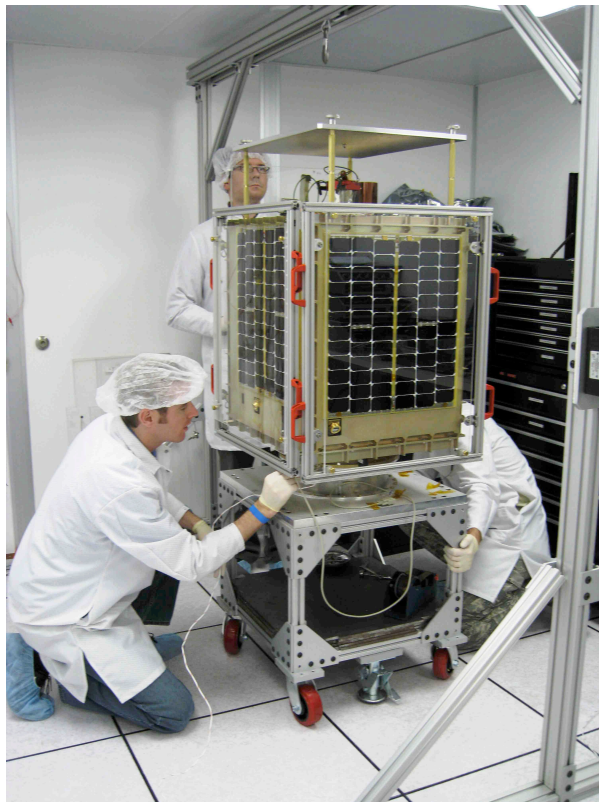


Figure 1.4: Construction of FalconSAT5 [5]

constraints, will determine the optimal orbit for transferring power between the ISS and FalconSAT6 with the maximum total access time at the minimum mean range. Next, the proposed optimized orbit will be scrutinized via various software tools for validity. Finally, an evaluation of what orbital configurations would be possible if hardware beyond what is currently available were to be used. Based on the results of these evaluations, a determination of the feasibility of such a wireless power transfer mission will be discussed. The end result shows that, unlike previous laser power beaming mission designs, exploring nearly 7000 possible orbits using a genetic optimizer one can quickly and effectively obtain an optimal solution to maximize the total access time while minimizing the mean range between two satellites.

In this thesis Chapter I introduces the research and discusses the significance of laser power beaming technology. Chapter II covers the literature review and provides a basic background of various laser power beaming missions. Chapter III discusses the development, validation, and verification of the design tool, while Chapter IV explores the design space using the model. Finally, Chapter V concludes the thesis with a discussion on the results obtained by the model and the need for future work.

II. Background

2.1 Chapter Overview

This chapter will analyze the background of and reasons for the wireless transmission of power. The discussion will begin with a look at the origins of wireless power transmission followed by justification for the use of a space-based laser for the transmission of power between two satellites as well as an overview of previous concepts. Additionally, an algorithm for calculating the relative motion between two satellites is presented. Next, a short discussion on the ISS body frame and the JEM/EF is presented. Finally, a discussion on the two orbital propagators used in this study will conclude the chapter.

2.2 The Roots of Wireless Energy

The quest for wireless energy dates back to the work of André-Marie Ampère who, in 1826, first described Ampere's Law showing that an electric current produces a magnetic field. In 1831 Michael Faraday described Faraday's Law of Induction which became an important law of electromagnetism. This was followed in 1864 by the work of James Maxwell, who had a consistent theory mathematically modeling electromagnetic radiation. It took Heinrich Rudolf Hertz in 1888 to prove the existence of electromagnetic radiation by building an "apparatus for generating electromagnetic waves", or a radio transmitter [20]. Finally, as shown in Figure 2.1, 1891 saw Nikola Tesla file for U.S. Patent No. 454,622 "System of Electric Lighting". At the World Columbian Exposition in Chicago in 1893 Tesla demonstrated the wireless illumination of electric light bulbs as shown in Figure 2.2[14]. This achievement at the World's Fair would serve as the culmination of nearly a century of work and would solidify the beginning of an era of wireless technology. Today, the work of these men and others permeates the world in which we live.

As Tesla discovered in his work from 1891-1893, the physics for the wireless transmission of power are the same as the wireless transmission of information (radio, for example) in that an engineer is concerned with the loss of efficiency over a distance [14]. For the transfer of information, when the received power drops below some threshold

(No Model.)

N. TESLA.
SYSTEM OF ELECTRIC LIGHTING.

No. 454,622.

Patented June 23, 1891.

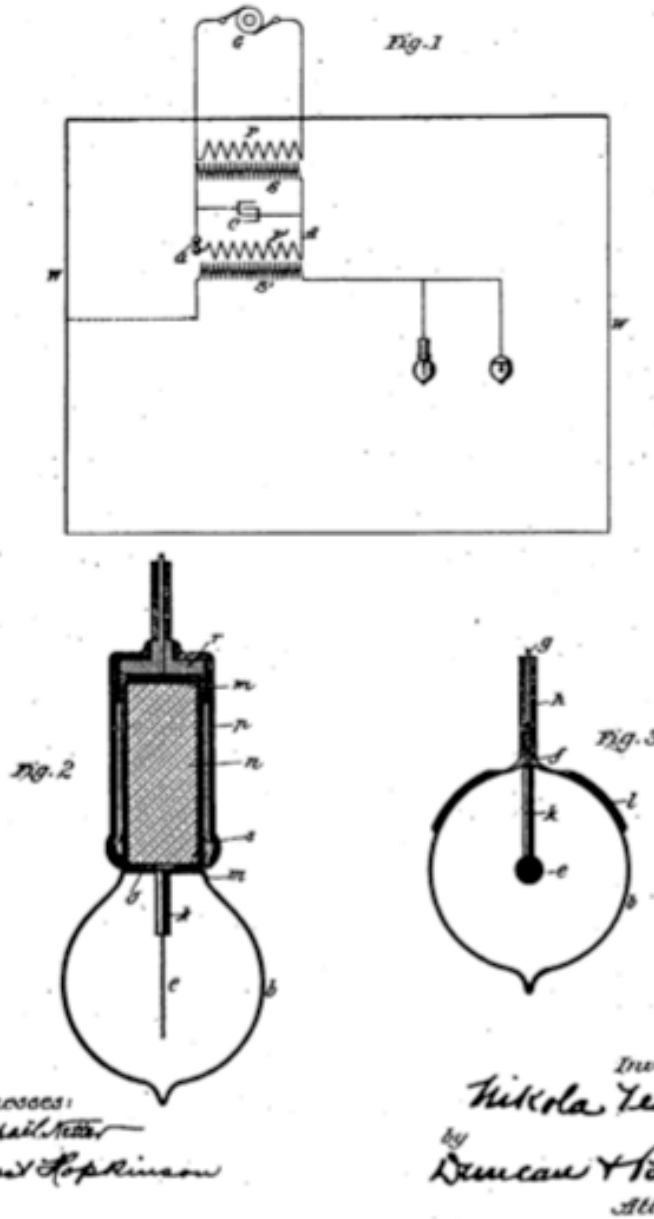


Figure 2.1: Drawing of Wireless Power Transfer in Nikola Tesla's 1891 U.S. Patent No. 454,622 [32]



Figure 2.2: The "City of Light" at the 1893 World Columbian Exposition in Chicago [32]

the ability to accurately recover the data will be in jeopardy. Energy transfer differs, however, in that the efficiency of transmitted to received power directly relates to the capabilities of the craft being powered and is therefore critically important. The work in the master's thesis "Minimizing Losses in a Space Power Beaming Experiment" [16] extensively explores this need for efficiency using the same laser that is the basis for this research.

2.3 Space-Based Lasers

Beaming power by microwave from space for use on Earth was first suggested by Dr. Peter Glaser in 1968, and following this suggestion there were several analyses of the possibility of beaming from space to space by microwave. In the 1980's, researchers at NASA Langley worked on the potential use of lasers for space-to-space power beaming, focussing primarily on the development of a solar-powered laser. In 1989 Dr. Geoffrey Landis suggested that power could be usefully beamed by laser from Earth to space. In particular, Dr. Landis proposed at the Princeton Conference on Space Manufacturing

in 1989 that Earth-based lasers could be used to provide power to a lunar base over the 354-hour lunar night [25]. In 1991, Dr. Rather at NASA Headquarters independently had exactly the same idea. Shortly after the meeting of Drs. Landis and Rather at the Resources of Near Earth Space conference in 1991 the SpacE Laser ENergy (SELENE) project was born. The idea of using an Earth based laser to extend the life of communications satellites past battery failure developed out of the laser power for the moon analysis of the SELENE project as well as the concept of rejuvenating “dead” satellites as seen in Figure 2.3 [28].

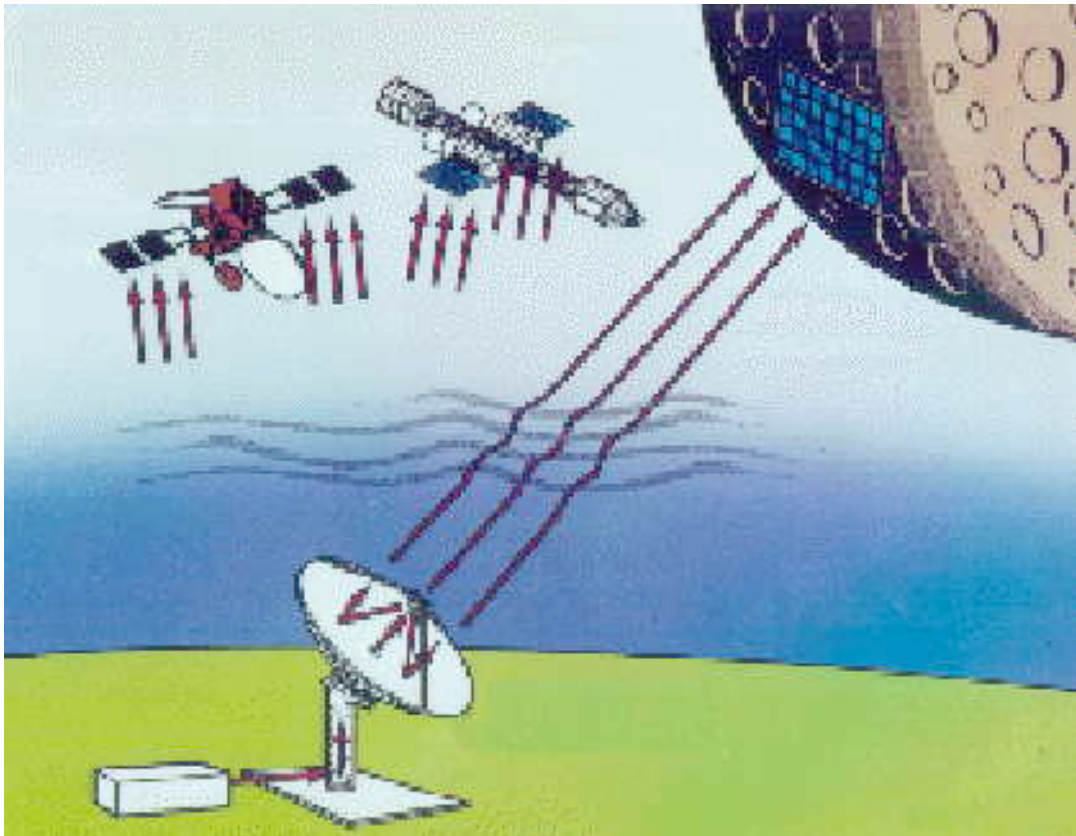


Figure 2.3: SELENE Concept [25]

When initially considering a laser power system of any kind, it quickly becomes apparent that there are many different configurations for how such a mission could look. For example, one could have a terrestrial based laser and beam power to either another terrestrial unit, or beam power to an orbiting spacecraft. As is intuitively apparent however, there are many factors within the Earth’s atmosphere that might make such a ground-to-ground or ground-to-space laser power beaming system impractical. Such a

system would require a very large power source as the energy loss of a laser beam propagating through the atmosphere is mainly the result of three attributes of the atmosphere. These atmospheric phenomenon include: molecular absorption, molecular scattering and particulate scattering. If one were to design a laser power beaming system which intersected the Earth's atmosphere, a system using the most effective laser wavelengths, from the standpoint of energy losses under various meteorological conditions, should be selected. [38]

If mission designers place the laser transmitter in orbit (along with the target satellite to be remotely powered) many of the losses associated with transmitting laser light through the atmosphere can be avoided. Coherent laser light offers a number of unique advantages as does the space environment, permitting speed-of-light applications such as optical communication, illumination, target designation, active remote sensing, and high-energy weapons. Laser technology has matured sufficiently in the past decade to provide highly reliable, cost-effective, energy-efficient and wavelength-flexible systems that can be applied to a variety of missions, such as remote sensing and communication. The unique characteristics of the space environment greatly enhance the utility of deploying lasers in space. These include the lack of any medium to attenuate the beam and ready access to the entire global surface [29]. As seen in Figure 2.4, on orbit laser systems may manifest themselves in many forms depending on the intended mission. Although actually intended to fire into Earth's extreme upper atmosphere, the Space Based Laser seen in Figure 2.5 was a concept from 1999 that would enable the system to have greater coverage over the Earth with a fraction of the atmospheric losses [9].

The use of an Earth-based laser to power an electric thruster for space propulsion was first proposed by Dr. Grant Logan of Lawrence Livermore Laboratories in 1988, with the technical details worked out in 1989. His proposal was a bit optimistic about technology (he proposed using diamond solar cells operating at a six-hundred degrees to convert ultraviolet laser light). His ideas, with the technology scaled down to be possible with more practical, nearer-term technology, were adapted into the SELENE program. The SELENE program was a serious research effort for about two years, but never had great support from NASA Headquarters as the cost of taking the concept to operational

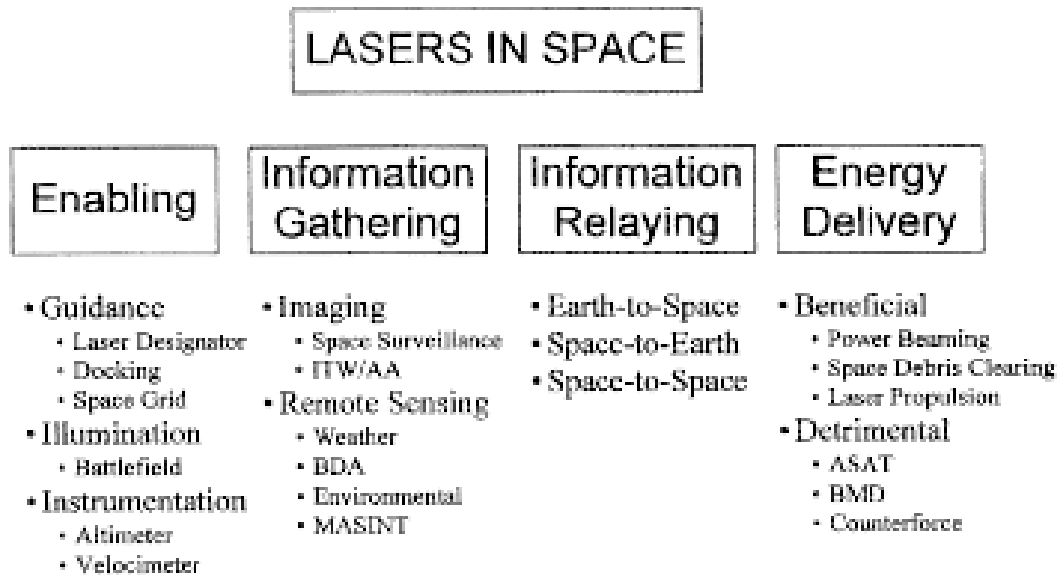


Figure 2.4: A Functional Taxonomy for Lasers in Space [29]

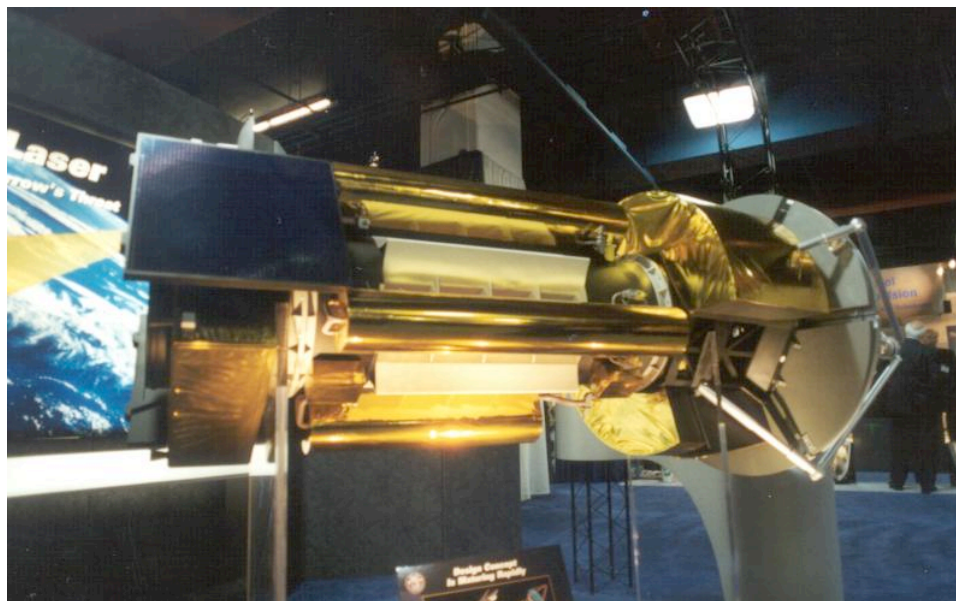


Figure 2.5: Image of the Space Based Laser - Integrated Flight Experiment [9]

status was too high and the pay-off too far-term. The SELENE project concluded around 1993 before reaching the goal of demonstrating the technology in space [25].

2.4 ISS Attributes

2.4.1 ISS Body Frame. As this will be important in Chapters III and IV and as a point of reference, Figure 2.6 clearly shows the right-handed body frame of the ISS. As seen in Figure 2.6(a) the x-axis points in the direction of travel while Figure 2.6(c) shows the z-axis nadir pointing. Figure 2.6(b) shows the y-axis normal to the x-z plane and completing the coordinate system.

The actual addition of the laser to the model will be discussed in depth in Section 3.5.1.2 and shown in Figure 3.11; however, it is important to note here that the laser will be mounted so that it points along the positive x-axis (in the velocity direction).

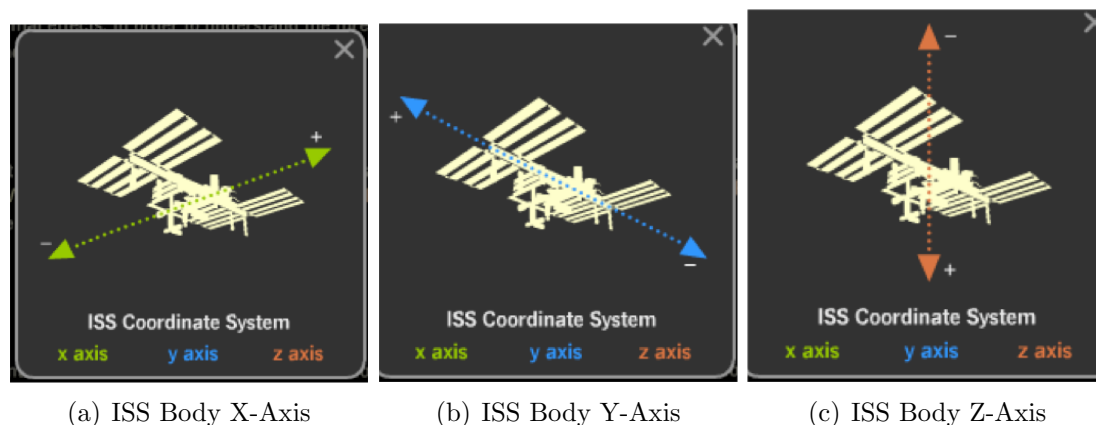


Figure 2.6: ISS Body Frame [8]

2.4.2 Japanese Experiment Module. The Japanese Experiment Module (JEM) called Kibo is Japan's first human space facility and enhances the unique research capabilities of the ISS. Experiments in Kibo focus on space medicine, biology, Earth observations, material production, biotechnology, and communications research. Kibo experiments and systems are operated from the Mission Control Room at the Space Station Operations Facility (SSOF), at Tsukuba Space Center in Ibaraki Prefecture, Japan. As seen in Figure 2.7, Kibo consists of six components: two research facilities – the Pressurized Module and Exposed Facility, a Logistics Module attached to each of them, a

Remote Manipulator System, and an Inter-Orbit Communication System unit. Kibo also has a scientific airlock through which experiments are transferred and exposed to the external environment of space.

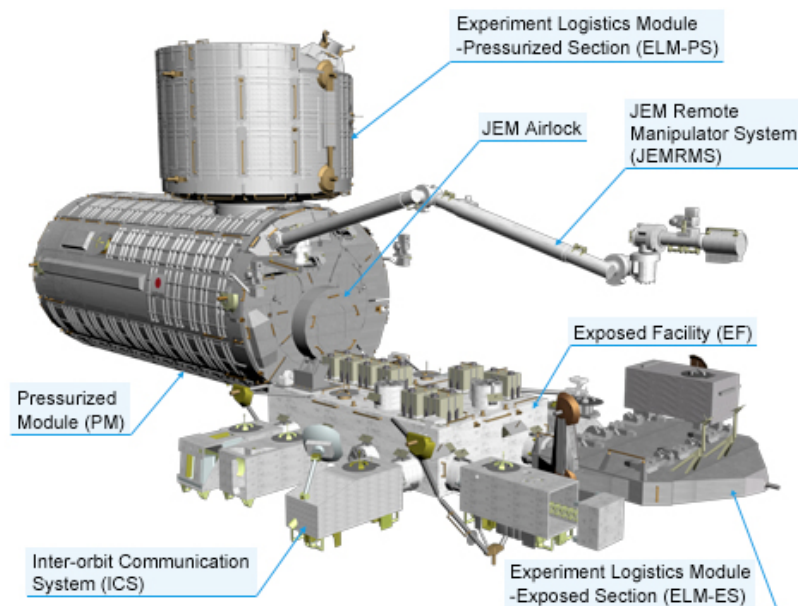


Figure 2.7: Diagram of the Japanese Experimental Module [7]

2.4.2.1 Pressurized Module. The Pressurized Module (PM), provides a shirt-sleeve environment in which astronauts conduct microgravity experiments. There are a total of 23 racks, including 10 experiment racks, inside the PM providing power supply, communications, air conditioning, hardware cooling, water control, and experiment support functions. As seen in Figure 2.8, the PM is 11.2 meters long and 4.4 meters in diameter. [7]

2.4.2.2 Exposed Facility. As can be seen in Figure 2.9, the Exposed Facility (EF), is a unique platform on the ISS that is located outside of the Pressurized Module and is continuously exposed to the space environment as seen in Figure 1.2. Items positioned on the exterior platform focus on Earth observation as well as communication, scientific, engineering, and materials science experiments. Because the EF's available services are perfectly suited for this experiment, the proposed laser as discussed in [16] will be mounted to one of the external mounting points on the EF. As this is a feasibility

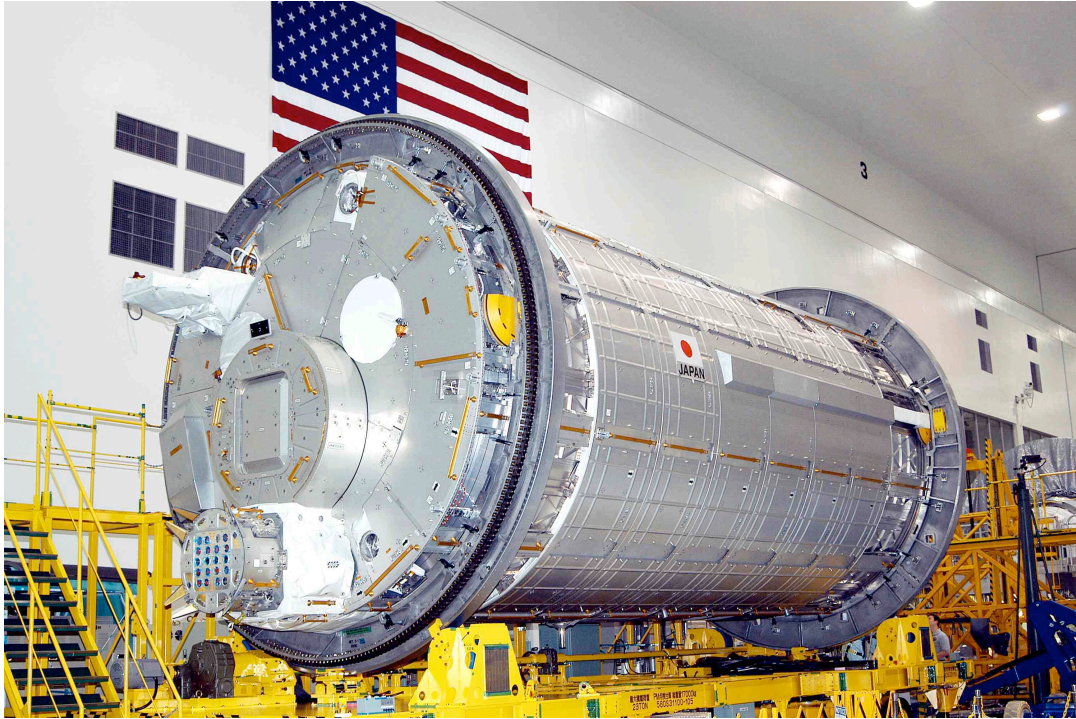


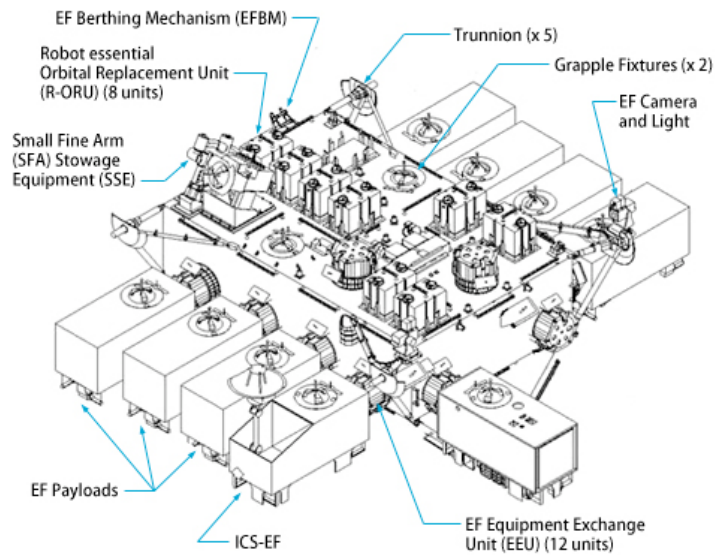
Figure 2.8: Kibo's Pressurized Module Under Construction [7]

study, one of the attachment locations on the EF was chosen as seen in Figure 3.11 and discussed in Section 3.5.1.2 and used for the entire research. For any future work as discussed in Section 5.3, the location of the laser may be located anywhere the mission requirements dictate. The module's specifications can be seen in Table 2.1 [6]. An excellent view of the EF while under construction can be seen in Figure 2.10.

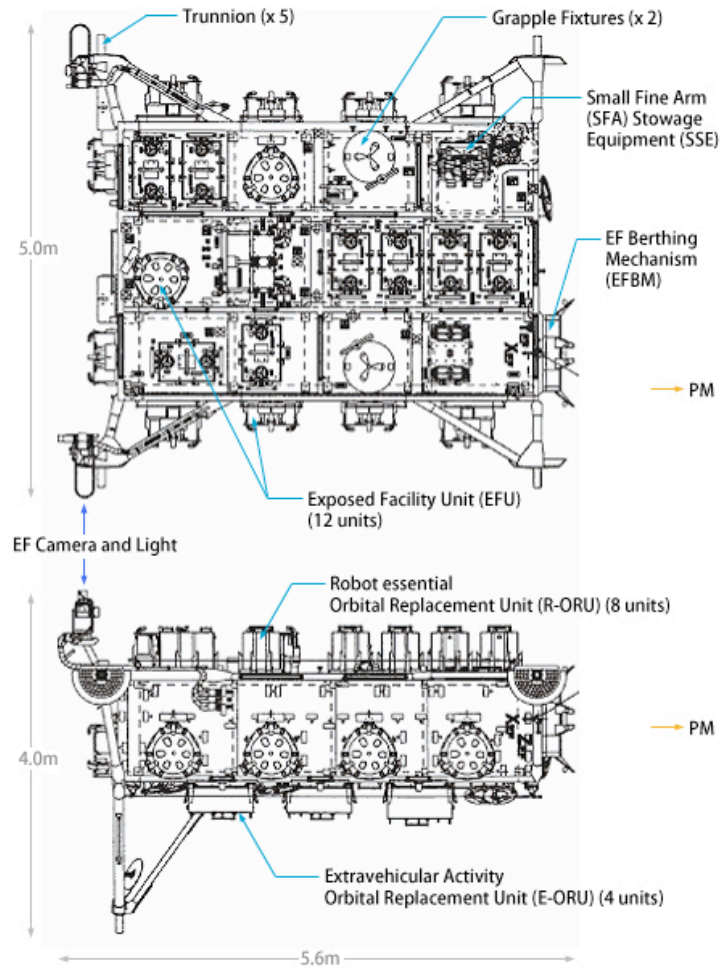
Table 2.1: Japanese Experiment Module - Exposed Facility Specifications

Item	Specification
Shape	Box shaped
Width	5.0m
Height	3.8m
Length	5.2m
Mass (at launch)	4.1tons
Number of payload attachment locations	12
Power (provided from US segment)	Max. 11kW 120V (Direct current)
Lifetime	More than ten years

2.4.2.3 Other Facilities.



(a) Planform View



(b) Top and Side Views

Figure 2.9: Diagram of the Kibo Exposed Facility[6]

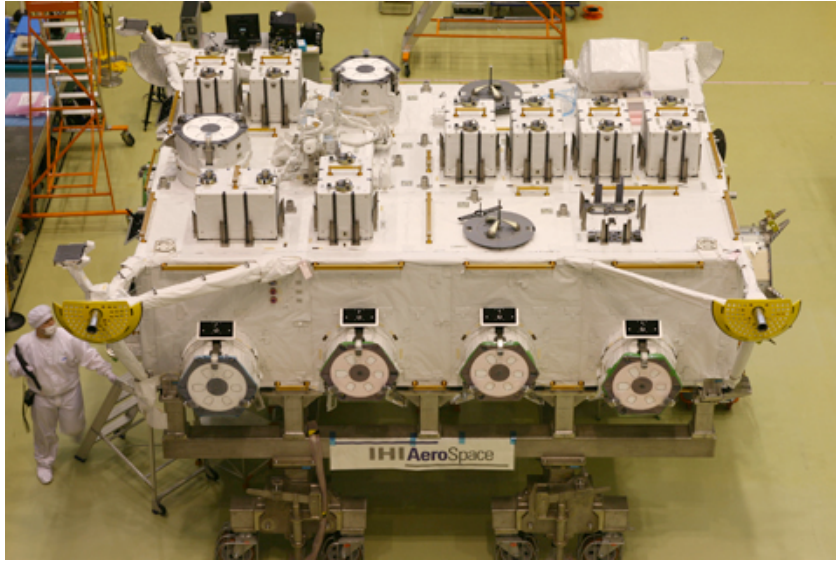


Figure 2.10: Kibo's Exposed Facility Under Construction [6]

Experiment Logistics Modules. The Experiment Logistics Modules (ELMs), serve as on-orbit storage areas that house materials for experiments, maintenance tools and supplies. The PM and the EF each have an ELM [6].

Remote Manipulator System. The Remote Manipulator System (RMS) consists of two robotic arms that support operations outside of Kibo. The Main Arm can handle up to 6.4 metric tons of hardware and the Small Fine Arm, when attached to the Main Arm, handles more delicate operations. Each arm has six joints that mimic the movements of a human arm. Astronauts operate the robot arms from a remote computer console inside the PM and watch external images from a camera attached to the Main Arm on a television monitor at the RMS console. The arms are specifically used to exchange experiment payloads or hardware located on the EF and ELM - Exposed Section from inside the PM through a scientific airlock, support maintenance tasks of Kibo, and handle orbital replacement units. The Main Arm measures 9.9 meters long, and the Small Fine Arm measures 1.9 meters [6].

Inter-Orbit Communication System. The Inter-Orbit Communication System (ICS) allows the operators in the Mission Control Room at the SSOF at Tsukuba Space Center to send commands to Kibo and receive system, payload, and

video data from Kibo for scientific payload operations. The Mission Control Room uses the Tracking and Data Relay Satellite System (TDRSS) to communicate with the ICS. An external ICS unit handles communications with TDRSS, while an internal ICS unit located in the PM handles data exchange throughout the Kibo facilities [6].

III. Methodology

3.1 Chapter Overview

This chapter discusses the development of the design tool. The chapter begins with a discussion the orbital propagators used in this work followed by a brief discussion on Hill's Equations. The chapter continues with a discussion on the selection of software used to create the design tool and then continues to describe the steps taken in the actual development of the design tool. The chapter concludes with a discussion on the validation and verification of the design tool.

The tool developed for this research is designed to find an optimal solution balancing the need to maximize the amount of access time between the ISS and FalconSAT6 while minimizing the range between the spacecraft. To accomplish this goal, an orbital model was constructed in Analytical Graphics Inc.'s Satellite Tool Kit v9.0.1TM and controlled via Phoenix Integration's ModelCenter v8.0TM. The Satellite Tool Kit (STK) orbital model mainly consists of two components: a component representing the ISS as well as one for FalconSAT6. A laser transmitter attached to the ISS on the JEM/EF provides the accurate point of origin for power transmission and a receiver on FalconSAT6 provides the target.

3.2 Orbital Propagators

For this research, the J4 orbital propagator is used for FalconSAT6's propagator while SGP4 is used for the ISS. A brief discussion on each of the orbital propagators will be presented here to provide background and help validate the use of different propagators for each of the two satellites evaluated in this study. Further discussion on the use of the different propagators can be found in Sections 3.5.1.2 and 3.5.1.3.

3.2.1 J4Perturbation. Two-Body, J2Perturbation, and J4Perturbation are analytical propagators that generate ephemeris by evaluating a formula. Two-Body's formula is exact (i.e. the formula generates the known solution for a vehicle moving about a central body considering only the effect of the body viewed as a point mass) but is not an accurate model of a vehicle's actual force environment. J2Perturbation includes the

point mass effect as well as the dominant effect of the asymmetry in the gravitational field (i.e. the J2 term in the gravity field, representing North/South hemisphere oblateness); J4 additionally considers the next most important oblateness effects (i.e., the J2² and J4 terms in addition to J2). None of these propagators model atmospheric drag, solar radiation pressure, or third body gravity; they only account for a few terms of a full gravity field model. These propagators are often used in early studies (where vehicle data is usually unavailable for producing more accurate ephemeris) to perform trending analysis; J2 Perturbation is often used for short analyses (weeks) and J4Perturbation often for long analyses (months, years). They are particularly useful for modeling “ideal” maintained orbits without having to model the maintenance maneuvers themselves. [12]

The solutions produced by the J2Perturbation and J4Perturbation propagators are approximate, based upon Keplerian mean elements. In general, forces on a satellite cause the Keplerian mean elements to drift over time (secular changes) and oscillate (usually with small amplitude). In particular, the J2 and J4 terms cause only periodic oscillations to semi-major axis, eccentricity, and inclination, while producing drift in argument of perigee, right ascension, and mean anomaly. STK’s J2Perturbation and J4Perturbation propagators model only the secular drift in the elements (the drift in mean anomaly can best be seen as a change to the period of motion of the satellite) [12].

3.2.2 SGP4. The Simplified General Perturbations (SGP4) propagator, a standard Air Force Space Command (AFSC) propagator, is used with two-line mean element (TLE) sets. It considers secular and periodic variations due to Earth oblateness, solar and lunar gravitational effects, gravitational resonance effects, and orbital decay using a drag model. A mission designer can input the initial conditions for the SGP4 propagator manually, but it is much more common to input TLE sets from a TLE file. As is discussed in Section 3.5.1.2, a .txt file with the desired TLE was created and the simulation was directed to use this TLE as the initial condition for the SGP4 propagator.

As seen in Figure 3.1, the result from a 2007 study by Dr. T.S. Kelso, “Validation of SGP4 and IS-GPS-200D Against GPS Precision Ephemerides” shows how the approximate error of SGP4 propagates over time. Figure 3.1 shows radial errors in red,

in-track errors in green, and cross-track errors in blue. Although the in-track errors quickly grow to roughly $10km$ this effect is expected and does not degrade the results of the simulation. As is discussed in Sections 3.5.1.2 and 3.5.1.3, this is a feasibility study and each propagator is being used for the spacecraft and situation for which it is best suited, there is no significant deficiency in the results stemming from this use of the J4 and SGP4 propagators [12]. To avoid these large errors in satellite position, NASA of course updates the ISS's TLE approximately every two days (as reinforced by the low errors near the middle of Figure 3.1). As discussed in Section 5.3, the updates in the ISS's TLE need to be included in any real time mission planning.

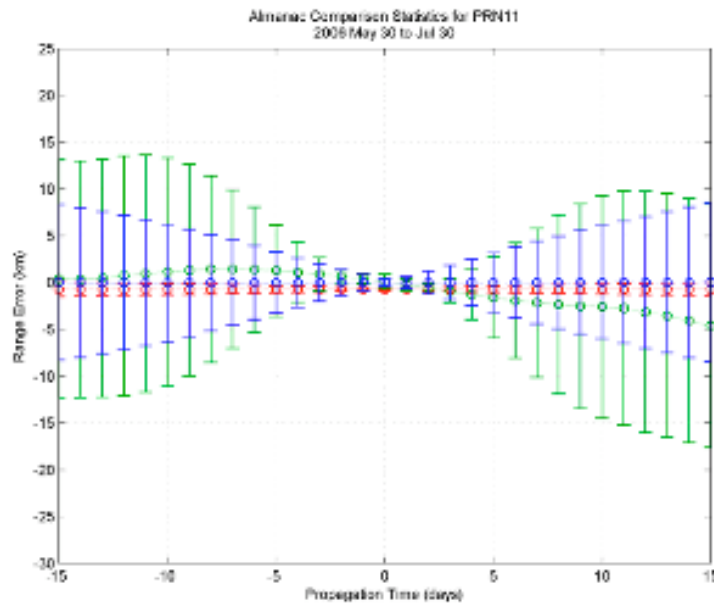


Figure 3.1: PRN11 Almanac Comparison Statistics [24]

Since the SGP4 propagator incorporates both J2Perturbation and J4Perturbation [34] terms with the addition of terms such as the lunar and solar effects as well as a simple atmospheric drag model [12] one would expect that as the simulation is run, the errors between the ISS's orbit and that of FalconSAT6 will stay approximately the same. This trend of similar error propagation between the SGP4 model and the J4 model is further reinforced by the use of one TLE for the ISS for the entire simulation time as discussed in Section 3.5.1.2. For further information on the comparison between the J4 and SGP4 propagators, please refer to [34].

3.3 Hill's Equations

Although not used in the calculation or validation of the solution, the Clohessy-Wiltshire Equations (also known as and will be referred to in this research as Hill's Equations) are presented as a point of comparison and as a reference for possible future work as discussed in Section 5.3. Using these equations, a mission planner could, knowing the two spacecrafts' position and velocity relative to each other, predict the relative motion of the target satellite (in this case FalconSAT6) relative to the principle satellite (in this case the ISS) over a given time span [34]. These equations are listed in Equations 3.1 - 3.6.

$$x(t) = \frac{\dot{x}_0}{\omega} \sin(\omega t) - \left(3x_0 + \frac{2\dot{y}_0}{\omega}\right) \cos(\omega t) + \left(4x_0 + \frac{2\dot{y}_0}{\omega}\right) \quad (3.1)$$

$$y(t) = \left(6x_0 + \frac{4\dot{y}_0}{\omega}\right) \sin(\omega t) + \frac{2\dot{x}_0}{\omega} \cos(\omega t) - (6\omega x_0 + 3\dot{y}_0)t + \left(y_0 - \frac{2\dot{x}_0}{\omega}\right) \quad (3.2)$$

$$z(t) = z_0 \cos(\omega t) + \frac{\dot{z}_0}{\omega} \sin(\omega t) \quad (3.3)$$

$$\dot{x}(t) = \dot{x}_0 \cos(\omega t) + (3\omega x_0 + 2\dot{y}_0) \sin(\omega t) \quad (3.4)$$

$$\dot{y}(t) = (6\omega x_0 + 4\dot{y}_0) \cos(\omega t) - 2\dot{x}_0 \sin(\omega t) - (6\omega x_0 + 3\dot{y}_0) \quad (3.5)$$

$$\dot{z}(t) = -z_0 \omega \sin(\omega t) + \dot{z}_0 \cos(\omega t) \quad (3.6)$$

These equations may be used with the understanding of three underlying assumptions.

1. The reference satellite can be referred to as: chief, station, or target. The other satellite can be referred to as: deputy, orbiter, or interceptor. This research will refer to the satellite combination as: target and interceptor. Each satellite's orbit is determined as a two-body problem.
2. The target is on a circular orbit and the interceptor must be very close to a circular orbit.
3. The magnitude of the vector from the target to the interceptor must be much less than the magnitude of the vector from the center of the Earth to the target.

3.4 Software Used in the Construction of the Design Tool

3.4.1 *Satellite Tool Kit v9.0.1.* Analytical Graphics Inc.'s Satellite Tool Kit is a Commercial-off-the-Shelf (COTS) software package designed to allow users to design and develop complex dynamic simulations of real-world aerospace problems. The multitude of built-in tools as well as optional component add-ons allow scientists and engineers the ability to quickly and accurately create complex aerospace simulations. These simulations are comprised of various components that are assembled to produce the desired model. Some examples of useful components include: satellites, ground stations, air vehicles, ground vehicles, ships, and many more. Additionally, as seen in Figure 3.2 using the built in 2D and 3D visualization tools one can easily and intuitively depict the interaction between various components in the model. Finally, utilizing the access and azimuth, elevation, and range (AER) tools also native to STK a designer is quickly able to quantify the interaction between various components. [12]

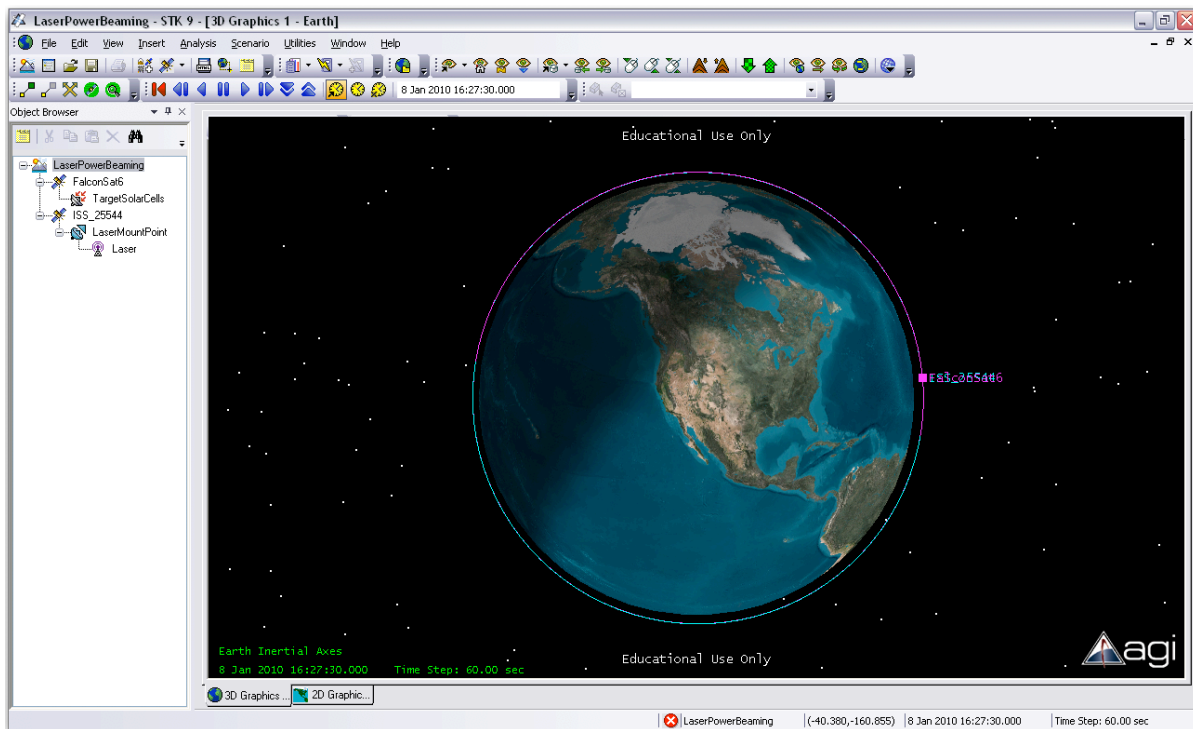


Figure 3.2: STK Main Window

3.4.2 *ModelCenter v8.0.* Phoenix Integration's ModelCenter is a multi-disciplinary modeling environment that can be used to study and optimize the trade space of a de-

sign. ModelCenter can combine analyses developed with a variety of tools including MATLABTM, MathcadTM, ExcelTM, command line executables, and many more. In this research, instead of creating a multiple component model as would be natural with a product such as ModelCenter, a single STK module was implemented as seen in Figure 3.3. This module was then rigorously analyzed using the built-in suite of design and optimization tools. Model Center's parametric, design of experiments, and visualization tools are used to conduct a variety of sensitivity studies to gain insight into what aspects of the design are the key drivers influencing the desired results. ModelCenter also provides a rich set of built-in optimization tools that can be used to determine values for the key drivers that optimize the design for a given goal while ensuring constraints are not violated. These optimization tools include a gradient optimizer, a genetic optimizer called DarwinTM, and an optimizer that utilizes surrogate models of the design space during optimization called DesignExplorerTM[31]. In this case, the ModelCenter simulations were constructed so that total access time between the satellites was maximized while average range was minimized within specified minimum and maximum constraints. Due to its unique ability to compute multi-objective solutions, ModelCenters genetic optimization tool Darwin will be used exclusively throughout this research [27]. A more detailed explanation on genetic optimization may be found in Section 3.4.2.1.

3.4.2.1 Darwin Optimization. ModelCenter's Darwin tool utilizes a genetic algorithm to find optimal design configurations defined by discrete variables. Genetic algorithms are stochastic algorithms that utilize processes analogous to natural selection to search through the design space. They have been experimentally proven to be robust in their application to many search problems, and are ideally suited for design problems with discretely valued design variables. Because they do not require objective or constraint gradient information, genetic algorithms are able to effectively search discontinuous and noisy design spaces. Genetic algorithms search using several designs (a population of designs) and thus, are much more likely to find the globally best design. They are capable of finding many near-optimal designs as well, thus providing the designer with many design alternatives. Genetic algorithms use a list of values to model a single design configuration. In general, the number of items in the list is equal

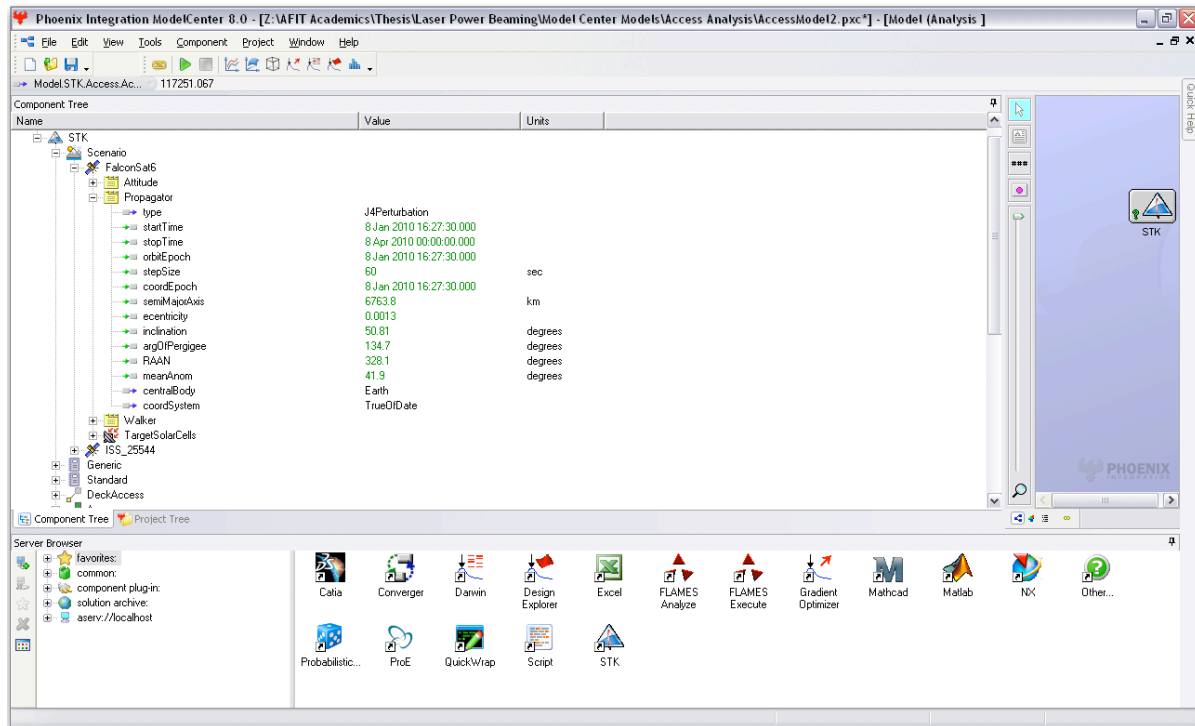


Figure 3.3: ModelCenter Main Window

to the number of variables specified for the design problem. Each item in the list can have any value defined in the enumerated set for the corresponding variable.

The genetic algorithm process begins by generating a random set of design configurations. This set of designs is called the first generation. The user-specified number of members in each generation is called the population size, N_p . Each design is then analyzed and ranked from best to worst based on its objective and constraint values. Next, two (parent) designs from the population are selected and recombined to create two child designs using crossover and mutation operators. Designs with a higher rank are given a greater probability of being selected to create children. The crossover and mutation operators are implemented according to a user specified probability. In general, crossover is implemented with a high probability ($\approx 100\%$) and mutation with a low probability ($\approx 15\%$).

The process of selecting parents and creating children continues until N_p new designs are created and all children are analyzed and ranked. The highest ranked parent design and all but the lowest ranked child design are then used to create the next gener-

ation of designs. One generation after another are created until a user-specified number of generations have been created without improvement in the best design. [27].

3.4.2.2 Pareto-optimal Design. In general, the solution to multi-objective optimization problems (such as this thesis) is a “family” of designs often referred to as the Pareto-optimal set. As seen in Figure 3.4, a Pareto-optimal (or non-dominated) design has the property that no other design can be found that is better in all objectives. A design is referred to as non-optimal (dominated) when another design can be found that has better values for all objectives. Darwin uses a ranking scheme based on the Pareto-optimal concept when ranking each generation of designs. Non-dominated designs are given the greatest probability of selected for crossover and mutation. For multi-objective optimization studies, Darwin will display the Pareto-optimal set of designs found during the search.

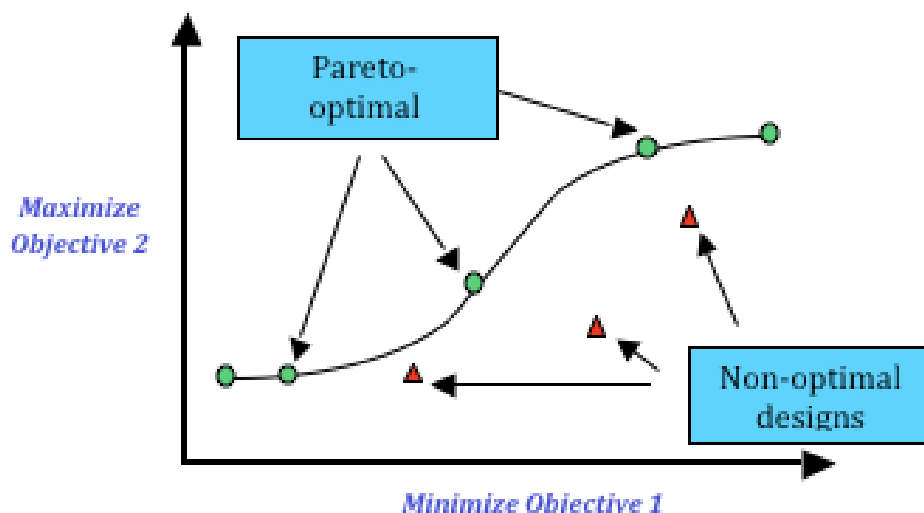


Figure 3.4: Pareto Front [27]

3.5 Model Construction

As mentioned in Section 3.1 the simulation for this research essentially consists of two main parts: the first from the STK model and the second from the ModelCenter controlling segment. The methodology behind the composition of each main part will be discussed in turn throughout this section.

3.5.1 Satellite Tool Kit Model. As discussed in Section 3.1, the STK model consists mainly of two built-in components, namely two satellites. One satellite is defined to be the International Space Station while the other is defined as FalconSAT6. Additionally, each satellite can, and does, have subcomponents (such as transmitters and receivers) attached to it. Here, the details of each satellite component, and its respective subordinate components will be discussed. Additionally, an examination into the global STK settings (that is, the settings that affect the entire model) will be conducted.

3.5.1.1 Global Configuration. The scenario time in STK was set to encompass approximately a three-month time span. As can be seen Figure 3.5, the epoch was set to: 8 Jan 2010 16:27:30 (UTC) (JD=2455205.18576389) and the end of the scenario was set to 8 Apr 2010 00:00:00 (UTC). This particular three month time span is arbitrary, however the duration was chosen for its balance between predicted available access time and computing time for the simulation to run. As will be discussed in Section 5.3, for future designs this time span may be changed to suit the desired mission design.

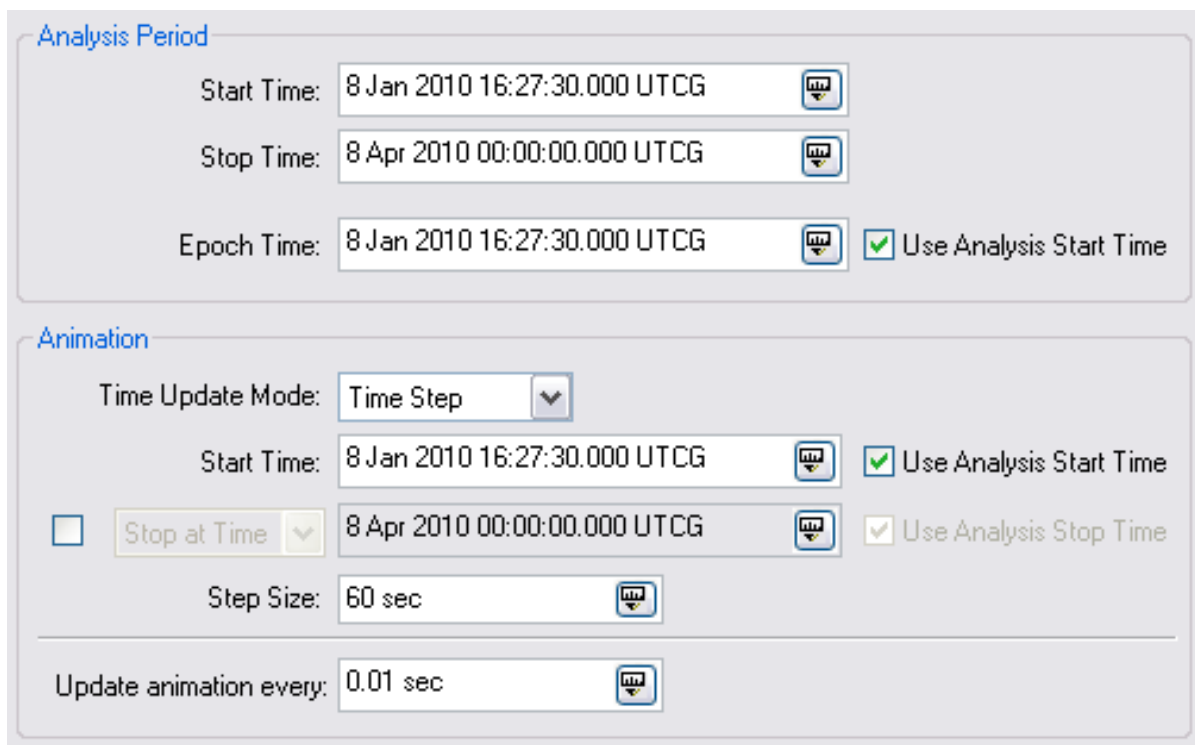


Figure 3.5: STK Analysis Period

3.5.1.2 International Space Station. The STK selections chosen during the construction of the model were all made with the emulation of reality as the primary driver. This component of the model has the largest number of details that must all be accurately chosen to produce a viable model. The first step in inserting the ISS into the STK model is to determine the source of the orbital parameters. The primary method of inserting a prominent spacecraft (such as the ISS) into an STK model should be to automatically download the orbital parameters directly from AGI's server. This method however will lead to a simulation that is not useful for the purposes of this thesis. That is, as NASA and AGI update the orbital parameters on the server, STK will automatically download the new parameters even if the scenario time in STK is unchanged, thus changing the ISS's orbit. If the desired results were an updated, real time analysis; then this solution would be ideal. However, since the desired behavior of this model is that of repeatability, a better, although less precise, technique is required.

The orbital elements for the ISS at epoch were therefore downloaded and validated from CalSky and the resulting two-line element set was saved to a text file to prevent STK from automatically updating the ISS's orbital data as seen in Figure 3.6. As discussed in Section 3.2 different propagators are used for the two different spacecraft. Also seen in Figure 3.6 is the evidence of the use of the SGP4 propagator for the ISS. This propagator was chosen over J2 or J4 as it is uniquely suited for use in STK given a specific two-line element (TLE) set. J2 and J4 are more appropriate as propagators in STK given the six orbital elements. As J4 is used as the propagator for FalconSAT6, its use will be discussed in Section 3.5.1.3.

The TLE used in the model is shown in Table 3.1. As mentioned above, this TLE was downloaded and validated from CalSky. This validation was accomplished graphically as shown in Figure 3.7. With the simulation set to the epoch time and STK allowed to freely download new TLEs from the server, the orbital elements associated with the TLE shown in Table 3.2 were also retrieved from CalSky and were inserted as the orbital parameters for FalconSAT6. The result was both spacecraft co-located at the same location at the same time. Additionally, their orbits propagated in unison. Next, leaving FalconSAT6 with these same orbital parameters, the ISS was transitioned

Propagator: SGP4

Use Scenario Analysis Period

Start Time: 8 Jan 2010 16:27:30.000 UTCG

Stop Time: 8 Apr 2010 00:00:00.000 UTCG

Step Size: 60 sec

Advanced...

Identification

SSC Number: 25544

or

Search Database...

Common Name: ISS

Int'l Designator: 1998-067A

TLE Source

Automatic Update

On propagation, retrieve elements from:

AGI Server Setup...

File Preview...

Define/Import Elements

Use	TLE Epoch	Age	Rev #
<input checked="" type="checkbox"/>	8 Jan 2010 16:27:30.000 UTCG	-0.0 mins	63834

Figure 3.6: ISS Orbit Definition in STK

to using the TLE obtained from CalSky as its source for orbital data as seen in Figure 3.6. The result from this last change is displayed in Figure 3.7 and revealed no change in the relative position of the two spacecraft. This therefore shows that the TLE obtained from CalSky agrees with the orbital elements downloaded from the AGI server and can safely be used for the rest of the simulation.

Table 3.1: International Space Station Two Line Element Set at Epoch Time [10]

1	25544U	98067A	10008.68576389	.00010907	00000-0	68829-4	0	3337
2	25544	051.6475	330.1976	0007655	160.0825	206.4481	15.77242795638342	

Table 3.2: International Space Station and FalconSAT6 Orbital Elements at Epoch Time [10]

Semi-major Axis:	6716.398km
Eccentricity:	0.0007655
Inclination:	51.6475°
Argument of Perigee:	160.0825°
Right Ascension of Ascending Node:	330.1976°
Mean Anomaly at Epoch:	206.4481°

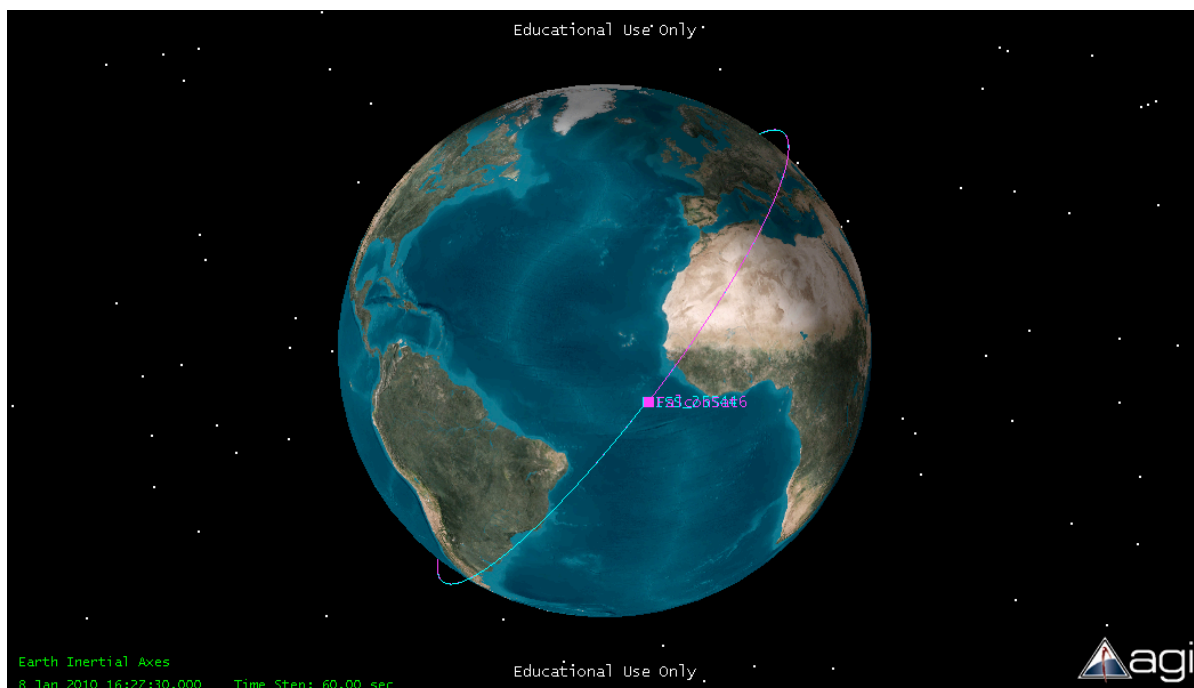


Figure 3.7: Demonstration of the ISS and FalconSAT6 Co-located

As mentioned above, this method of inserting the ISS into the model could introduce error into the simulation, even though it achieves the goal of having a repeatable model. This error could be due to the fact that while this research will use the TLE shown in Table 3.1 for three months, NASA updates their ISS TLE every few days. Therefore, after a few days have passed in the simulation, the TLE shown in Table 3.1 will be obsolete and errors will be introduced into the model. This consequence is acceptable, however, since this research is merely a feasibility study and not a plan with a real world epoch in mind.

Next, to ensure the greatest detail and accuracy for the actual rendering of the ISS itself (as well as X,Y,Z location of the JEM/EF), the built in .mdl rendering file for the ISS was discarded and replaced with a highly detailed and accurate one obtained directly from the Space Test Program (STP) as seen in Figure 3.8. This model enabled the accurate placement of the laser on one of the JEM/EF mounting points.

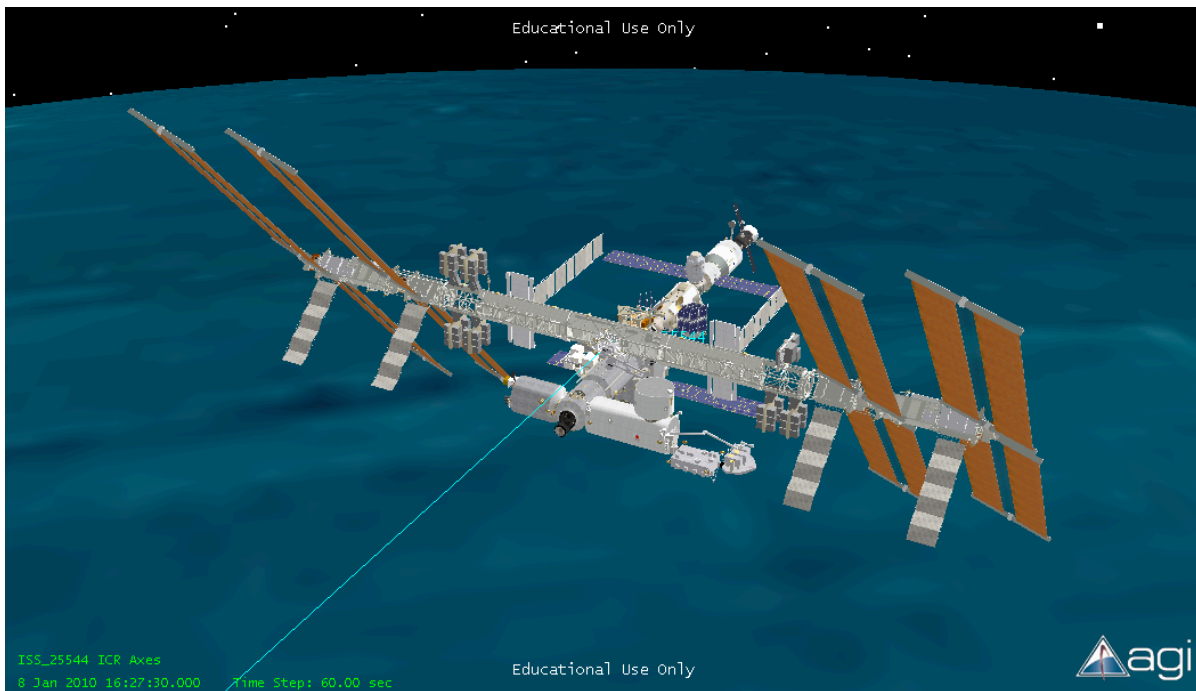


Figure 3.8: ISS Model from the Space Test Program

Once the ISS had been properly inserted into the STK model with the correct orbit that would allow for a repeatable simulation as well as an accurate graphical rendering of the station, the laser and mission constraints were added. For the purposes of the

STK simulation, the laser consists of two separate components as seen in Figure 3.9. This technique compensates for the STK limitation that transmitters cannot be located in any X,Y,Z location in the body frame on a spacecraft, whereas sensors can. As shown in Figure 3.9, a sensor was “attached” to the ISS and called LaserMountPoint as it will serve as the mounting point for the actual laser. Additionally, due to STK’s limitation concerning the placement of a transmitter, for the purpose of this simulation all physical constraints normally attributed to the laser will be assigned to the LaserMountPoint and will be discussed here instead of relative to the transmitter. As shown in Figure 3.9, since the actual transmitting laser (called Laser for this simulation) is a child of the LaserMountPoint, when the simulation is executed the Laser will take on all of the attributes of the LaserMountPoint.

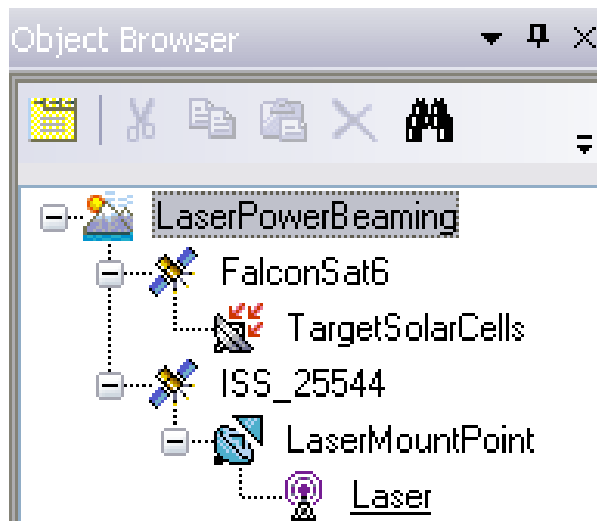


Figure 3.9: STK Object Browser

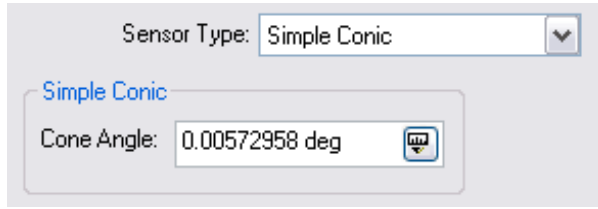
The first step in defining the LaserMountPoint/Laser is identifying its type and dimension to STK. As seen in Figure 3.10(a) a simple conic type of beam was chosen with an angle of approximately $.00573^\circ$. The simple conic was chosen as it most easily represents the physical shape of the laser beam as it travels away from the ISS. The cone angle is based on the work done in the complementary thesis to this work entitled “Minimizing Losses in a Space Power Beaming Experiment” [16] and represents the angle at which the laser beam diverges from a perfectly columnated beam as it propagates

away from the ISS[16]. As seen in Figure 3.10(b) this value produces a reasonable representation of the spot size at the operable range of FalconSAT6.

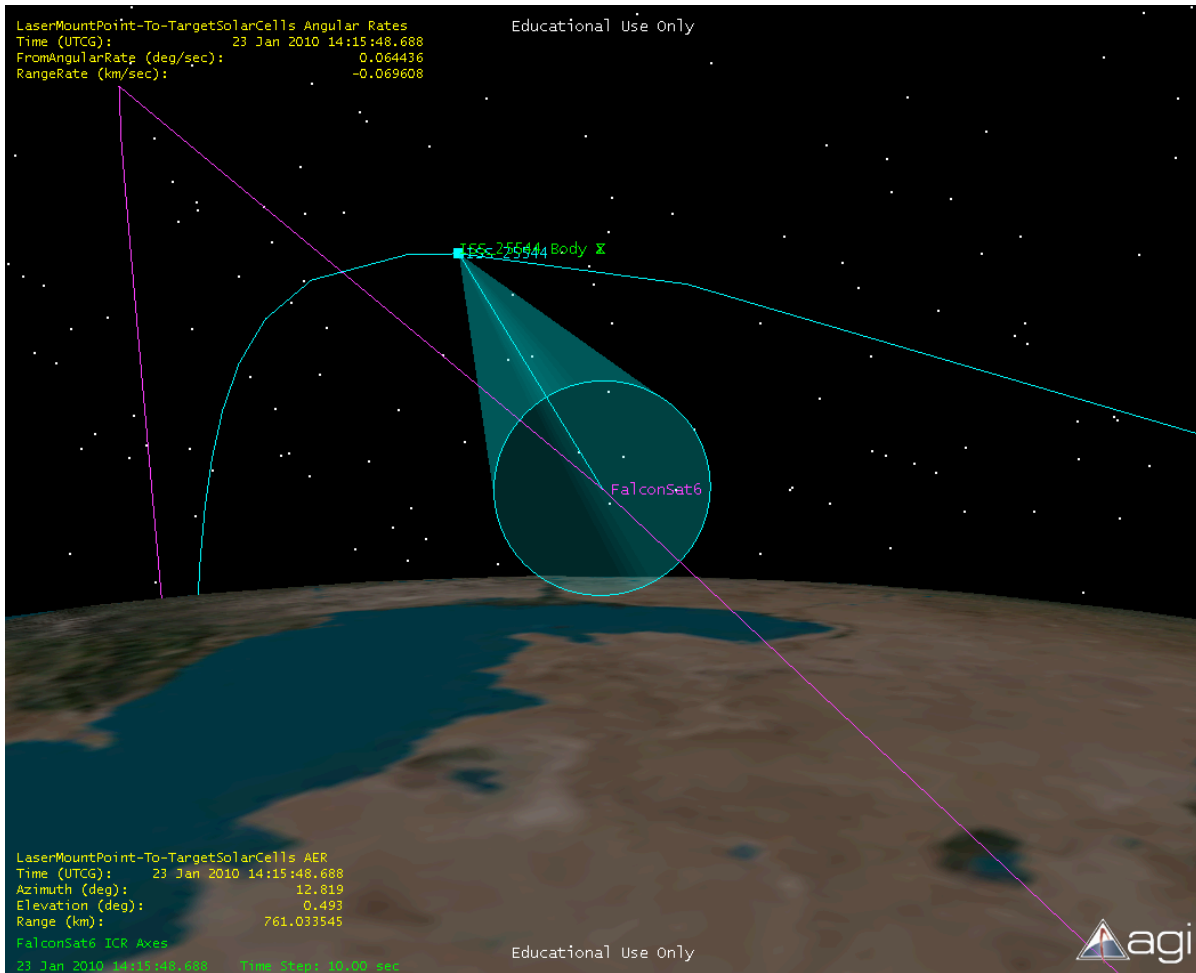
After defining the beam properties of the laser, it was necessary to properly locate the LaserMountPoint/Laser pairing physically on the ISS. If allowed to place the LaserMountPoint/Laser on the ISS in the default location, STK would place it at the center of the body frame. This trait is undesirable here as this would ultimately locate the laser in the middle of a module. To properly locate the LaserMountPoint/Laser on the JEM/EF, trial and error was used to determine the correct location in STK's ISS body frame for one of the JEM/EF's mounting points. As can be seen in Figure 3.11(b) this task was accomplished graphically via the interface shown in Figure 3.11(a). Also, the final X,Y,Z coordinates of the LaserMountPoint/Laser are listed in in Figure 3.11(a).

Once the laser was correctly configured in both dimension and location, it needed to be properly targeted. The only choice for this step, and the topic for this thesis, was to target FalconSAT6. The actual construction of the FalconSAT6 model will be covered in Section 3.5.1.3 however as targeting is a function of the LaserMountPoint/Laser it is covered here. As can be seen in Figure 3.12(a) FalconSAT6 was selected from the available list of targets and assigned as the LaserMountPoint/Laser's target. Additionally "Tracking" was selected because, as the name implies, this function allows the LaserMountPoint/Laser to track the target satellite, in this case FalconSAT6. Figure 3.12(b) demonstrates the result of the targeting selections described in Figure 3.12(a). The blue line extending from the ISS and intersecting the dot marked FalconSAT6 represents the laser emanating from the JEM/EF.

With the beam dimension, laser location, and targeting settings fully configured, the final step of adding the real world physical constraints to the model was accomplished. As seen in Figure 3.14(a) constraints are defined for the azimuth, elevation, and range of the LaserMountPoint/Laser. The $\pm 20^\circ$ azimuth and $\pm 20^\circ$ elevation constraints effectively form a 40° cone about the Body-X axis as seen in Figure 3.11(b). The constraint value selected is based on the work in [16] and is a nominal angle that a generic COTS fast-steering mirror can subtend. This angle also attempts to prevent the laser from ever allowing the ISS to obscure the beam. A detailed discussion of the obscuration

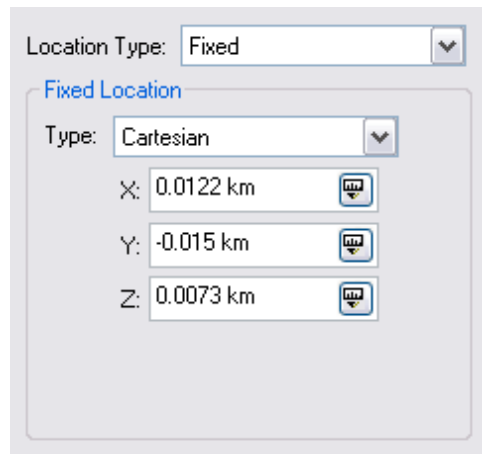


(a) Type of Sensor and Cone Angle

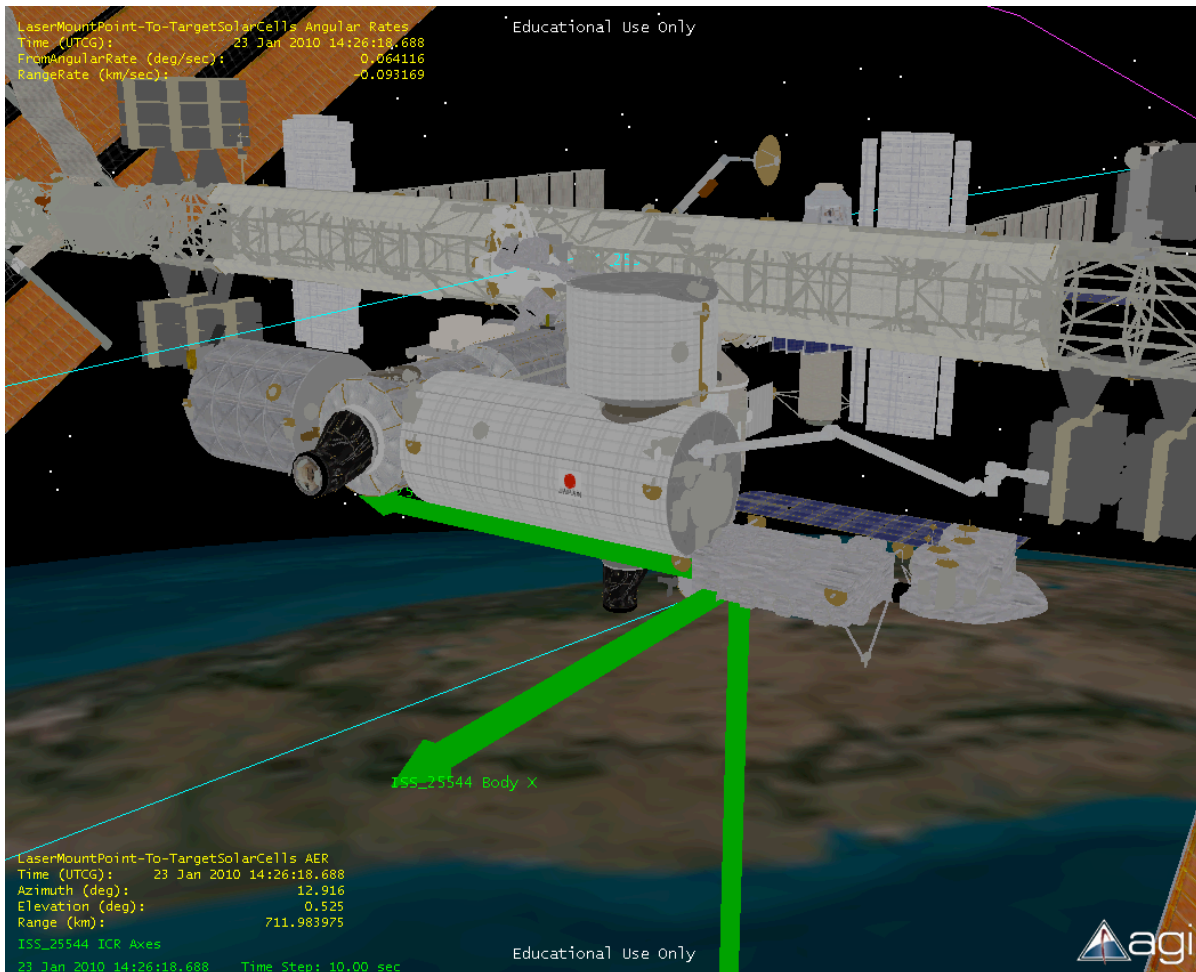


(b) Laser Spot Size at FalconSAT6 Range

Figure 3.10: Laser Dimensions

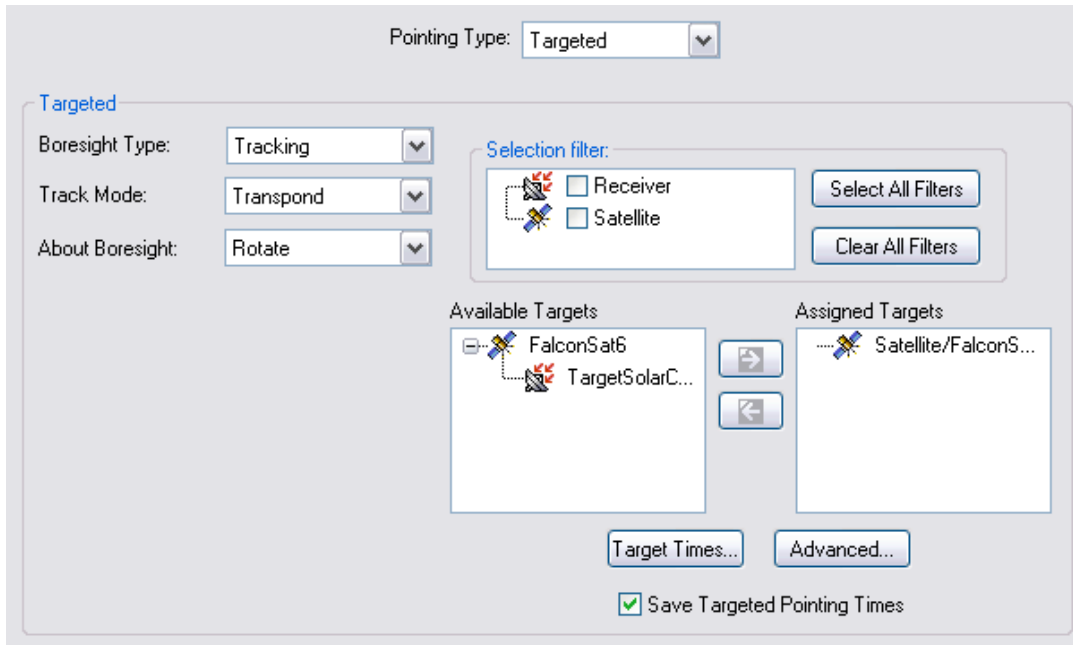


(a) X,Y,Z Location in ISS Body Axes

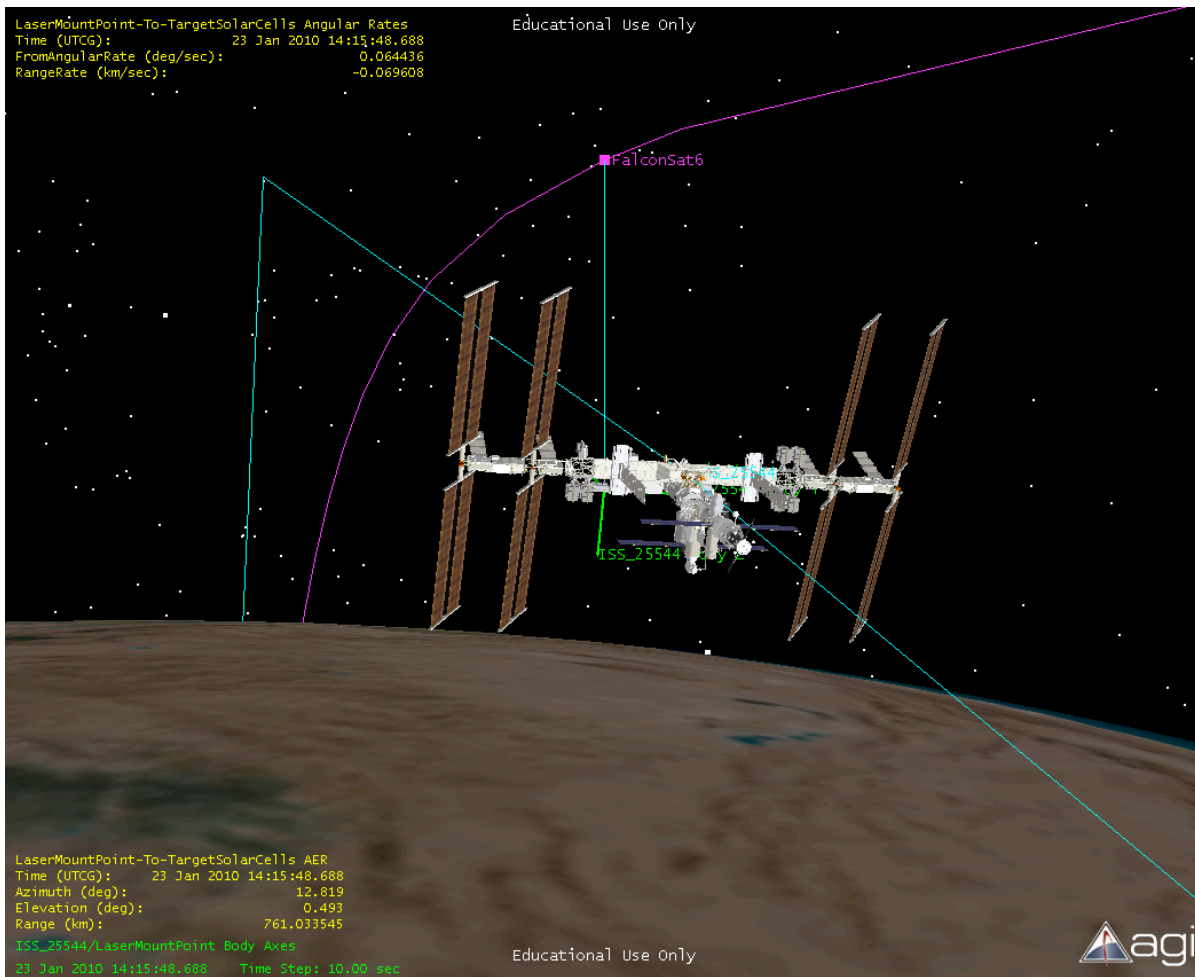


(b) Laser on JEM/EF

Figure 3.11: Laser Location on ISS



(a) Tracking Configuration



(b) Laser Tracking FalconSAT6

Figure 3.12: Laser Tracking Parameters

analysis can be found in Section 4.4. Next, the range constraint was defined. Here, the minimum and maximum values for the range were selected for quite different reasons. The minimum range in all directions from the ISS was set to $40km$ as this satisfies two requirements. First, a $40km$ “bubble” around the ISS satisfies NASA’s $10km - 25km$ safety zone surrounding the ISS including a factor of safety of over 60%. Second, also based on the work in [16], $40km$ is outside the lethal fluency for the type and power of laser being considered for this mission. The other component of the range constraint, the maximum range was also defined. The range of $883km$ was also chosen based on the work in [16] as this is the maximum effective range of the laser. Considering the laser spot size at this range as well as the size of the proposed solar cells, system losses, and available power, this is the largest range that sufficient power can be transmitted to FalconSAT6 to complete the mission[16].

The next step of defining the LaserMountPoint/Laser’s real world physical constraints was identifying the temporal constraint as shown in Figure 3.14(b). This constraint serves two distinct purposes. First, $30sec$ was chosen as the minimum duration that would be allowed for any one access because, based on the work in [16], $30sec$ is a reasonable amount of time for the laser system to: locate and acquire the target satellite, confirm accurate tracking, and transmit enough power for the batteries to receive a charge. A lower value could potentially have been chosen, however as this is a feasibility study, a theorized worst-case scenario for a minimum access time was desired. In addition to allowing for a worst-case acquisition time, $30sec$ also allows for a worst case tracking rate of the laser system. Using $30sec$ as a minimum access time allows for an angular rate as shown as

$$\frac{40^{\circ}}{30sec} = 1.333deg/sec \quad (3.7)$$

This angular rate for a fast-steering mirror is clearly a worst case scenario. Many reasonably priced COTS fast-steering mirrors can achieve angular rates orders of magnitude less than this. Again however, as this is a feasibility study, a reasonable worst-case angular rate is desired.

Next, the access association between the ISS and FalconSAT6 had to be established. The actual construction of the FalconSAT6 component will be covered in Section 3.5.1.3; however, as the access association concerns the LaserMountPoint, it will be discussed here. As shown in Figure 3.13 the access assignment must be between the LaserMountPoint on the ISS and the TargetSolarCells on FalconSAT6.

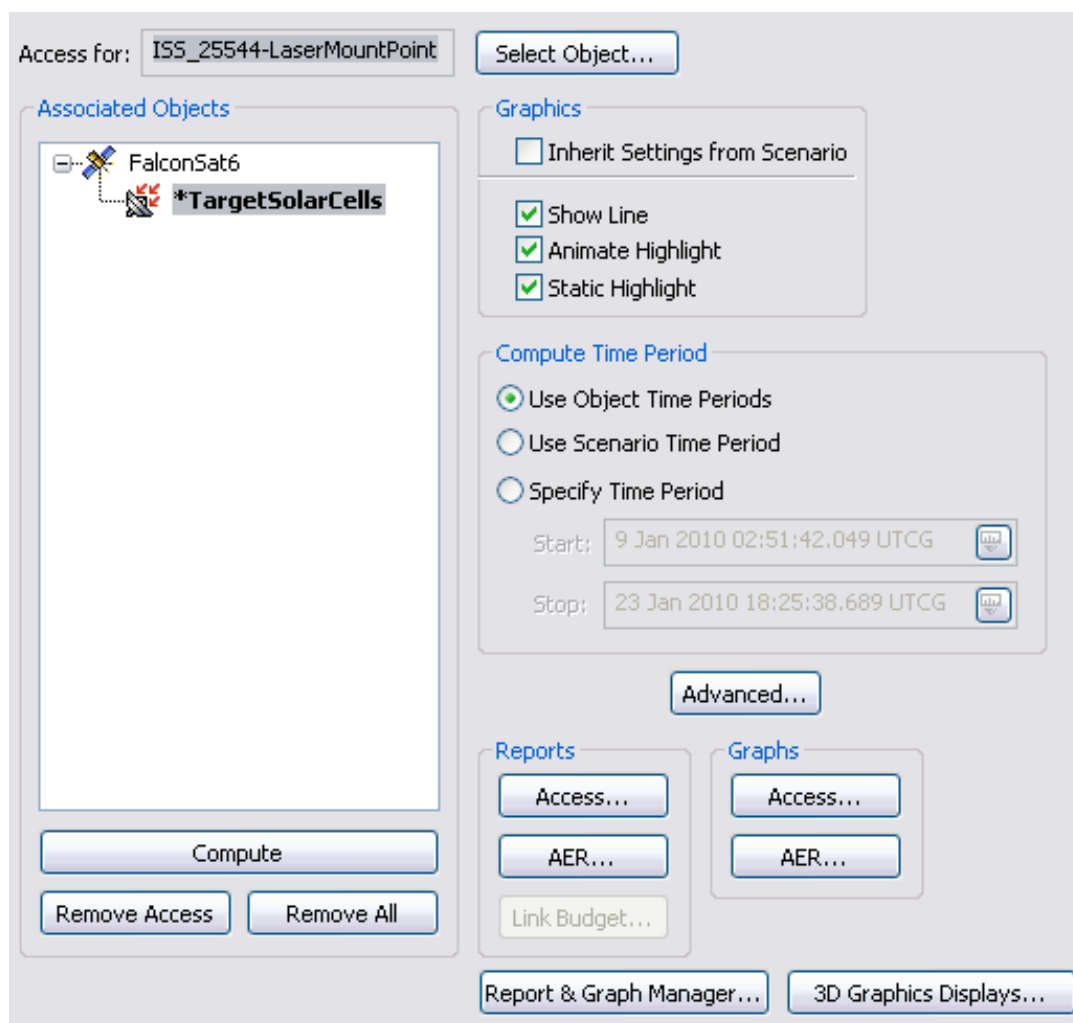


Figure 3.13: ISS to FalconSAT6 Access Assignment

Finally, once all parameters for the LaserMountPoint were correctly set, the actual laser transmitter was attached to the sensor named LaserMountPoint. As previously discussed, this laser will assume all of the same traits and constraints of the sensor it is attached to. Once attached to the sensor, the transmitter component will be defined as a “Laser Transmitter Model” and take on the properties of a laser. As this thesis does

not discuss the use of a specific laser, all default settings for the transmitter frequency and wavelength were accepted.

The screenshot displays a grid of control panels for 'LaserMountPoint Basic Constraints'. The panels are arranged in three rows and three columns:

- Row 1:**
 - Azimuth Angle:** Min: -20 deg, Max: 20 deg. Exclude Time Intervals.
 - Elevation Angle:** Min: -20 deg, Max: 20 deg. Exclude Time Intervals.
 - Range:** Min: 40 km, Max: 883 km. Exclude Time Intervals.
- Row 2:**
 - Azimuth Rate:** Min: [empty], Max: [empty]. Exclude Time Intervals.
 - Elevation Rate:** Min: [empty], Max: [empty]. Exclude Time Intervals.
 - Range Rate:** Min: [empty], Max: [empty]. Exclude Time Intervals.
- Row 3:**
 - Angular Rate:** Min: [empty], Max: [empty]. Exclude Time Intervals.
 - Altitude:** Min: [empty], Max: [empty]. Exclude Time Intervals.
 - Propagation Delay:** Min: [empty], Max: [empty]. Exclude Time Intervals.

At the bottom of the interface, there are three global options: Line of Sight, Field of View, and Sensor AzEl Mask.

(a) Azimuth, Elevation, and Range

The screenshot shows the 'Duration' settings panel. It contains two rows of controls:

- Min:** 30 sec
- Max:** [empty]

(b) Temporal

Figure 3.14: LaserMountPoint Basic Constraints

3.5.1.3 FalconSAT6. As the purpose of this research is the to study the optimization of FalconSAT6's orbit, the initial setup for this spacecraft was much less involved relative to that of the ISS. Similar to the ISS, FalconSAT6 was inserted into the model as one of the primary modules as seen in Figure 3.9. This was done simply by creating a satellite in STK and defining it with the orbital parameters of the ISS as seen in Table 3.2. As discussed in Section 3.5.1.2, assigning FalconSAT6 the same orbital

elements as the ISS provides a verification method for the ISS’s orbit. Additionally, as will be discussed in Section 3.6, the orbital elements for FalconSAT6 were initially set to match those of the ISS to examine a “best case scenario” for the access time, and, as will be discussed in Chapter IV, give ModelCenter a place to start the optimization process.

As seen in Figure 3.15, while defining the orbit for FalconSAT6 the J4 propagator was selected. This propagator was chosen because, in STK and as discussed in Section 3.2, it is best suited for the given input of orbital elements (verses the TLE given for the ISS). Again, as this is a feasibility study, having different propagators will not adversely affect the result of the research.

Propagator: J4Perturbation Initial State Tool...

Use Scenario Analysis Period

Start Time: 8 Jan 2010 16:27:30.000 UTCG

Stop Time: 8 Apr 2010 00:00:00.000 UTCG

Step Size: 60 sec

Orbit Epoch: 8 Jan 2010 16:27:30.000 UTCG Semimajor Axis: 6716.4 km

Coord Epoch: 8 Jan 2010 16:27:30.000 UTCG Eccentricity: 0.0007655

Coord Type: Classical Inclination: 51.6475 deg

Coord System: TrueOfDate Argument of Perigee: 160.083 deg

Prop Specific: Special Options... RAAN: 330.198 deg

Mean Anomaly: 206.448 deg

Figure 3.15: FalconSAT6 Orbital Definition

Once the satellite was installed in the model, the default graphical rendering of a generic satellite was replaced with the USAFA’s STK image file for FalconSAT5 as shown in Figure 3.16. This enables accurate access calculations between the ISS and FalconSAT6 as the relative size and cross section will be correct. Additionally, as will be discussed in Chapter V, having an accurate size for the FalconSAT6 bus as well as the attached solar panels will aid in the development of possible follow-on work.

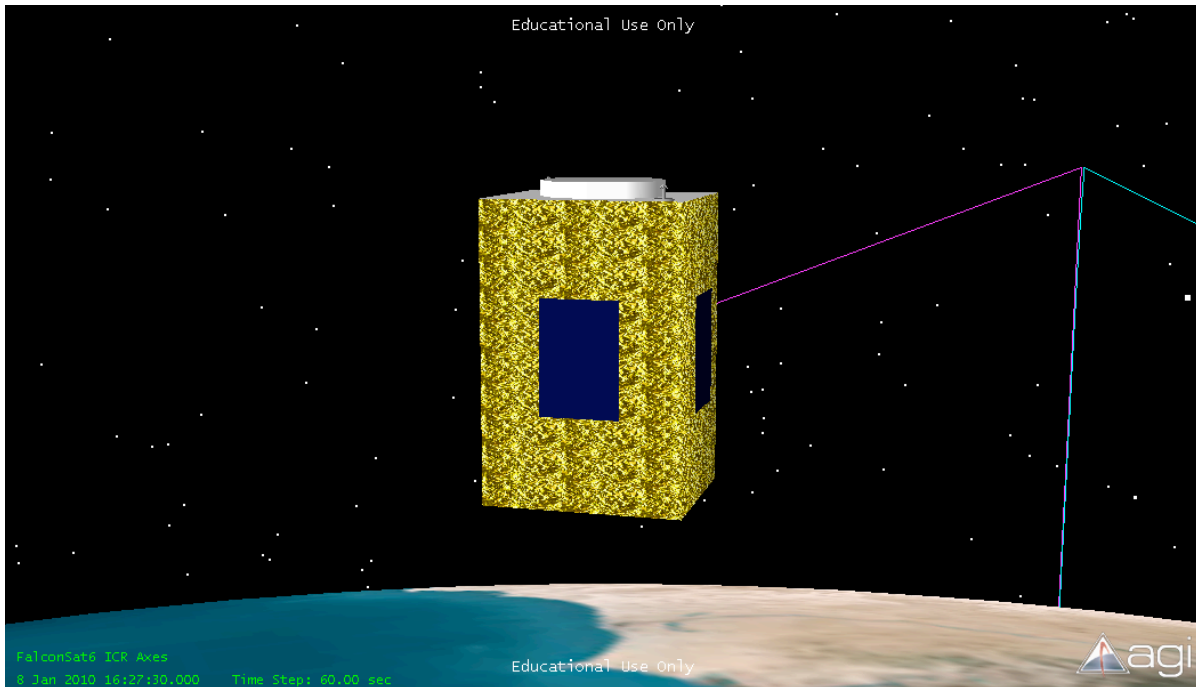


Figure 3.16: USAFA’s FalconSAT5 STK Model

Attaching the solar panels was the final step in placing FalconSAT6 into the overall model. As placing the solar panels at the center of mass of FalconSAT6 is far less consequential than for the ISS due to its small size relative to both the ISS and the laser spot size as shown in Figure 3.10(b), the process is much less complex relative to the placement of the laser on the ISS. The solar panel was attached to FalconSAT6 simply by adding a receiver object and associating it to FalconSAT6 as shown in Figure 3.9. This receiver was named TargetSolarCells. The receiver was then defined as a “Laser Receiver Model” and, like the “Laser Transmitter Model”, all default frequencies and wavelengths were accepted.

3.5.2 ModelCenter Simulation. The STK model described in Section 3.5.1 is only one part of the greater simulation. The actual analysis takes place in ModelCenter. For this research effort, a single STK component served as the entire model in ModelCenter; which was extensively explored using ModelCenter’s built in design, data visualization, and optimization tools. Compared to the construction of the actual model in STK, the setup in ModelCenter for this research was simple. As seen in Figure 3.3 to actively control a STK model from within ModelCenter, a STK component must be

added to the component pane in ModelCenter's main window. Once this task was accomplished and the correct STK file was associated with the new component, the STK model had to be verified to ensure it was producing accurate and reliable results.

3.5.3 Summary of Model Constraints, Assumptions, and Limitations. The summary of the model's constraints as discussed in Section 3.5 is displayed in Table 3.3. Additionally, this model is constrained to using only the ISS and one other satellite (in this case, FalconSAT6). If the analysis of the interaction between the ISS and other satellites is desired, then one would need to add those additional satellites to the model. This can be accomplished manually via STK or one can download satellites from STK's extensive database (similar to the manner which the ISS was initially added to the model as discussed in Section 3.5.1.2). The model is also limited to finding solutions to the problem as constrained in Table 3.3. All of these parameters can (and should) be changed to fit the needs of the current design proposal as discussed in Section 5.3. Finally, other than a $3kW$ input power laser and a BHT-200, this model makes no assumptions of which hardware should be used in a mission of this type (control system, solar panels, etc.).

3.6 Model Verification and Validation

As was mentioned in Section 3.5.1.3, FalconSAT6's orbital elements were initially set to the values shown in Table 3.2. That is, they were set to those of the ISS at the epoch time thus exactly co-locating the two satellites at the epoch time. To verify and validate the model, a parametric study was then conducted via ModelCenter as shown in Figure 3.17. Each orbital element was individually varied over a specified range as shown in Table 3.4 while the other five elements were held constant at the ISS's orbital parameters. Table 3.4 describes the ranges over which each of the orbit elements were individually varied.

The only two maximum constraints placed on the problem at this point were: the $883km$ maximum range as discussed in Section 3.5.1.2 and the decision that no retrograde orbits beyond a sun-synchronous orbit of 98° would be considered due to the

Table 3.3: Summary of Model Constraints and Assumptions

Parameter	Value	Reason
Laser Input Power	$3kW$	Maximum power delivered to one attachment point on JEM/EF
Dwell Mirror Angles	$\pm 20^\circ$	Angle in both azimuth and elevation; Help prevent laser obscuration from the ISS
Individual Contact Time	$30sec$	Allows for a slower dwell mirror; Accounts for delays in acquiring FalconSAT6; Provides enough time for batteries to receive a feasible charge
Minimum Total Access Time	$10,000sec$	So many solutions have a total access time great than $10,000sec$, a minimum acceptable time had to be selected; $10,000sec$ of total access time translates into approximately $400sec$ of BHT-200 firing time
Minimum Range to ISS	$40km$	Outside of NASAs $10km-25km$ safety bubble around the ISS; Outside of the lethal laser fluence on FalconSAT6s solar panels
Maximum range from ISS	$883km$	Maximum effective range of the laser
Simulation Time	3 months	8 Jan 2010 16:27:30 - 8 Apr 2010 00:00:00; Balance between predicted available access time and computing time for the simulation

Table 3.4: FalconSAT6 Orbital Parameter Ranges Used in Parametric Studies

Orbital Element	Value Range
Semi-major Axis	$6716.4km - 7600km$
Eccentricity	0.0 - 0.9
Inclination	$0.0^\circ - 98^\circ$
Argument of Perigee	$0.0^\circ - 360^\circ$
Right Ascension of Ascending Node	$-180^\circ - 360^\circ$
Mean Anomaly	$-180^\circ - 360^\circ$

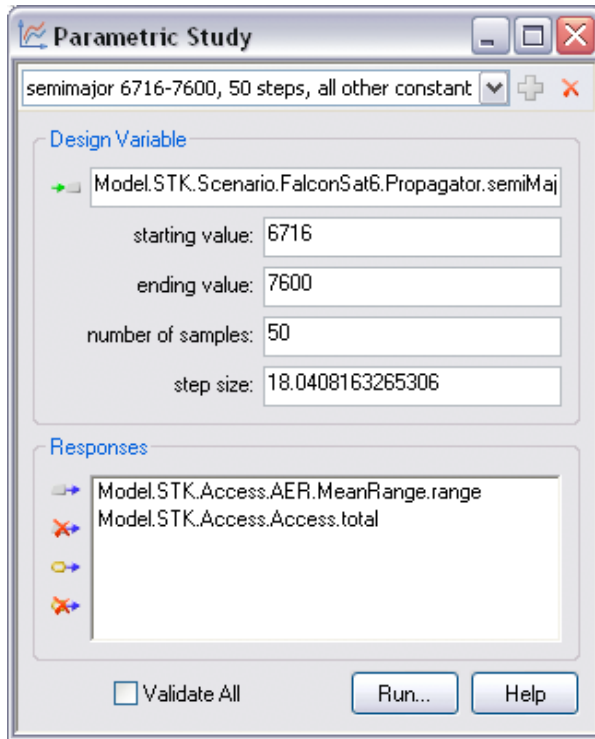


Figure 3.17: ModelCenter Parametric Study Tool

unlikeliness of being launched into such an orbit. As shown in Table 3.4 all other orbital elements were varied through their entire possible ranges. Additionally, a minimum semi-major axis of $6716.4km$ was chosen as this is the semi-major axis of the ISS at the epoch time. For this thesis, only orbits higher than the ISS were considered to both extend the mission duration by reducing atmospheric drag and eliminate any possible dangers or complications caused from firing a laser towards the Earth's surface. As will be discussed in Section 5.3 however, future work may also consider orbits lower than the ISS as a means to initiate or facilitate the de-orbiting of FalconSAT6.

3.6.1 Model Initial Conditions. As the input to each of the six individual parametric studies was an orbital element, the outputs were mean range and total access time. The output graphs from the parametric studies shown in Figures 3.18 - 3.29 were used to initially explore the data over the suspected useful ranges of each of the parameters. During the verification and validation process, careful consideration was given to each graphical relationship to verify that the simulation was producing the expected results (results that could be determined at this point without the use of the

model). As mentioned in Section 3.5.1.3, in addition to enabling the validation of the TLE and orbital elements to be used in the simulation, initially co-locating FalconSAT6 with the ISS enabled what is suspected to be the best case scenario to be evaluated. Intuitively, if FalconSAT6 was co-located with the ISS, the expected result would be the maximum access time possible given the constraints of the mission described in Section 3.5.1.2. As shown in Table 3.5, the total access time over the three month simulation was 1244293.626sec or 14.4015days. Although, this is clearly not the entire three month duration of the simulation, it demonstrates the point that, within the limitations of the STK simulation, co-locating the two spacecraft will produce a sizable total access time. As described in Section 3.2, the two satellites in the simulation did not stay in “formation” flight for the entire three month time span mainly because of the different drag models of the orbital propagators used. This result was the first indication that the model was running correctly.

Table 3.5: Global Statistics for STK Access Report with FalconSAT6 Co-located with the ISS

	Access	Start Time (UTCG)	Stop Time (UTCG)	Duration (sec)
Min Duration	10	23 Jan 2010 18:06:19.744	23 Jan 2010 18:25:38.689	1158.945
Max Duration	5	9 Jan 2010 08:34:53.151	23 Jan 2010 11:22:52.078	1219678.927
Mean Duration				124429.363
Total Duration				1244293.626

The AER report was then used to validate the model. Table 3.6 shows that both the azimuth and elevation remained within the $\pm 20^\circ$ cone defined in Figure 3.14(a). Additionally, Table 3.6 shows that the range also remained within the parameters defined in Figure 3.14(a). This result in the AER report was the second indication that the simulation was running correctly. Next, the orbit elements themselves were used to additionally validate the model.

3.6.2 Orbital Elements. Figures 3.18 - 3.29 give insight into the accurate execution of the model. Figures 3.18 and 3.19 are both outputs as a result of varying semi-major axis over the range shown in Table 3.4 and holding the other five orbital elements constant at the ISS’s epoch time. In both figures, the expected result is shown.

Table 3.6: Global Statistics for STK AER Report with FalconSAT6 Co-located with the ISS

	Access Time (UTCG)	Azimuth (<i>deg</i>)	Elevation (<i>deg</i>)	Range (<i>km</i>)
Min Elevation	9 Jan 2010 05:43:21.776	3.921	-6.659	40.000987
Max Elevation	23 Jan 2010 15:37:27.247	351.957	11.518	40.000961
Mean Elevation			-0.625	
Min Range	23 Jan 2010 15:37:27.247	351.957	11.518	40.000961
Max Range	16 Jan 2010 09:54:37.726	359.707	-1.444	306.994651
Mean Range				210.252152

Figure 3.18 shows an extremely high total access time at the ISS's semi-major axis (as shown in Table 3.2) at the epoch time followed by a steep decline toward zero access time as semi-major axis is increased. Meanwhile, Figure 3.19 shows the range steadily climbing as semi-major axis is increased until the range constraint shown in Figure 3.14(a) is reached and the model no longer records any access. In addition to producing the expected result of increasing range with an increasing semi-major axis, Figure 3.19 also demonstrates that the range constraints have been correctly applied.

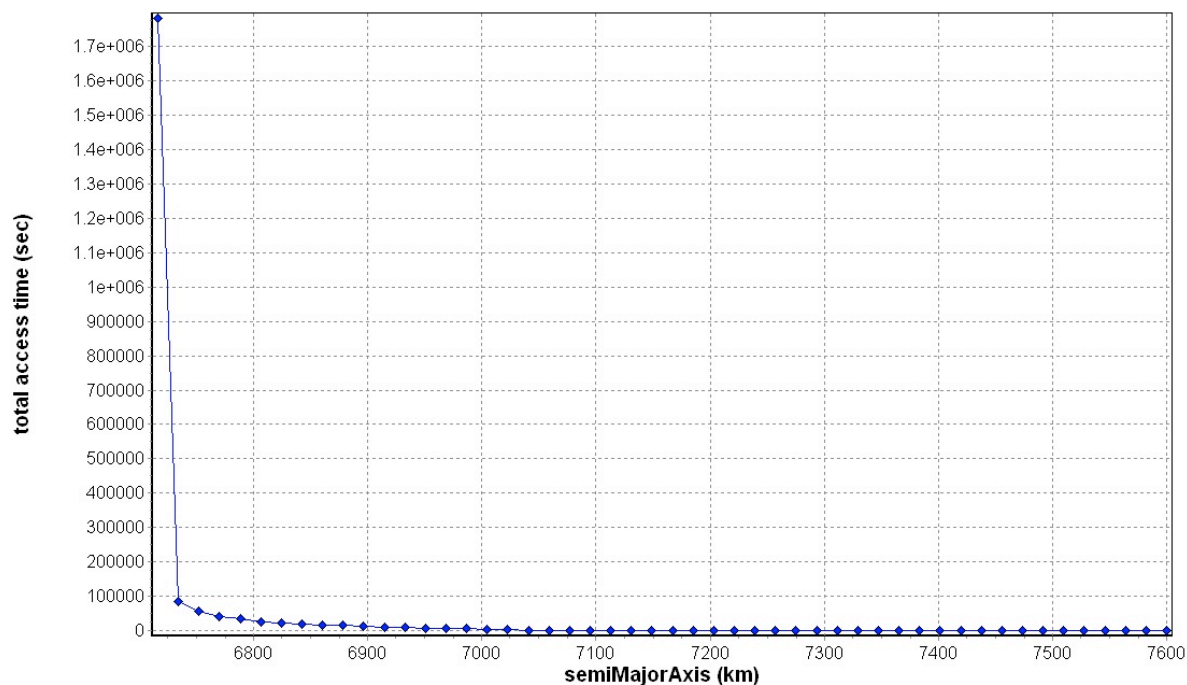


Figure 3.18: Total Access Time as a Function of Semi-Major Axis

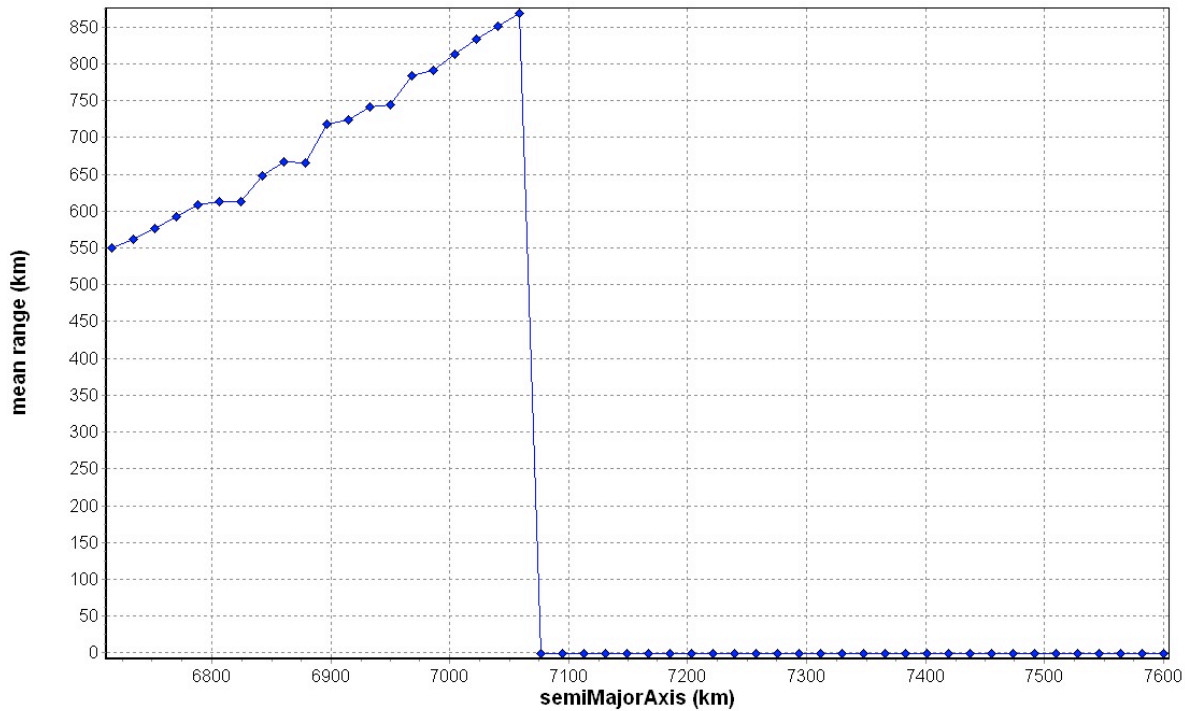


Figure 3.19: Mean Range as a Function of Semi-Major Axis

Figures 3.20 and 3.21 depict total access time and mean range as a function of eccentricity. Figure 3.20 shows the expected result of a very high total access time at approximately the ISS’s eccentricity (as shown in Table 3.2) then quickly approaching zero as the orbit becomes more eccentric. Mean range, however, produces an interesting result. There is no single region where the mean range either approaches zero or becomes very large. This result could be due to a coupling effect between semi-major axis and eccentricity or the geometry of the constrained problem. For this analysis of eccentricity, semi-major axis has been held constant at $6716.4km$. Therefore, as the orbit increases in eccentricity it is possible that the orbit periodically intersects with the Earth’s surface creating the discontinuous regions of zero mean range. This phenomenon will be further explored in Chapter IV.

Inclination is evaluated in Figures 3.22 and 3.23. Both of these figures are an excellent and clear indication that the model was performing as expected. Figure 3.22 indicates a very high total access time at the inclination of the ISS while approaching zero at all other inclinations. Conversely, Figure 3.23 shows a minimal mean range

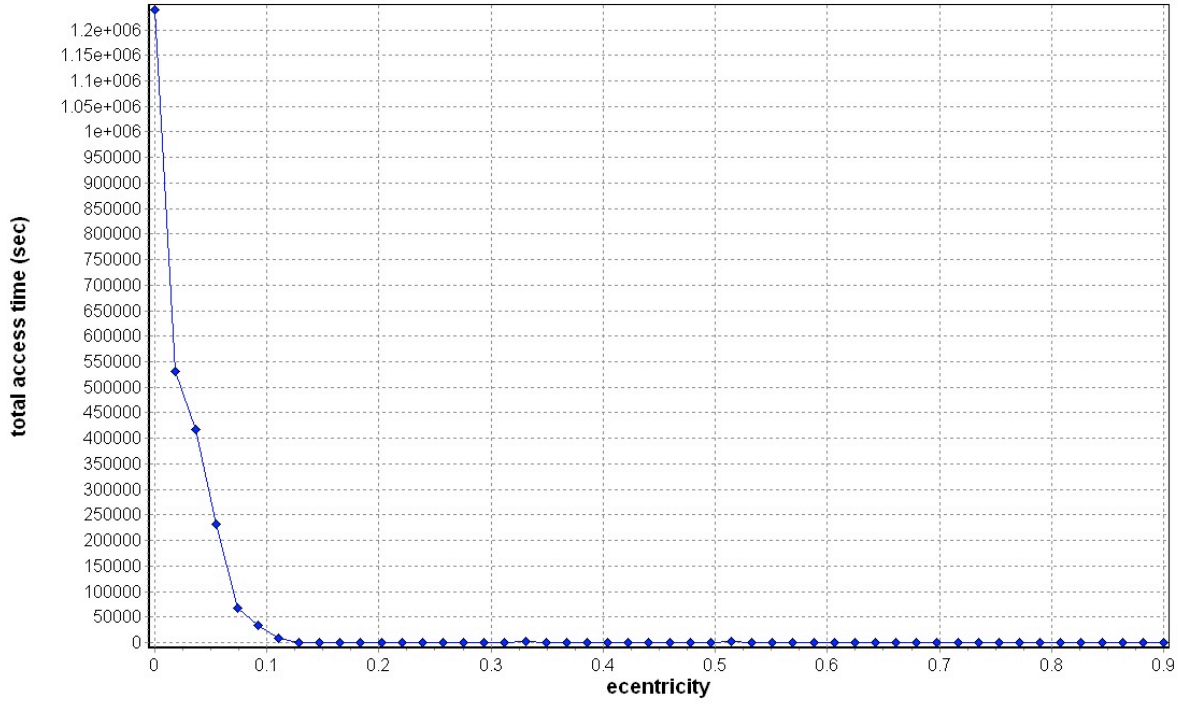


Figure 3.20: Total Access Time as a Function of Eccentricity

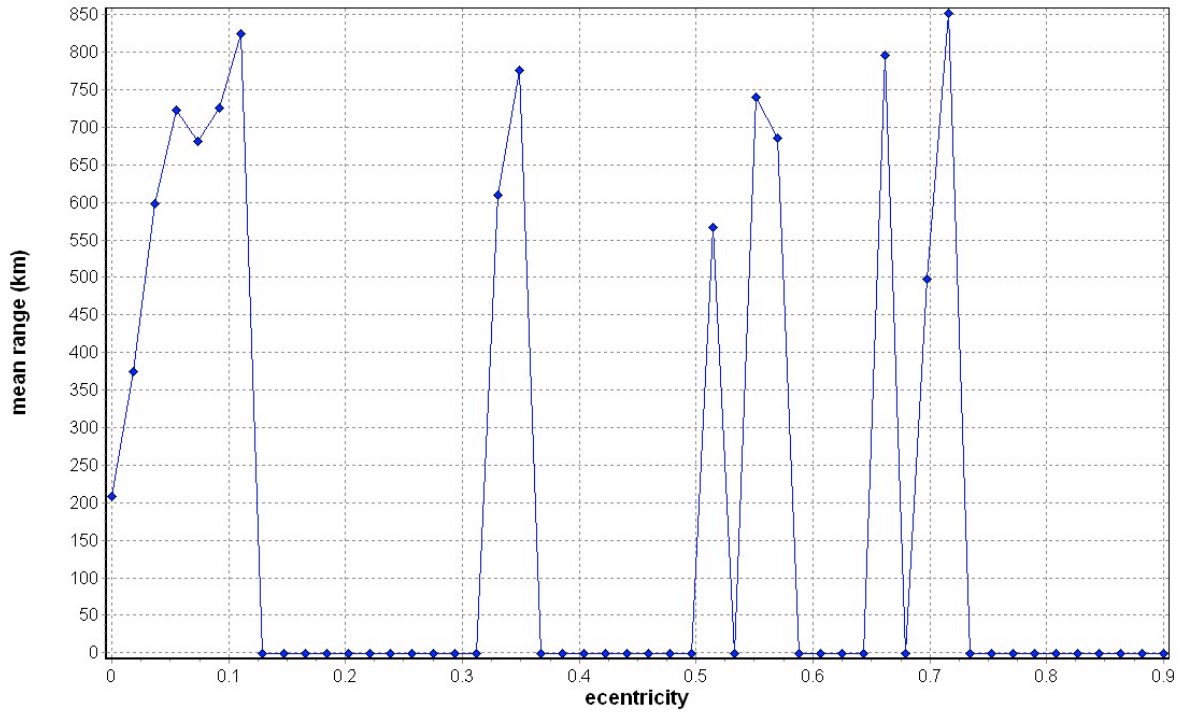


Figure 3.21: Mean Range as a Function of Eccentricity

between the satellites at the ISS's inclination (as shown in Table 3.2) while showing a relatively large mean range at all other inclinations. Intuitively, with all other variables held constant, this is the expected result from varying inclination and reinforces the validity of the model.

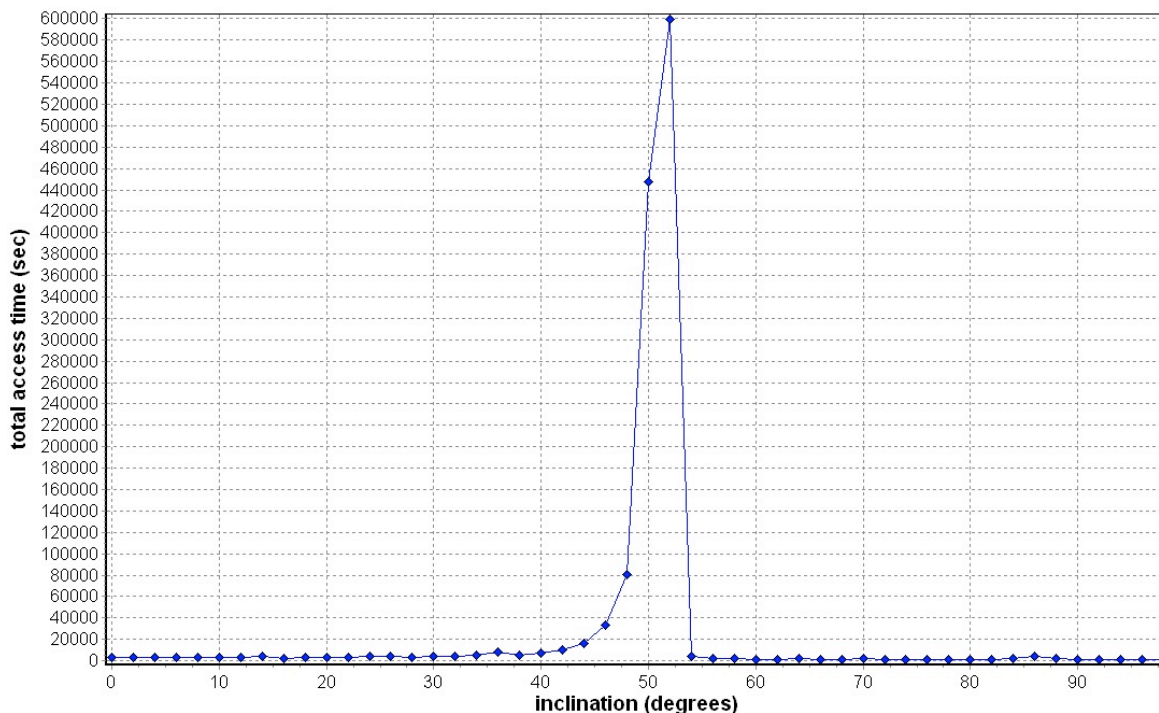


Figure 3.22: Total Access Time as a Function of Inclination

Finally, in Figures 3.24 - 3.29, argument of perigee, right ascension of ascending node, and mean anomaly are all evaluated. Similar to semi-major axis, eccentricity, and inclination, these figures all present the expected result. At the ISS's value for each respective orbital element, (as shown in Table 3.2) Figures 3.24, 3.26, and 3.28 show a prominent spike in total access time while total access time is relatively low for all other values. Also, in Figures 3.25, 3.27, and 3.29 mean range is approximately zero at and near the ISS's value at epoch time, while indicating a relatively large value at other values.

On face value it appears that many of the graphs have regions where the output is undesirable and there are extensive areas of input values that can be eliminated based on these graphs. However, since there are six input variables involved in this problem and

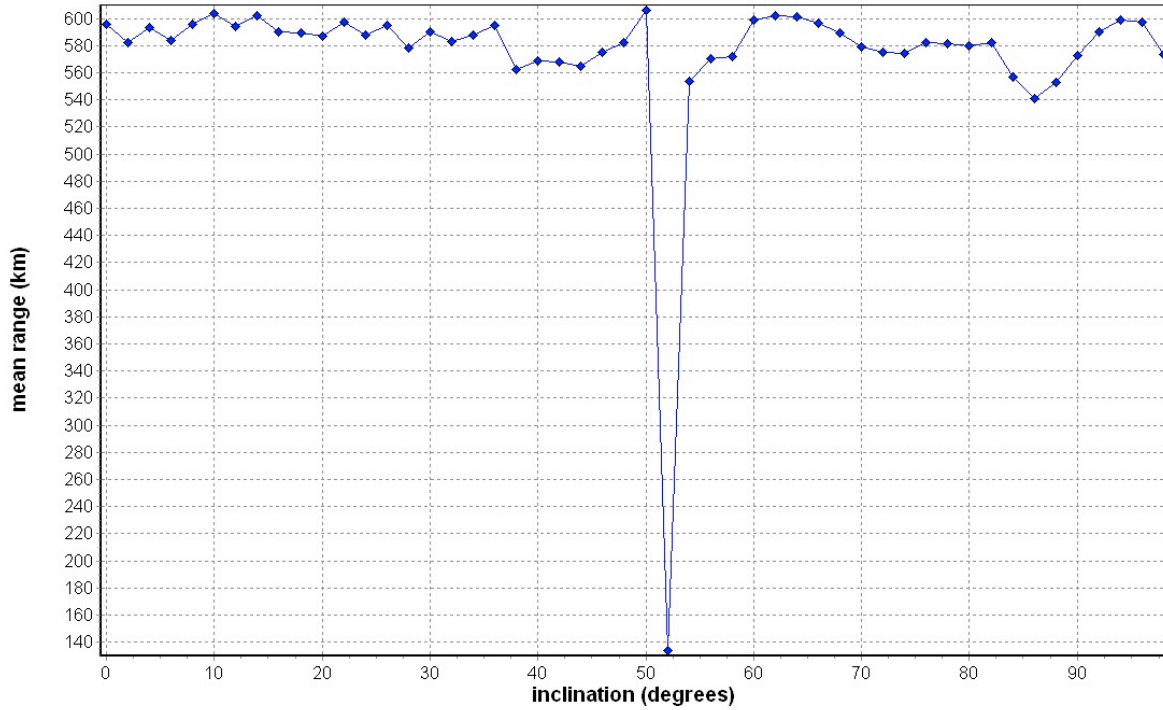


Figure 3.23: Mean Range as a Function of Inclination

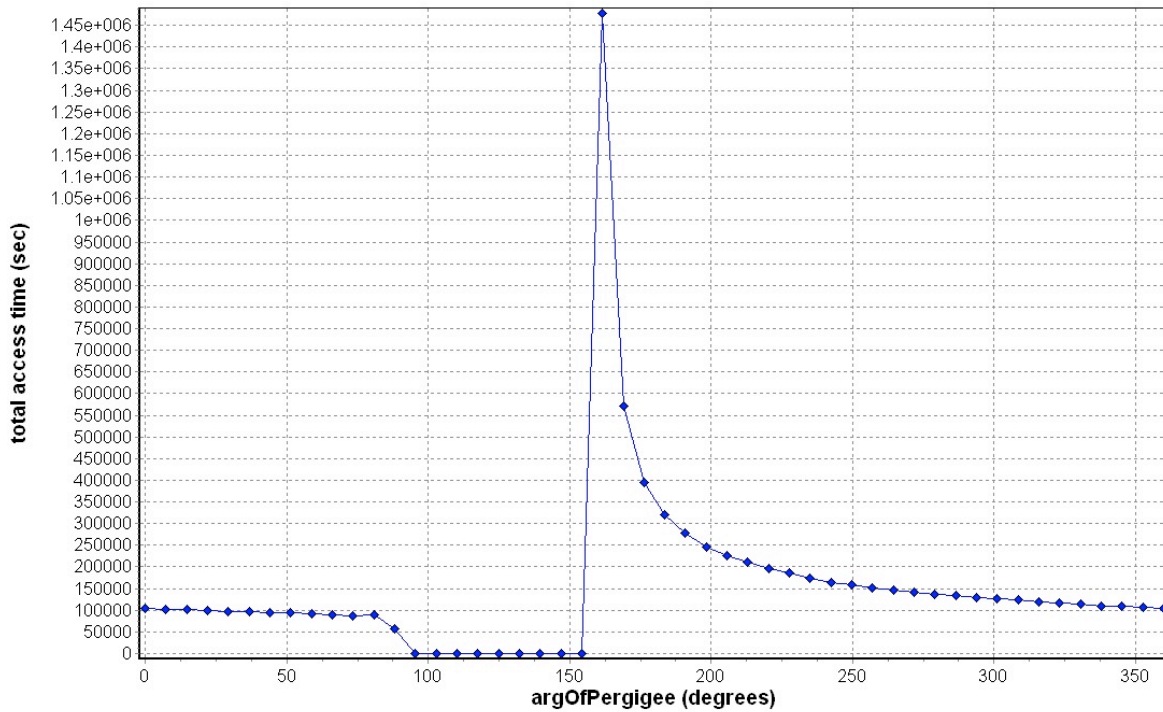


Figure 3.24: Total Access Time as a Function of Argument of Perigee

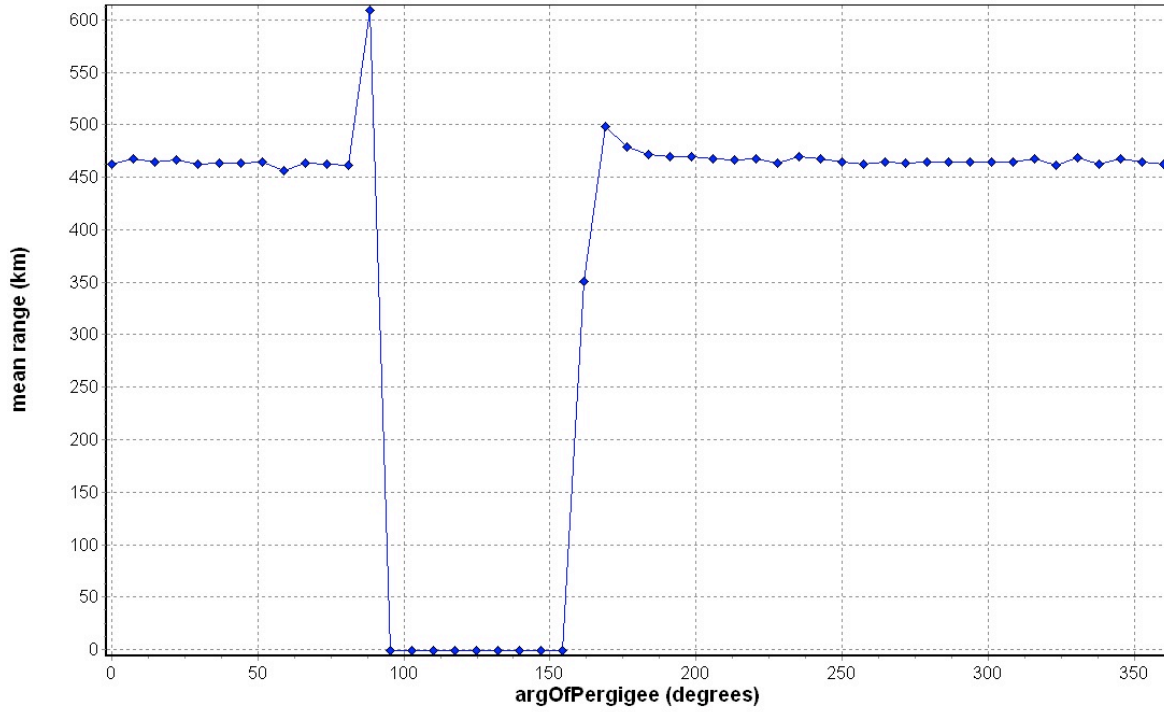


Figure 3.25: Mean Range as a Function of Argument of Perigee

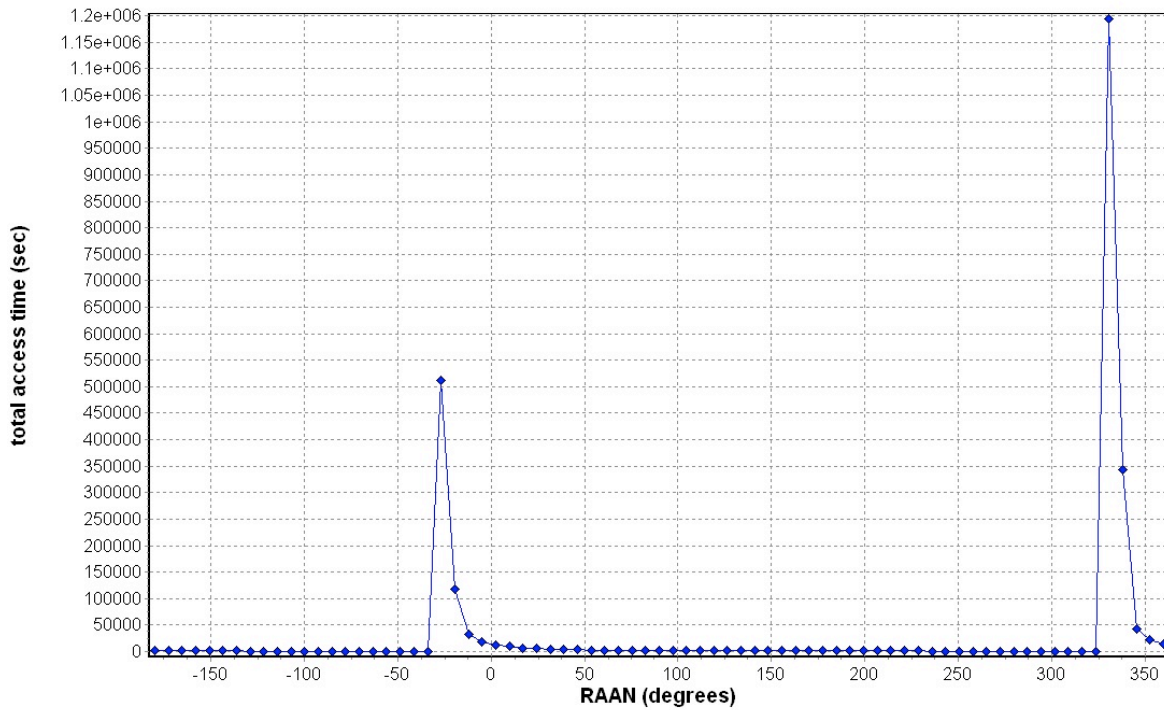


Figure 3.26: Total Access Time as a Function of Right Ascension of Ascending Node

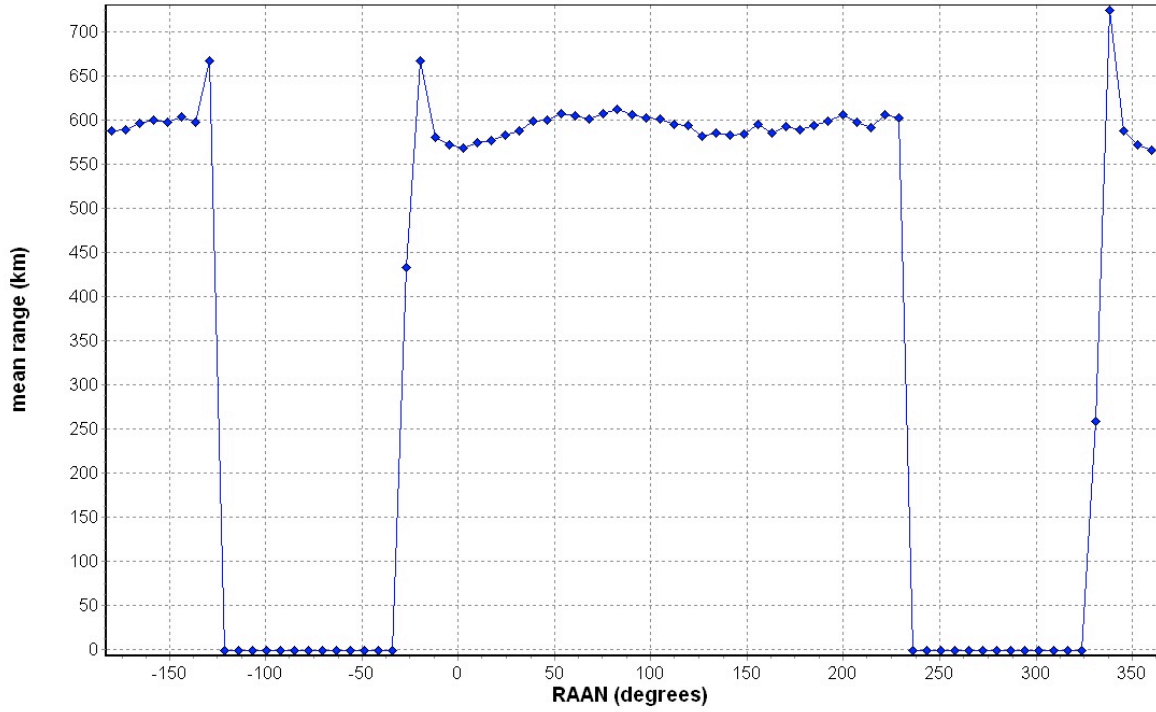


Figure 3.27: Mean Range as a Function of Right Ascension of Ascending Node

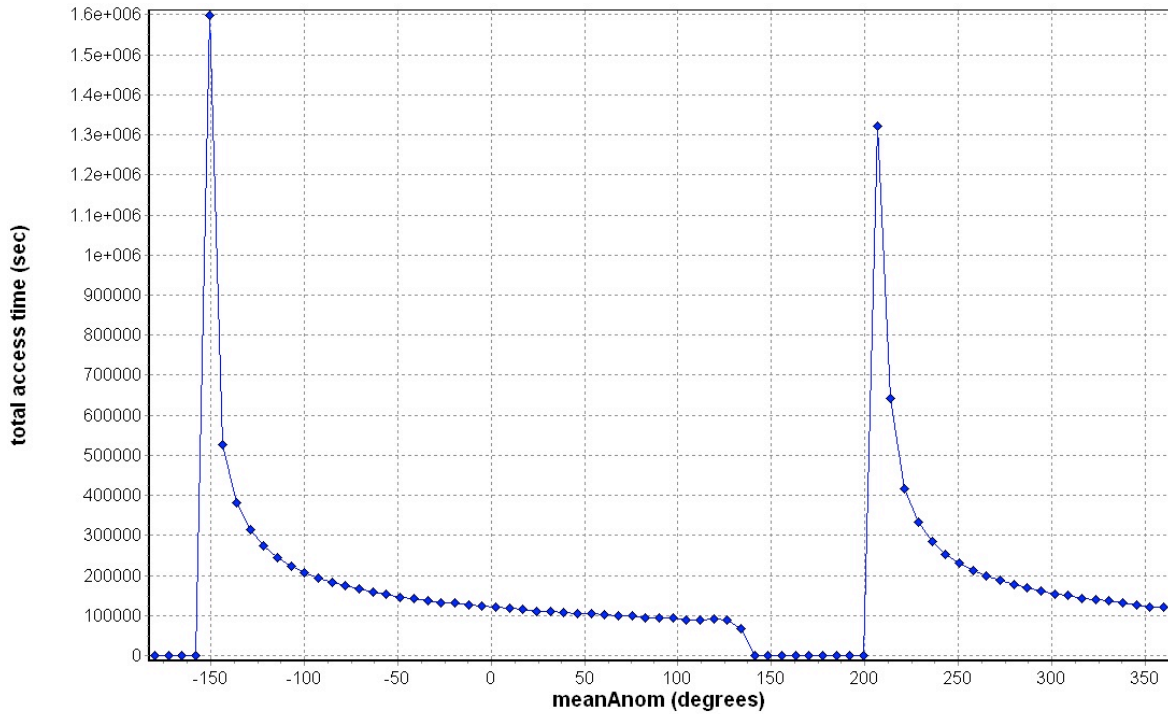


Figure 3.28: Total Access Time as a Function of Mean Anomaly

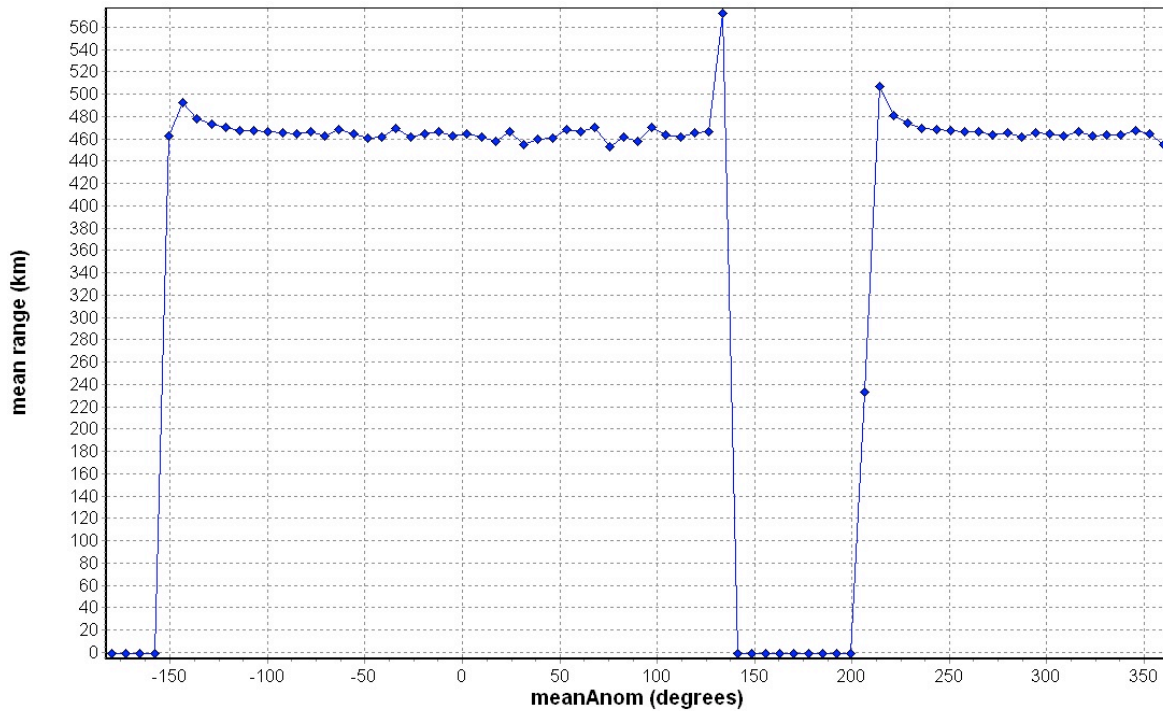


Figure 3.29: Mean Range as a Function of Mean Anomaly

only one orbital element at a time is being varied throughout these parametric studies, none of the data regions will be curtailed at this point. After carefully analyzing the results of the constraint evaluations in Tables 3.5 and 3.6, as well as the behavior of the six orbital elements in Figures 3.18 - 3.29, it can be concluded that the STK and ModelCenter simulation described in this chapter produce consistent and correct results for the purpose of evaluation in Chapter IV.

3.7 Summary

This chapter has shown the detailed development, implementation, verification, and validation of the model to be used in optimization of a satellite's orbit. The simulation used in this research is made up of a detailed STK model containing a component representing the ISS and one representing FalconSAT6. This STK model was inserted into ModelCenter as a single component and the built in tool contained in STK and ModelCenter were used to verify and validate the construction of the model and the results it produces.

IV. Results and Discussion

4.1 Chapter Overview

Following the construction, verification, validation, and initial exploration of the combined STK and ModelCenter simulation using various parametric studies as discussed in Chapter III, the model was fully explored using ModelCenter's built-in suite of data exploration and optimization tools. In this chapter the use of ModelCenter's Design of Experiments tool will be discussed followed by an in depth evaluation of the data using ModelCenter's genetic optimization tool called Darwin. The chapter will conclude with an evaluation of the optimized solution using STK's built in obscuration tool as well as a discussion on potential mission designs using a more powerful laser.

4.2 Design of Experiments

After making an initial exploration into the data using various parametric studies, the data was dissected using the design of experiments tool in ModelCenter. The setup of the parametric study's graphical user interface can be seen in Figure A.1.

Using the same six orbital parameters with the same value ranges as described in Table 3.4 and requesting the same outputs of total access time and mean range, an in depth view of the key drivers was obtained. Along with representing the six inputs and two outputs in one succinct plot, ModelCenters design of experiments tool identified the variables that have the largest impact on the desired solutions as well as the coupling of variables that significantly affect the solution. The variable influence profiles for both total access time and mean range are displayed in Figures 4.1 and 4.2 respectively.

As is evident from Figures 4.1 and 4.2, some variables are more influential on the result than others. Namely, as seen in Figure 4.1, total access time for the simulation is most influenced by eccentricity, followed by semi-major axis, and then the coupling between semi-major axis and eccentricity. Additionally, as seen in Figure 4.2, mean range is influenced mostly by the coupling between semi-major axis and eccentricity followed by semi-major axis. Mean anomaly also influences the solution, but to a lesser degree. Figures 4.1 and 4.2 both give interesting insight into the simulation while confirming that the model was producing realistic results. One would expect that as semi-major

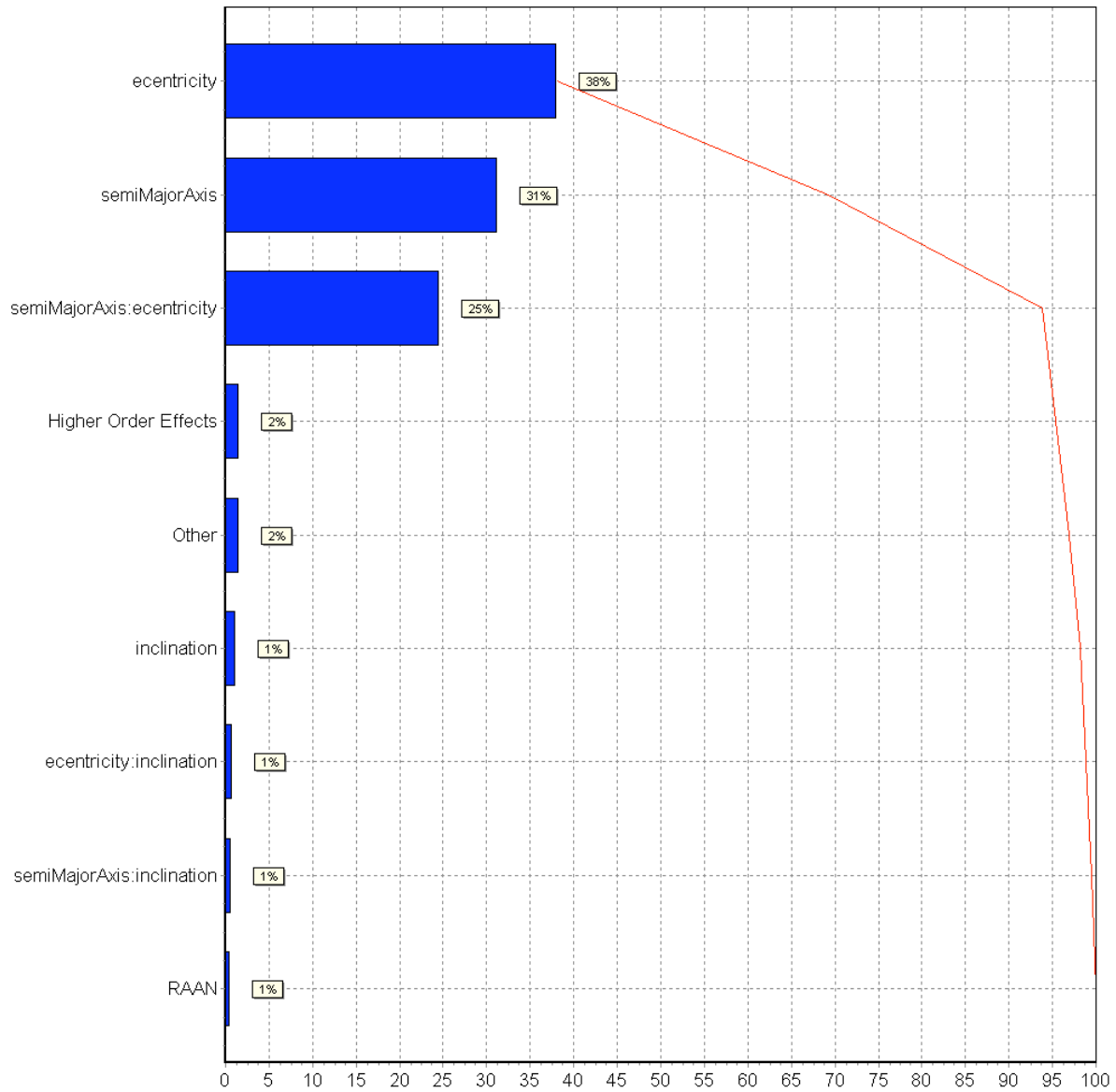


Figure 4.1: Variable Influence Profile with respect to Total Access Time

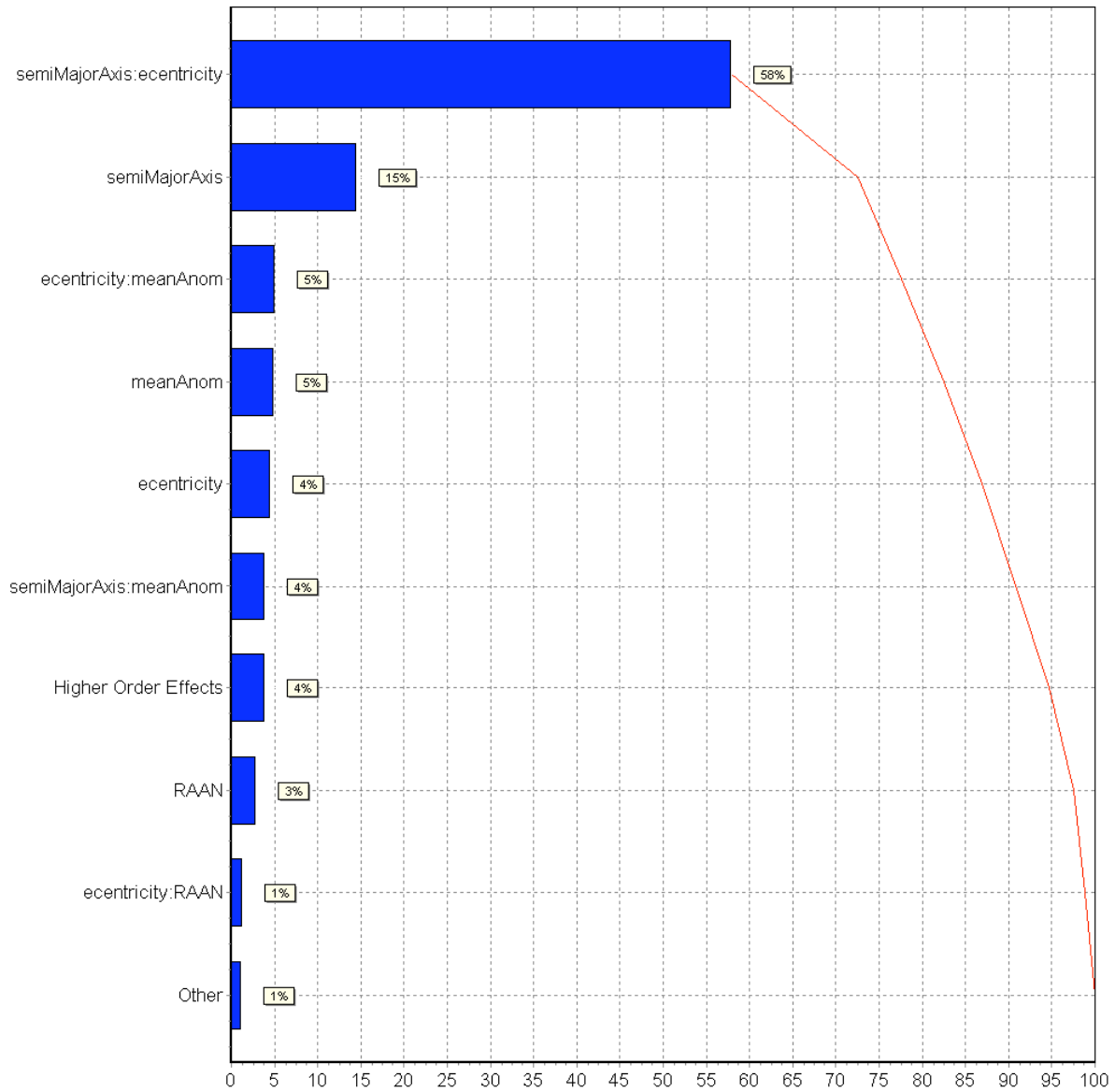


Figure 4.2: Variable Influence Profile with respect to Mean Range

axis and eccentricity increase, the mean range between the satellites would be greatly affected. Also, as those same variables are changed, it is also reasonable that total access time would be greatly effected.

Using the information from the design of experiments, it can be seen that there is a strong influence on both mean range as total access time from the coupling of semi-major axis and eccentricity. To verify and visualize this phenomenon, three-dimensional carpet plots of the space were obtained with mean range and total access time as the outputs. The setup of the carpet plot tool’s graphical user interface can be seen in Figure A.2. The carpet plots were created by varying both semi-major axis and eccentricity over their entire ranges as described in Table 3.4. The variables were each divided into ten equal steps creating a 100 run plot. The carpet plots for mean range and total access time are displayed in Figures 4.3 and 4.4.

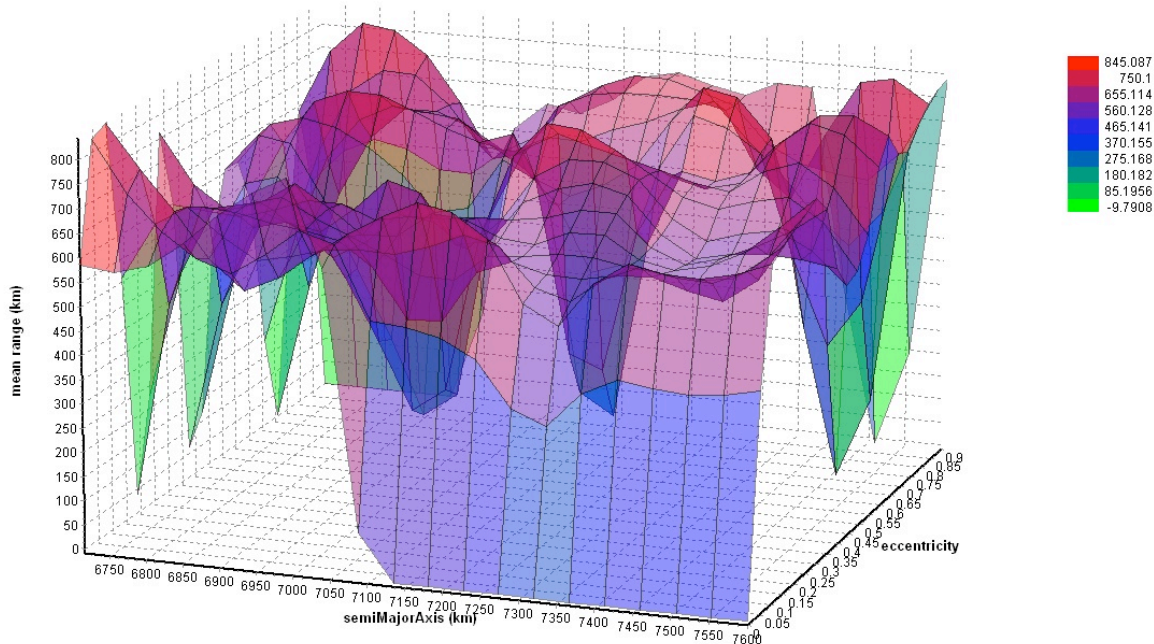


Figure 4.3: 3-Dimensional Carpet Plot of Mean Range as a Function of Semi-Major Axis and Eccentricity

The carpet plots shown in Figures 4.3 and 4.4 clearly display the effect described in the variable influence profiles shown in Figures 4.1 and 4.2. Mean range is highly dependent on the coupled value of semi-major axis and eccentricity; however, total access

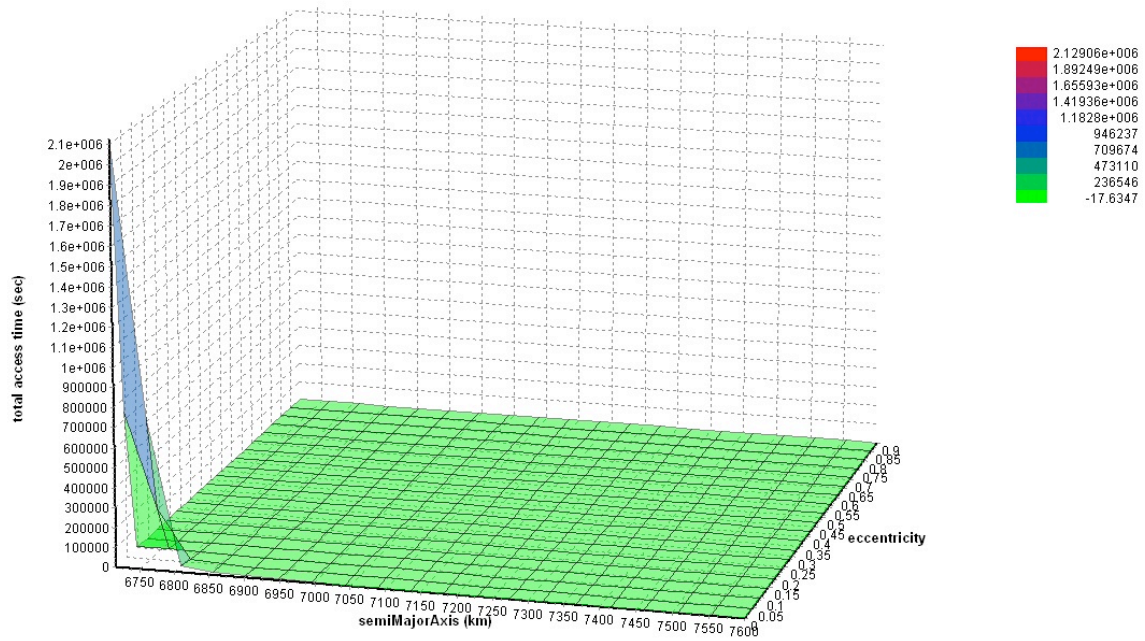


Figure 4.4: 3-Dimensional Carpet Plot of Total Access Time as a Function of Semi-Major Axis and Eccentricity

time is clearly dependent on both semi-major axis and eccentricity, but the coupling of the two orbital elements to a lesser degree.

Although Figure 4.3 is not immediately intuitive, the figure makes sense and helps validate the model when one considers that this plot is only representing the range when there is an access between the ISS and FalconSAT6. If ranges outside of access times were considered, the plot may look very different as a majority of the time the satellites would potentially be thousands of kilometers apart due to the phasing of the orbits. In this case, orbital elements such as mean anomaly, right ascension of ascending node, and argument of perigee could more greatly influence the range between the satellites.

4.3 Genetic Optimization

Using the data from Sections 3.6 and 4.2 one is now informed enough to begin fully exploring the design space with ModelCenter's genetic optimizer tool Darwin. A brief discussion on genetic optimization can be found in Section 3.4.2.1. No region of input values of any of the orbital elements was identified through the parametric studies

or the design of experiments as a candidate to be eliminated from the experiment. The simulation was very similar to the design of experiments discussed in Section 4.2. That is, the six orbital elements were utilized over their ranges as described in Table 3.4 and the desired outputs were still mean range and total access time. Using Darwin however, ModelCenter was asked to drive the system to a desired solution. Also, the model was constrained to maximize the total access time, minimize the mean range between the satellites, and constrain the mean range to the $40km$ to $883km$ window described in Section 3.5.1.2. The setup of the genetic optimizer's graphical user interface can be seen in Figure A.3.

The Darwin genetic optimizer in ModelCenter was allowed to explore the design space defined in Table 3.4 and Figure A.3 for approximately 13 hours, and as shown in Figure 4.5, approximately 7000 different orbits were considered to rigorously explore the available trade space. Each data point in Figure 4.5 represents an individual design point run by the optimization. A design point, in this case, being an orbit defined with all six orbital elements that meets the constraints discussed in Section 3.5.1.2. Although in Figure 4.5 there appears to be a clear trend of the maximum total access times occurring around $600km$, this unsorted, raw data must be further dissected to reveal the true nature of the solution.

To accurately determine which truly optimal solutions exist, Darwin's data visualizer was configured. First, the graphical representation of the objectives as discussed in Section 3.5.1.2 were set. Next, and most importantly, the real world physical mean range constraints also discussed in Section 3.5.1.2 were set. Additionally, as seen in Figure 4.5, it appears that there are a multitude of solutions with relatively large total access times. To further bound the design problem a minimum total access time of $10000sec$ or $166.66min$ was set as an additional constraint. This $10000sec$ constraint was determined by the work in [16] as a value that would allow approximately four hundred firings of a BHT on board FalconSAT6. The combination of these two configuration steps clearly revealed the feasible solutions to the optimization problem and made the examination of the true solutions more clear. As this particular optimization is the chief focus of this research, the $10000sec$ constraint was only applied to this case for the purpose of more

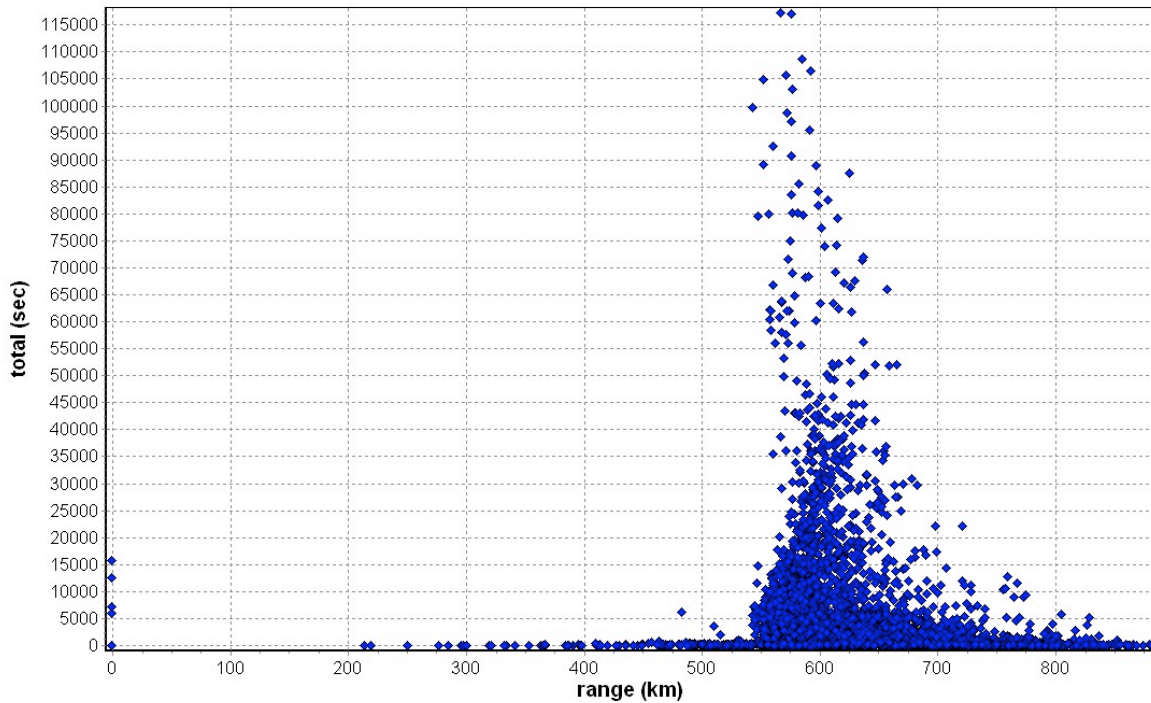


Figure 4.5: 2-Dimensional Plot of Total Access Time vs. Mean Range - All Solutions

accurately dissecting the data. The additional cases described in Section 4.5 were not analyzed in as great of depth and were therefore not constrained to a minimum total access time. The setup of the data visualizer's graphical user interface can be seen in Figure A.4.

In addition to the standard 2-Dimensional and 3-Dimensional plots easily obtainable from nearly all data manipulation software packages, as discussed in Section 3.4.2, ModelCenter has the capability to display up to 7-Dimensional information on one graph. For ease of readability and understanding, this research however, nothing greater than 5-Dimensional graphs will be used. Figures 4.6 - 4.8 are all examples of these multi-dimensional data representations. The significance of each figure will be discussed in turn. Additional multi-dimensional figures are shown in Appendix B.

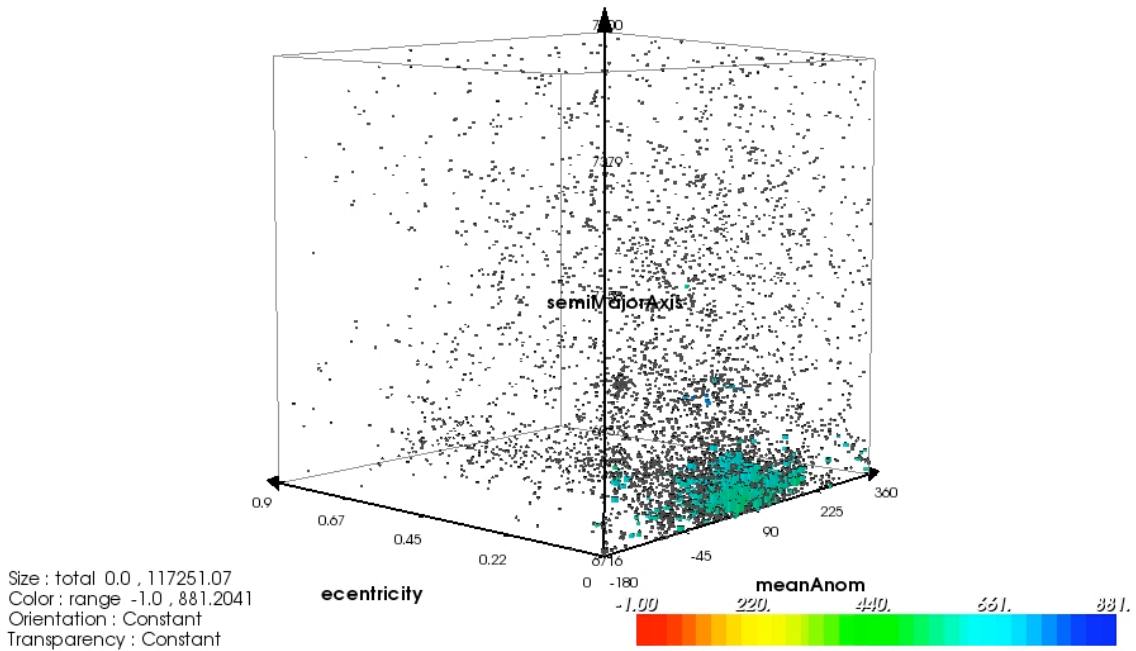
Figure 4.6 provides the initial look at the complex design space of this research. Here, mean anomaly, eccentricity, and semi-major axis are displayed on the X, Y, and Z axes respectively. Additionally, the total access time is represented by the size of the data point, while the mean range is represented by the color. As is apparent in Figure

4.6(a), a majority of the feasible solutions (shown here in various shades of blue and green) are in the expected region. That is, a very low eccentricity and a semi-major axis close to that of the ISS. In terms of semi-major axis and eccentricity, however, the majority of feasible solutions are centered around approximately 60° . This difference in mean anomaly from the ISS's is sensible as this optimized orbit differs from that of the ISS and therefore a difference in satellite phasing (in the form of the mean anomaly) is required to gain the greatest total access time between the satellites.

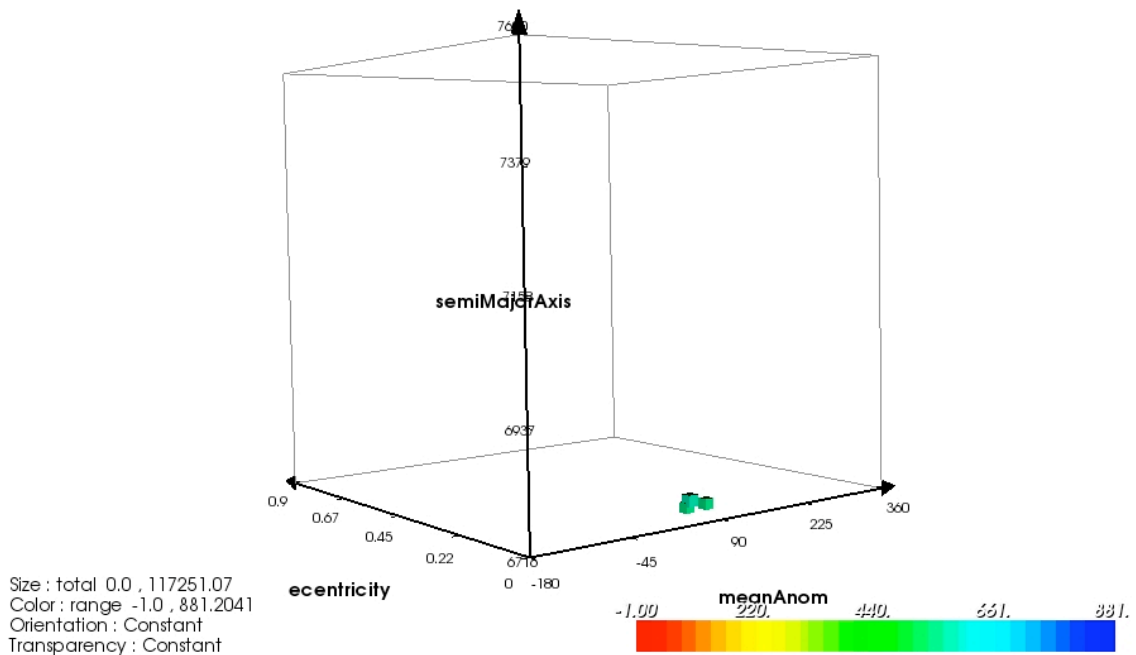
It is obvious from this first look at the data that although figures such as Figure 4.6(a) are useful and will be considered throughout this chapter, a more succinct depiction of the important data is necessary. Figure 4.6(b) provides the Pareto front required to draw meaningful conclusions about the model and extract the optimized solution. As is apparent with both the infeasible and non-Pareto solutions removed, the suspected optimized solution is identified by one of the three data points on the Pareto front. See Section 3.4.2.2 for a more detailed discussion on Pareto fronts

Similar to the discussion for Figure 4.6, Figure 4.7 depicts an interesting result. In Figure 4.7 eccentricity, semi-major axis, and mean range are represented on the X, Y, and Z axes respectively while total access time is represented by both the color and size of the data points. The feasible points are displayed in color, while the infeasible ones are shown in gray. Considering Figure 4.7(a), it can be clearly seen that there is an effective “floor” to the minimum values that the mean range can be while still producing a viable total access time. Additionally, it is clear by the large cluster of feasible solutions near the z-axis that a low semi-major and eccentricity (similar to that of the ISS) will produce the greatest total access time between the satellites. This observation is reinforced by the Pareto front in Figure 4.7(b) where the Pareto solutions are clustered near the z-axis.

It should also be mentioned at this point that although the mean ranges of the Pareto solutions in Figure 4.7(b) are approximately $500km$ (quite far from the minimum constraint of $40km$ as described in Section 3.5.1.2), these are acceptable results. Because the proposed solutions are well within the limit of $883km$, it is sensible that to get more total access time a mean range close to $40km$ would be insufficient due to too great of a “flyby” speed.

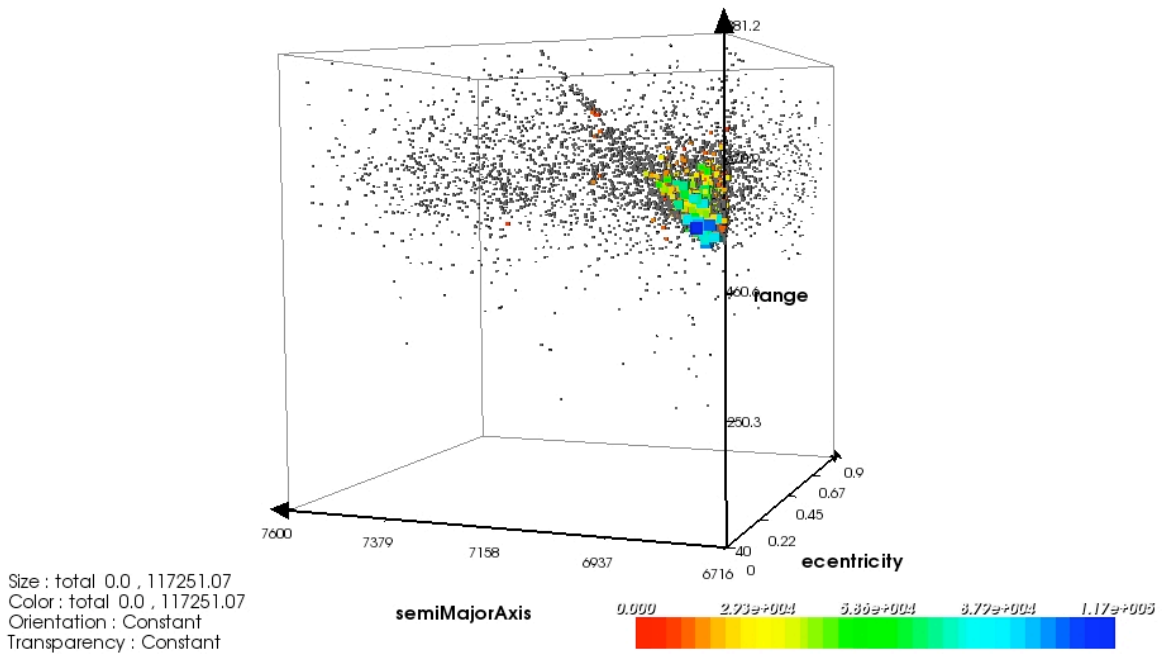


(a) All Solutions (Feasible Solutions Hi-lighted)

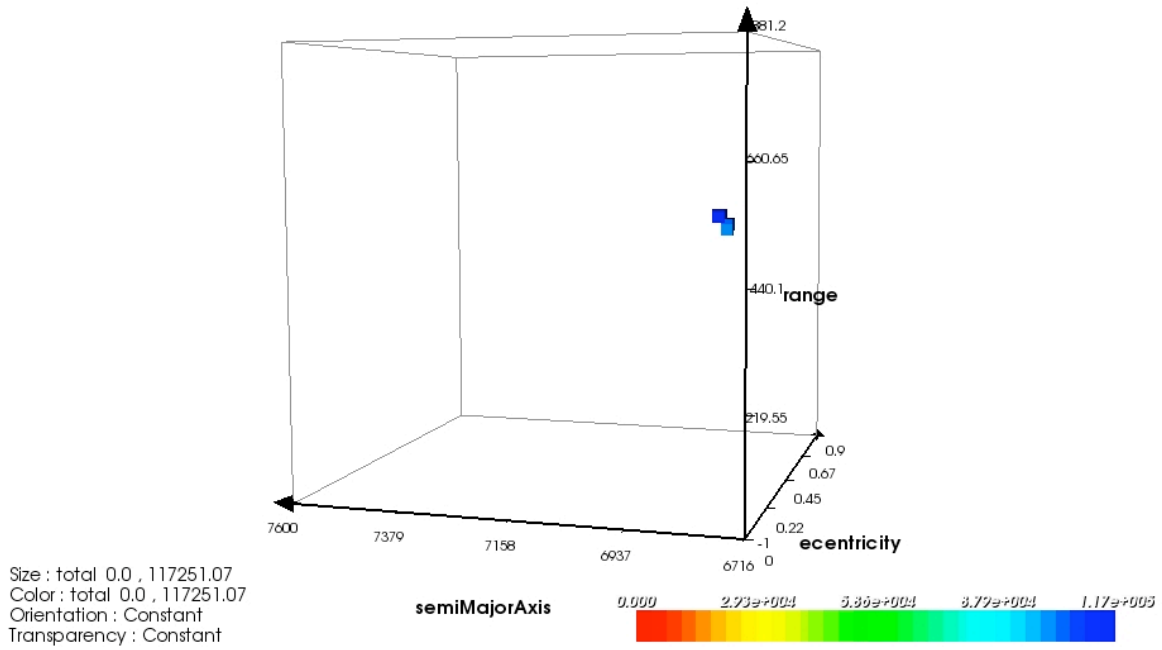


(b) Pareto Solutions

Figure 4.6: 5-Dimensional Plot of Eccentricity, Semi-Major Axis, Mean Anomaly, Mean Range, and Total Access Time



(a) All Solutions (Feasible Solutions Hi-lighted)



(b) Pareto Solutions

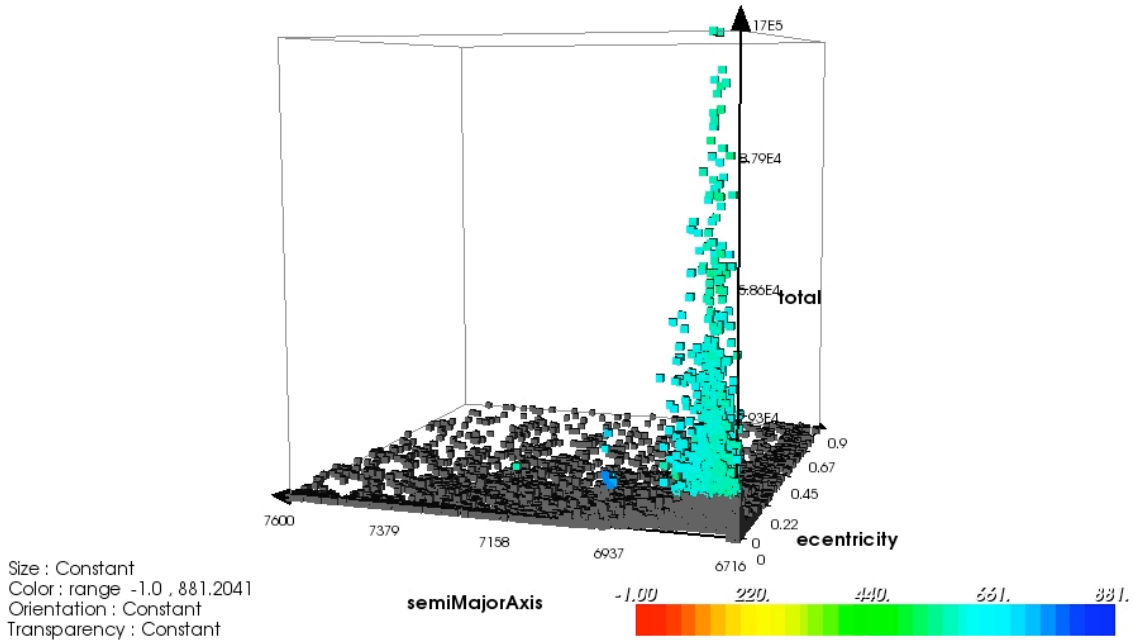
Figure 4.7: 4-Dimensional Plots of Eccentricity, Semi-Major Axis, Mean Range, and Total Access Time

The final multi-dimensional plots to be evaluated are shown in Figure 4.8. Similar to Figures 4.6 and 4.7, Figure 4.8(a) shows a clear trend in a localized region toward a desirable total access time. Figure 4.8 represents eccentricity, semi-major axis, and total access time on the X, Y, and Z axes respectively. Mean range is represented by the color of the data points. Again, the feasible points are displayed in color, while the infeasible ones are shown in gray. Consistent with the results from Figure 4.7(a), the vast majority of feasible data points in Figure 4.8(a) are the same color. This indicates that, consistent with the rest of the results, feasible solutions all lie around the same region of mean ranges (approximately 500km to 600km). Additionally, all of the feasible solutions are clustered around a relatively small semi-major axis and eccentricity (again, similar to the ISS). The Pareto front shown in Figure 4.8(b) clearly indicates the designs of interest, with the likely optimal solution at the top of the z-axis.

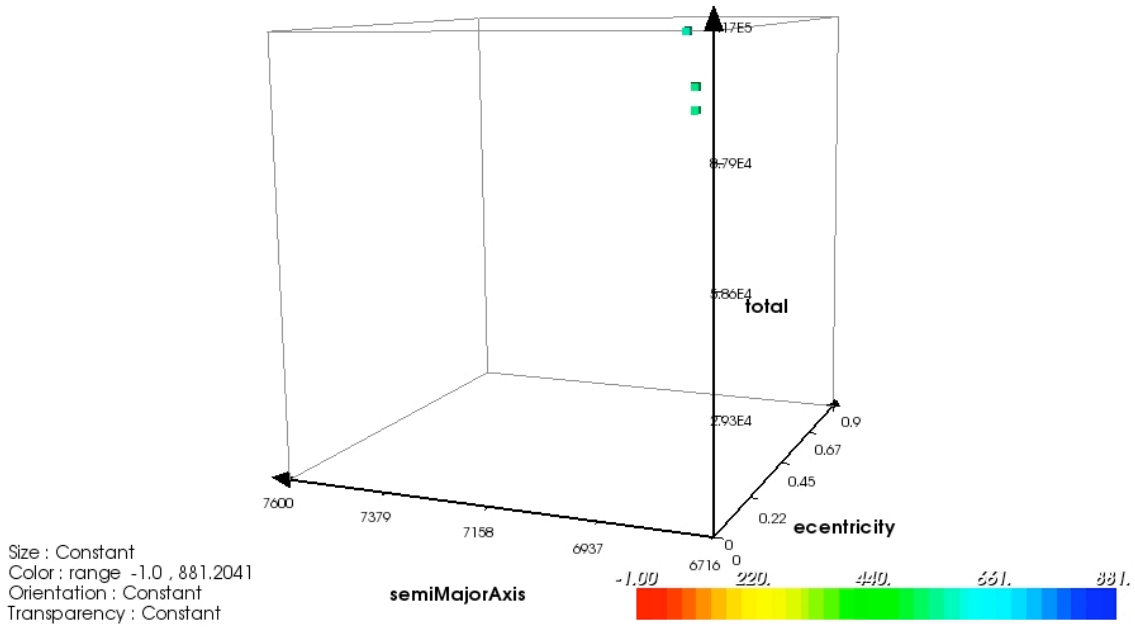
4.3.1 Darwin Results. After carefully analyzing the data and variable relationships presented in Figures 4.5 - 4.8, one may now begin to accurately draw conclusions of what an orbit optimized to wirelessly transfer power from the ISS to FalconSAT6 will look like. Figure 4.9 provides an ideal means of summarizing the data into a concise form for interpretation. Figure 4.9 clearly looks similar to Figure 4.5 except now the data has been annotated based on the insight gained from our multi-dimensional analyses for ease of interpretation and understanding.

Figure 4.9 is a 2-Dimensional plot with mean range and total access time representing the X and Y axes respectively. The design points are color coded in response to the configuration accomplished in Figure A.4(a). That is, the more blue the data point, the closer it is to meeting the main objective of maximizing total access time. Additionally, data points forming the Pareto front are highlighted with black crosses and those design points deemed infeasible from the configuration in Figure A.4(b) are in gray. It can clearly be seen that the bulk of the highly desirable design points are localized around a relatively narrow band of mean range values.

Typically when analyzing a Pareto front, as discussed in Section 3.4.2.2, it would be desirable to select a design point that is the best compromise between two or more



(a) All Solutions (Feasible Solutions Hi-lighted)



(b) Pareto Solutions

Figure 4.8: 4-Dimensional Plots of Eccentricity, Semi-Major Axis, Total Access Time, and Mean Range

competing variables. In this research however, the problem has been constrained so that the maximum total access time at a given range will always be the desirable solution over those with fewer total access times (as no solution is able to be found outside the permissible ranges as discussed in Section 3.5.1.2). In this case, as seen in Figure 4.9, there is only one “peak” in the data around a narrow window of ranges. Therefore, the top value of this peak should be the optimal solution. The maximum value in this simulation, “Design 4083” has been highlighted on Figure 4.9 as the optimal solution and will be discussed.

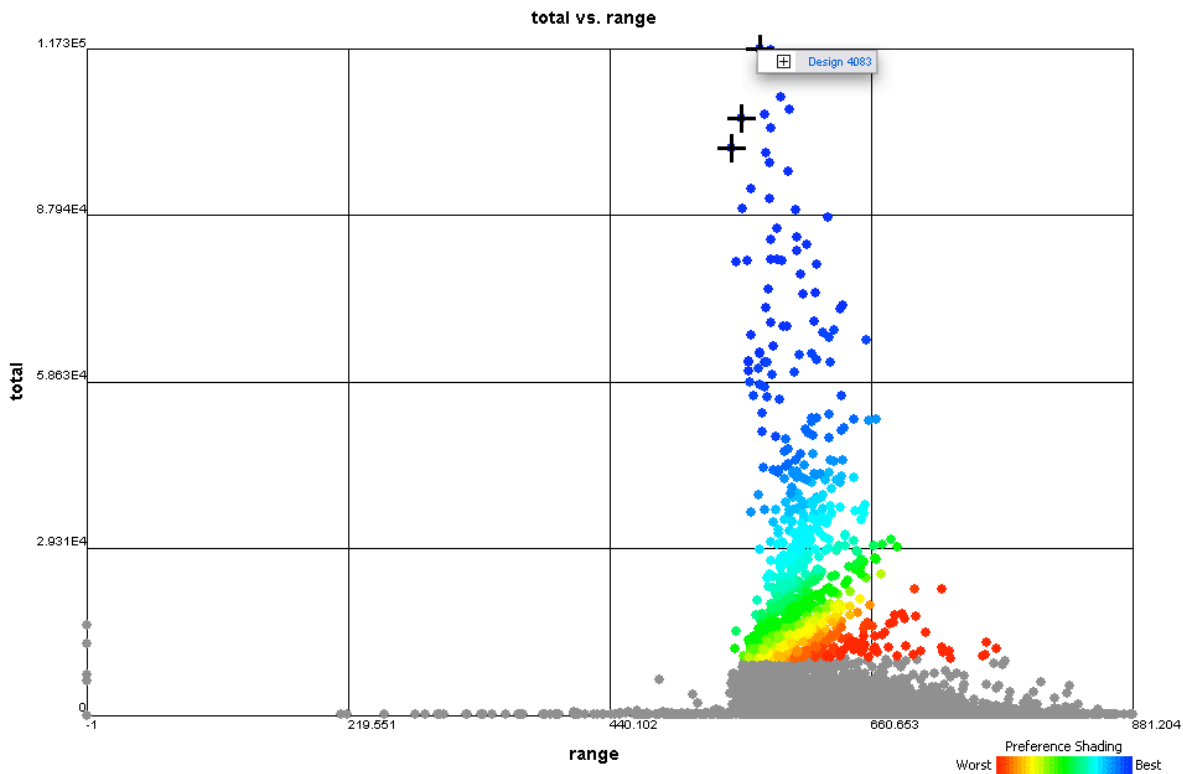


Figure 4.9: 2-Dimensional Plot of Total Access Time vs. Mean Range with Pareto front, Infeasible Solutions, and Optimal Solution (Design 4083) Hi-lighted

The details of design 4083 (along with seven other excellent design candidates) can be seen in ModelCenter’s data explorer interface in Figure 4.10. As is apparent in Figure 4.10, although the other candidate designs are also desirable, they have very similar orbital elements to that of design 4083. Therefore, both as the chief design and as a representative to the other candidate designs, only design 4083 will be discussed here.

An isolated view of design 4083's orbital elements as well as evidence of its satisfaction of the design requirements can be seen in Figure 4.11.

	4083	3215	3363	4036	6209	4682	5798	3929
design_variable [Model.STK.Scenario.FalconSat6.Propagator.semiMajorAxis]	6763.8	6754.3	6750.8	6765.2	6740.8	6750.5	6759.4	6750.2
design_variable [Model.STK.Scenario.FalconSat6.Propagator.eccentricity]	0.0013	0.0104	0.0175	0.0204	0	0.0088	0.018	0.0059
design_variable [Model.STK.Scenario.FalconSat6.Propagator.inclination]	50.81	50.96	51.01	50.63	51.16	50.79	51.05	51.47
design_variable [Model.STK.Scenario.FalconSat6.Propagator.argOfPerigee]	134.7	128.7	132.4	138	120.4	134.2	135.6	124.6
design_variable [Model.STK.Scenario.FalconSat6.Propagator.RAAN]	328.1	330.3	328.1	329.8	328.2	331.4	327.7	325.5
design_variable [Model.STK.Scenario.FalconSat6.Propagator.meanAnom]	41.9	34.6	36.3	48.5	43.3	70.4	47.1	39.5
constraint [Model.STK.Access.AER.MeanRange.range]	566.893	576.018	584.778	592.434	571.186	551.645	576.769	542.772
objective [Model.STK.Access.Access.total]	117251	117016	109662	106429	105589	104897	103121	99609.7
objective [Model.STK.Access.AER.MeanRange.range]	566.893	576.018	584.778	592.434	571.186	551.645	576.769	542.772
Model.STK.Scenario.FalconSat6.Attitude.Basic.Profile.constraintOffset	0	0	0	0	0	0	0	0
Model.STK.Scenario.FalconSat6.Propagator.type	J4Perturbati...	J4Perturbati...	J4Perturbati...	J4Perturbati...	J4Perturbati...	J4Perturbati...	J4Perturbati...	J4Perturbati...
Model.STK.Scenario.FalconSat6.Propagator.startTime	8 Jan 2010 ...	8 Jan 2010 ...	8 Jan 2010 ...	8 Jan 2010 ...	8 Jan 2010 ...	8 Jan 2010 ...	8 Jan 2010 ...	8 Jan 2010 ...
Model.STK.Scenario.FalconSat6.Propagator.stopTime	8 Apr 2010 ...	8 Apr 2010 ...	8 Apr 2010 ...	8 Apr 2010 ...	8 Apr 2010 ...	8 Apr 2010 ...	8 Apr 2010 ...	8 Apr 2010 ...
Model.STK.Scenario.FalconSat6.Propagator.orbitEpoch	8 Jan 2010 ...	8 Jan 2010 ...	8 Jan 2010 ...	8 Jan 2010 ...	8 Jan 2010 ...	8 Jan 2010 ...	8 Jan 2010 ...	8 Jan 2010 ...
Model.STK.Scenario.FalconSat6.Propagator.stepSize	60	60	60	60	60	60	60	60
Model.STK.Scenario.FalconSat6.Propagator.coordEpoch	8 Jan 2010 ...	8 Jan 2010 ...	8 Jan 2010 ...	8 Jan 2010 ...	8 Jan 2010 ...	8 Jan 2010 ...	8 Jan 2010 ...	8 Jan 2010 ...
Model.STK.Scenario.FalconSat6.Propagator.semiMajorAxis	6763.8	6754.3	6750.8	6765.2	6740.8	6750.5	6759.4	6750.2
Model.STK.Scenario.FalconSat6.Propagator.eccentricity	0.0013	0.0104	0.0175	0.0204	0	0.0088	0.018	0.0059
Model.STK.Scenario.FalconSat6.Propagator.inclination	50.81	50.96	51.01	50.63	51.16	50.79	51.05	51.47
Model.STK.Scenario.FalconSat6.Propagator.argOfPerigee	134.7	128.7	132.4	138	120.4	134.2	135.6	124.6
Model.STK.Scenario.FalconSat6.Propagator.RAAN	328.1	330.3	328.1	329.8	328.2	331.4	327.7	325.5
Model.STK.Scenario.FalconSat6.Propagator.meanAnom	41.9	34.6	36.3	48.5	43.3	70.4	47.1	39.5
Model.STK.Scenario.FalconSat6.Propagator.centralBody	Earth	Earth	Earth	Earth	Earth	Earth	Earth	Earth
Model.STK.Scenario.FalconSat6.Propagator.coordSystem	TrueOfDate	TrueOfDate	TrueOfDate	TrueOfDate	TrueOfDate	TrueOfDate	TrueOfDate	TrueOfDate
Model.STK.Scenario.FalconSat6.Walker.enable	false	false	false	false	false	false	false	false
Model.STK.Scenario.FalconSat6.Walker.type	Delta	Delta	Delta	Delta	Delta	Delta	Delta	Delta
Model.STK.Scenario.FalconSat6.Walker.numPlanes	2	2	2	2	2	2	2	2
Model.STK.Scenario.FalconSat6.Walker.numSatsPerPlane	2	2	2	2	2	2	2	2
Model.STK.Scenario.FalconSat6.Walker.RAANSpread	360	360	360	360	360	360	360	360
Model.STK.Scenario.FalconSat6.Walker.walkerParam	0	0	0	0	0	0	0	0
Model.STK.Scenario.FalconSat6.Walker.constellation								
Model.STK.Scenario.FalconSat6.Walker.constellationType	Satellite	Satellite	Satellite	Satellite	Satellite	Satellite	Satellite	Satellite
Model.STK.Scenario.FalconSat6.TargetSolarCells.type	Laser Recei...	Laser Recei...	Laser Recei...	Laser Recei...	Laser Recei...	Laser Recei...	Laser Recei...	Laser Recei...
Model.STK.Scenario.ISS_25544.Attitude.Basic.Profile.constraintOffset	0	0	0	0	0	0	0	0
Model.STK.Scenario.ISS_25544.LaserMountPoint.Laser.type	Laser Sourc...	Laser Sourc...	Laser Sourc...	Laser Sourc...	Laser Sourc...	Laser Sourc...	Laser Sourc...	Laser Sourc...
Model.STK.Scenario.ISS_25544.LaserMountPoint.definition.type	Simple Conic	Simple Conic	Simple Conic	Simple Conic	Simple Conic	Simple Conic	Simple Conic	Simple Conic
Model.STK.Scenario.ISS_25544.LaserMountPoint.definition.coneAngle	0.00573	0.00573	0.00573	0.00573	0.00573	0.00573	0.00573	0.00573
Model.STK.Scenario.ISS_25544.LaserMountPoint.pointing.type	Targeted	Targeted	Targeted	Targeted	Targeted	Targeted	Targeted	Targeted
Model.STK.Scenario.ISS_25544.LaserMountPoint.pointing.targetPath	"FalconSat6"	"FalconSat6"	"FalconSat6"	"FalconSat6"	"FalconSat6"	"FalconSat6"	"FalconSat6"	"FalconSat6"
Model.STK.Scenario.ISS_25544.LaserMountPoint.pointing.targetPath[0]	FalconSat6	FalconSat6	FalconSat6	FalconSat6	FalconSat6	FalconSat6	FalconSat6	FalconSat6

Figure 4.10: Darwin Data Explorer Window Showing Optimized Results in Tabular Form

As a verification of the optimization process, design 4083 was taken from Darwin's output and inserted as the orbital elements for FalconSAT6 directly into STK. This step was conducted in a very similar manner to the way the ISS co-location orbit was established as discussed in Section 3.5.1.2 and seen in Figure 3.15. Once design 4083's orbital elements were inserted for those of FalconSAT6's, the orbits of the two satellites were interrelated as seen in Figure 4.12. (Note the similarity between design 4083 and the ISS's orbit, this similarity will be discussed in Chapter V.)

As an additional verification that design 4083 is meeting all of the design specifications and expectations, an analysis into the angular rate and range rate between the two satellites was conducted. Periodically throughout the analysis period as discussed in Section 3.5.1, the angular rate and range rate were sampled. As discussed in Section 3.5.1.2, it is desirable to keep the angular rate between the ISS and FalconSAT6 under $1.333deg/sec$ as shown in Equation 3.7. Figure 4.13(b) is an example of the extremely

Design: 4083

Data Visualizer
Rank: 1 (total 6723 runs, 747 feasible, 0 runs with the same rank) [Set Preferences](#) [More](#) ▼

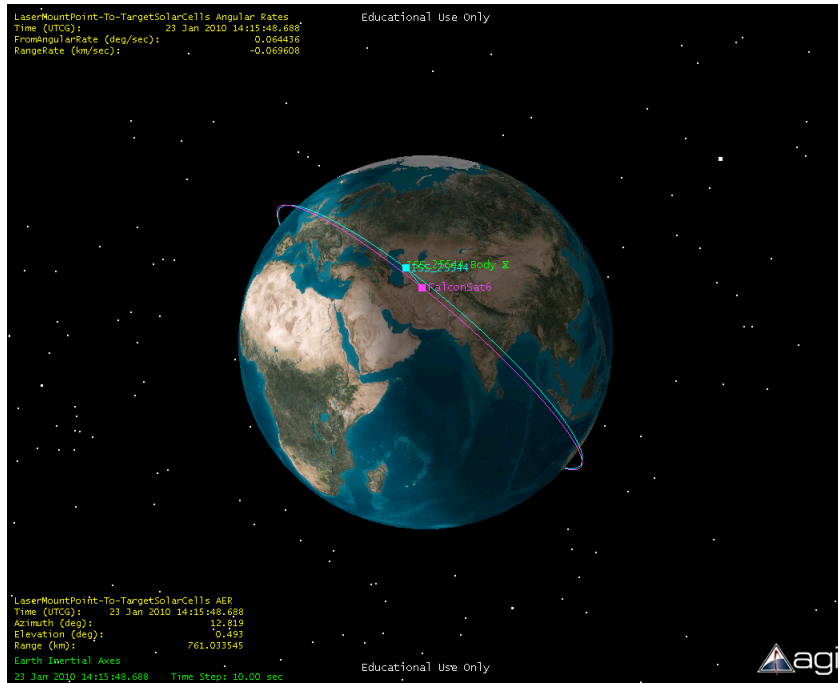
Variables

Name	Value
semiMajorAxis	6763.8
eccentricity	0.0013
inclination	50.81
argOfPerigee	134.7
RAAN	328.1
meanAnom	41.9
range	566.8929
total	117251.07

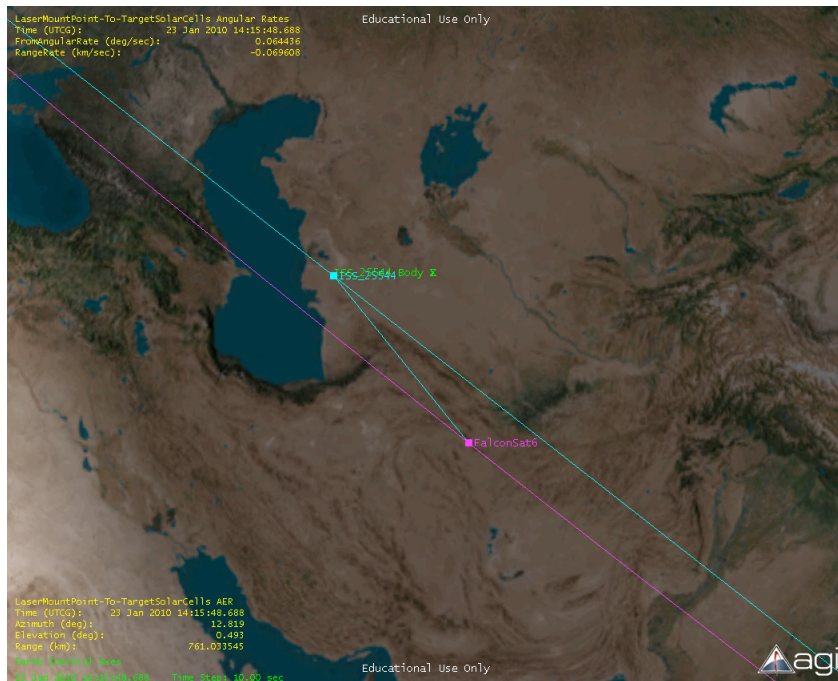
Figure 4.11: Detail View of Optimal Design 4083

low angular rates of $0.064436deg/sec$ and range rates of $-0.069608km/sec$ produced by design 4083.

Finally, STK's Access and AER reporting tools were utilized on the optimized FalconSAT6 orbit. As is evident in Table 4.1, STK verified ModelCenter's total access time from design 4083. The $4.076sec$ difference in computed total access time between the Darwin solution (as presented in Figure 4.11) and the STK solution (presented in Table 4.1) is approximately a .003% error and can be attributed to the round off of the values of the orbital elements that occurred when the ModelCenter solution was imported into STK. The complete access report for the analysis period can be seen in Appendix C. The summary of STK's AER report as shown in Table 4.2 also reinforces the fact that design 4083 is a viable solution. The minimum range of $145.177km$ and the maximum range of $883.000km$ are both within the constraints described in Section 3.5.1.2. Additionally, the azimuth and elevation angles never exceed the $\pm 20^\circ$ constraint



(a) Global View



(b) Close-in View

Figure 4.12: Association of Optimized FalconSAT6 Orbit (in pink) and ISS Orbit (in blue)


```
LaserMountPoint-To-TargetSolarCells AER
Time (UTCG):      23 Jan 2010 14:15:48.688
Azimuth (deg):    12.819
Elevation (deg):  0.493
Range (km):       761.033545
```

(a) Azimuth, Elevation, and Range

```
LaserMountPoint-To-TargetSolarCells Angular Rates
Time (UTCG):      23 Jan 2010 14:15:48.688
FromAngularRate (deg/sec): 0.064436
RangeRate (km/sec): -0.069608
```

(b) Angular Rate and Range Rate

Figure 4.13: Instantaneous Values for: Azimuth, Elevation, Range, Angular Rate, and Range Rate for Figure 4.12

also described in Section 3.5.1.2. A more detailed AER report can be seen in Appendix D.

Table 4.1: Global Statistics for STK Access Report with FalconSAT6 in Optimized Orbit

	Access	Start Time (UTCG)	Stop Time (UTCG)	Duration (sec)
Min Duration	10	4 Feb 2010 14:37:52.562	4 Feb 2010 14:46:14.867	502.305
Max Duration	20	16 Mar 2010 18:50:34.16	16 Mar 2010 21:07:52.963	8238.800
Mean Duration				4885.289
Total Duration				117246.924

Table 4.2: Global Statistics for STK AER Report with FalconSAT6 in Optimized Orbit

	Access Time (UTCG)	Azimuth (deg)	Elevation (deg)	Range (km)
Min Elevation	29 Jan 2010 13:41:31.534	355.65	-0.999	883.000128
Max Elevation	5 Mar 2010 14:41:47.473	12.590	19.999	145.177607
Mean Elevation			3.658	
Min Range	5 Mar 2010 14:41:47.473	12.590	19.999	145.177607
Max Range	22 Feb 2010 01:11:53.575	5.037	-0.272	883.000659
Mean Range				566.871968

4.4 Obscuration Analysis

The final step in producing a valid design and therefore a valid design tool was to insert the best design from Darwin back into STK and run STKs obscuration tool as

seen in Figure A.5 to ensure that there were not any serious losses in access time due to obscuration from the ISS. STK's obscuration tool uses a simplified graphical model of the ISS, as seen in Figure 4.14, to calculate when the laser is being obscured by the ISS during an access time. Obscuration levels should be extremely low due to the chosen mount point on the ISS as well as the constrained $\pm 20^\circ$ cone the laser is allowed to traverse. Based on the results yielding very large total access times from Darwin and the minimum total contact time that is required to fire the BHT onboard FalconSAT6 as determined by the work in [16], a moderate amount of obscuration (if it were a factor) is certainly tolerable for a successful mission..

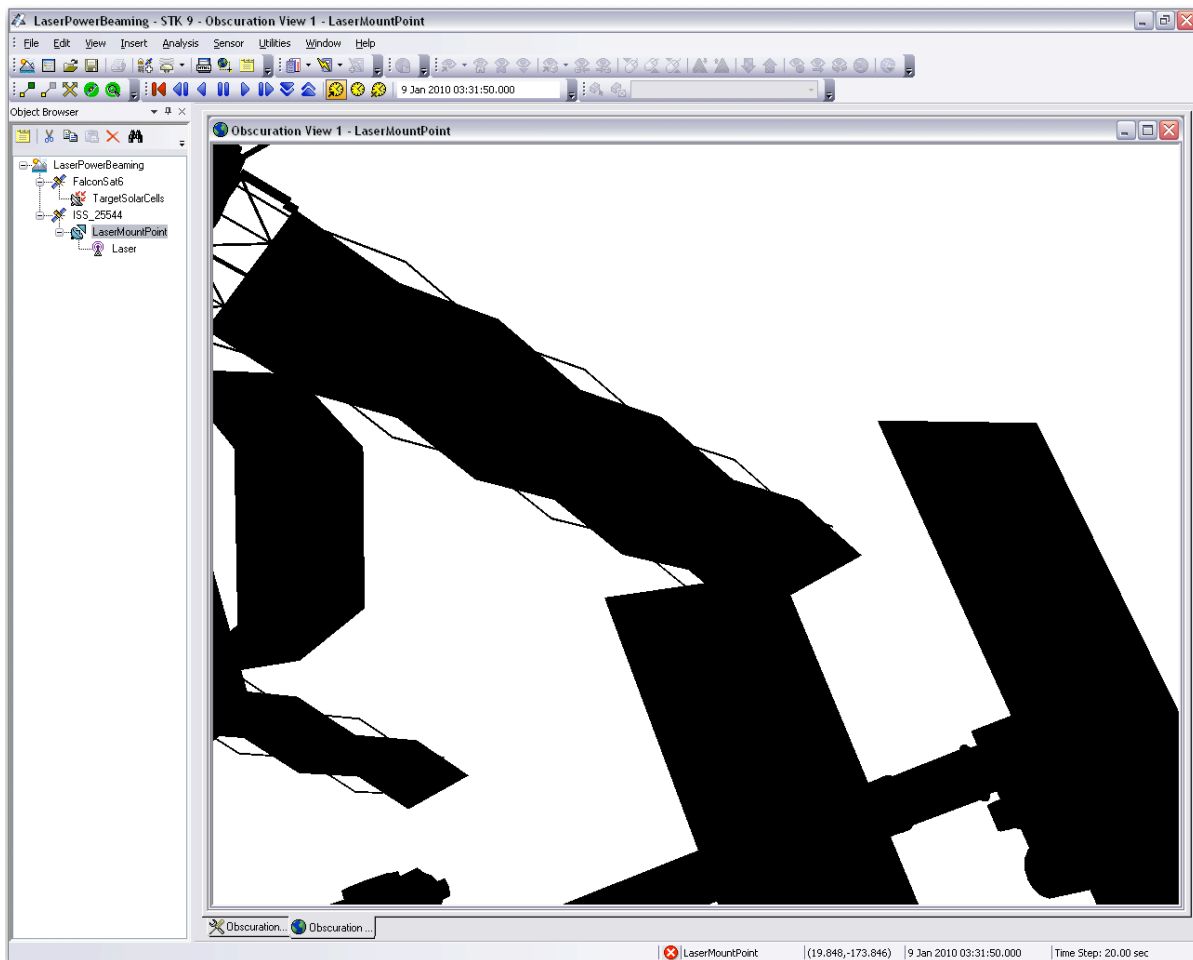


Figure 4.14: STK's Access Obscuration Window

A time step of 60sec was chosen for the obscuration analysis. Although a 60sec time step may seem quite large, the minimum duration for any single contact as seen in Table 4.1 is 502.305sec. This time step yielded eight samples during the shortest access. The

mean access time of 4885.289sec yields an average of 81 samples per access. Additionally, as STK executes the obscuration analysis graphically it takes much longer (in terms of computing time) for a single analysis than a standard assess report and therefore step size becomes a serious consideration. Finally, even at a 60sec time step, over the three month analysis period, the obscuration tool produced approximately 129,600 samples. Table 4.3 shows only three minutes over the entire three month period (and specifically the 117,246sec access time) that the laser was obscured by the ISS. This result translates into .0015% obscuration of the laser by the ISS and is therefore not a factor for completing this mission. Figure 4.15 displays the same information described in Table 4.3 in graphical form. It is apparent from Figure 4.15 that there are only two distinct spikes in the obscuration, both at the times listed in Table 4.3. The setup of the obscuration tool's graphical user interface can be seen in Figure A.5.

Table 4.3: Suspected Obscured Times During Analysis Period

Time (UTCG)	Percent Obscured	Percent Unobscured	Relative Obscured Area	Relative Unobscured Area
10 Feb 2010 12:10:30.000	100	0	1	0
10 Feb 2010 12:11:30.000	100	0	1	0
05 Mar 2010 14:41:30.000	100	0	1	0

As STK does not indicate the source of the obscuration (other than the user defined target of the analysis, in this case the ISS), an investigation into the obscuration report is necessary. To attempt to verify the results of the obscuration report and to gain some understanding of what part of the ISS was obscuring the laser, a view of STK's 3D Graphics Window at the three suspected obscuration times plus/minus approximately one minute was analyzed. At each suspected obscuration time, a view down the bore sight from the laser transmitter toward FalconSAT6 was analyzed. The result from the suspected 10 Feb 2010 12:10:30.000 obscuration time can be seen in Figure 4.16. As is apparent in Figure 4.16, there is nothing obscuring the laser at the suspected time (or within a minute of the suspected time as discussed above). The other two suspected obscuration times yield the exact same result. This could be due to one of two things. First, there is potentially an extremely short obscuration occurring somewhere

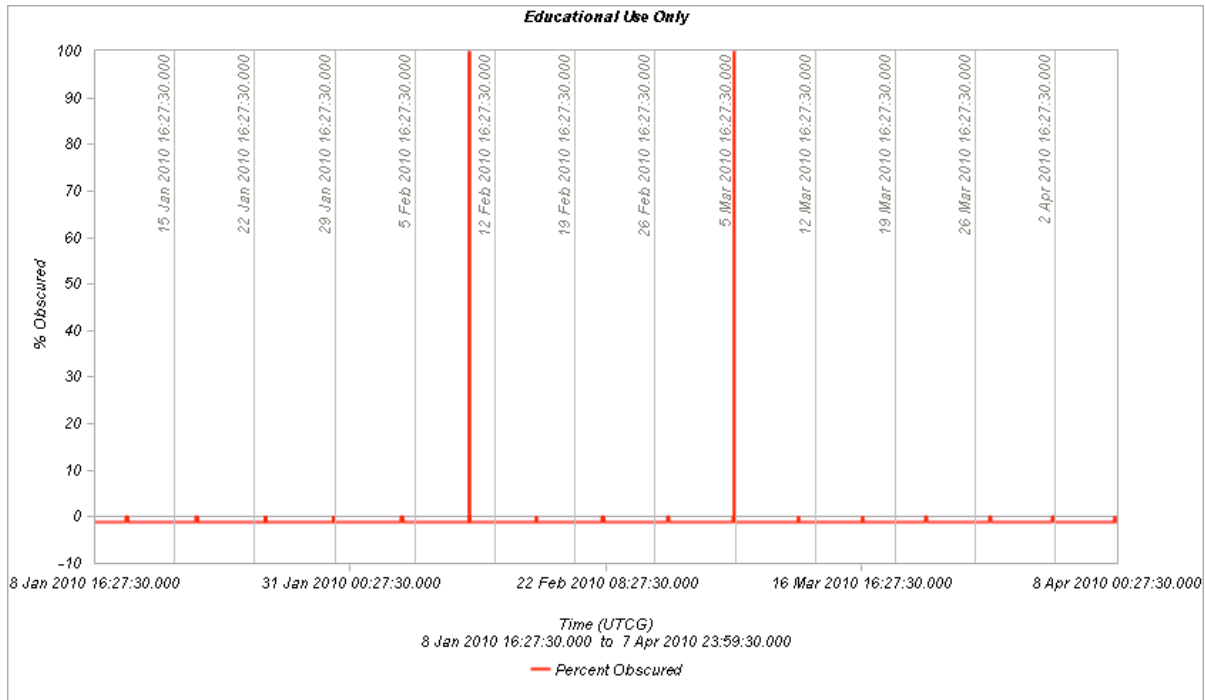


Figure 4.15: Graphical Obscuration Report

in the minute surrounding the suspected obscuration time. This would be indicated in the obscuration report that the laser is being blocked for the entire minute. Also, as the suspected obscuration time was visually analyzed at a 0.50sec time step as seen in Figure 4.16 with no obscuration detected on the 3D display window, it is possible that the $.0015\%$ error (as discussed earlier in this section) is computer error of some form and no obscurations exist for the analysis period. As this is only a feasibility study, this research will only recommend that when the actual mission is planned, careful consideration is given to even the smallest possible obscuration from the ISS. However, here, it is sufficient to say that even given the full 180sec of obscuration over the entire $117,246\text{sec}$ access time, obscuration is not a reason why the proposed mission is not feasible.

4.5 Expanded Constraints

Through this research it had been shown that a wireless power beaming mission between the ISS and a target satellite is feasible, however there are limitations in what is possible. The orbital elements from the optimal design (Design 4083) are very similar to that of the ISS as seen in Table 4.4. However, as discussed in Section 3.6.1, this

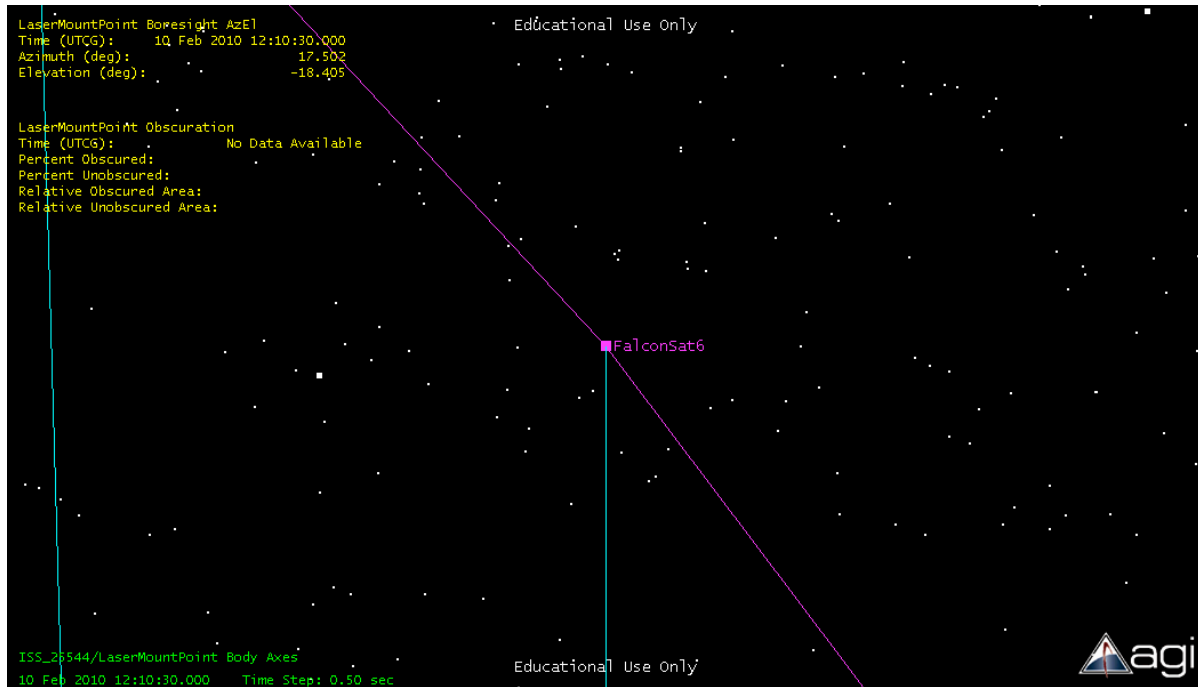


Figure 4.16: Bore Sight View of Laser at the 10 Feb 2010 12:10:30.000 Suspected Obscuration Time

result is expected because the truly optimal mission configuration would be to co-locate FalconSAT6 with the ISS as discussed in Section 3.6.1. With the key physical constraints of a minimum 30sec contact time and a maximum range of 883km as discussed in Section 3.5.1.2 the orbital options are limited to those that are relatively very near that of the ISS. Again, this has been shown to be feasible. However, if greater range or more contact time is desired, the constraints will need to be expanded.

Table 4.4: Differences in FalconSAT6's Optimized Orbital Elements from ISS's Orbital Elements

	ISS Orbital Elements	Optimized FalconSAT6 Orbital Elements	Difference
Semi-major Axis:	6716.398km	6763.8km	47.402km
Eccentricity:	0.0007655	0.0013	0.0005345
Inclination:	51.6475°	50.81°	0.8375°
Argument of Perigee:	160.0825°	134.7°	25.3825°
Right Ascension of Ascending Node:	330.1976°	328.1°	2.0976°
Mean Anomaly at Epoch:	206.4481°	41.9°	164.5481°

4.5.1 *1MW Laser and 15sec Minimum Access Time.* To determine which orbits might be possible with more flexible system constraints, the Darwin optimization as described in Section 4.3 was re-run with a minimum contact time of 15sec and a maximum range of 32,030km (versus the 30sec and 883km constraints described in Section 3.5.1.2). The new 15sec minimum contact time is derived from the assumption that a fast-steering with a faster slew rate than 1.33deg/sec could be obtained. Additionally, the new maximum range of 32030km is derived by [16] from the use of a 1MW laser verses the 3kW laser used in the determination of the original 883km maximum range. The access and AER reports from this second optimization simulation and the optimized orbital elements can be see in Tables 4.5 - 4.7. A detailed discussion on the execution of Darwin can be found in Section 4.3.

Table 4.5: Optimal Orbit with Minimum Access Time of 15sec and Maximum Range of 32030km Using a 1MW Laser

Semi-major Axis:	7458km
Eccentricity:	0.5262
Inclination:	61.36°
Argument of Perigee:	230.2°
Right Ascension of Ascending Node:	-20.3°
Mean Anomaly at Epoch:	269.6°

Table 4.6: Global Statistics for STK Access Report with FalconSat6 in Enhanced Orbit Using a 1MW Laser

	Access	Start Time (UTCG)	Stop Time (UTCG)	Duration (sec)
Min Duration	18	27 Feb 2010 21:49:26.317	27 Feb 2010 21:49:43.424	17.107
Max Duration	6	23 Jan 2010 01:33:40.725	23 Jan 2010 15:40:09.691	50788.967
Mean Duration				30335.850
Total Duration				788732.104

Note, in Table 4.7 the maximum range is less than the 32030km constraint set in the simulation. This would indicate that the 4413.80km maximum range noted in Table 4.7 is the maximum range obtainable with the given geometry of this mission. Additional work using the model in [16] is necessary to determine the amount of input power to the laser associated with this apparent “absolute” maximum range.

Table 4.7: Global Statistics for STK AER Report with FalconSat6 in Enhanced Orbit Using a 1MW Laser

	Access Time (UTCG)	Azimuth (<i>deg</i>)	Elevation (<i>deg</i>)	Range (<i>km</i>)
Min Elevation	29 Jan 2010 01:29:03.994	358.437	-18.542	4408.670578
Max Elevation	27 Feb 2010 21:49:43.424	340.679	20.000	134.065590
Mean Elevation			-7.974	
Min Range	27 Feb 2010 21:49:43.424	340.679	20.000	134.065590
Max Range	27 Mar 2010 10:00:06.559	358.498	-18.409	4413.804282
Mean Range				2331.238209

As is evident from Tables 4.6 - 4.7, as the problem becomes less constrained due to an increase in the capabilities of the hardware being used, more interesting and flexible orbits are possible. Evaluating Table 4.8 demonstrates that the difference in orbital elements allowed by increasing the capabilities of the laser and decreasing the minimum access time. When compared to the difference in orbital elements shown in Table 4.4 one can easily see the gain in available orbits by modifying the constraints. As this is a feasibility study, Table 4.8 excludes argument of perigee, right ascension of ascending node, and mean anomaly as these orbital elements are concerned with phasing and launch times and therefore not as readily comparable.

Table 4.8: Differences in FalconSAT6's Optimized Orbital Elements from ISS's Orbital Elements

	ISS Orbital Elements	FalconSAT6 Orbital Elements (1MW Laser)	Difference
Semi-major Axis:	6716.398 <i>km</i>	7458 <i>km</i>	742 <i>km</i>
Eccentricity:	0.0007655	0.5262	0.5254
Inclination:	51.6475°	61.36 °	9.71°

4.5.2 *6kW Laser and 30sec Minimum Access Time.* After demonstrating the benefit to the mission from using a 1MW laser (which, with current technology is fairly unlikely to be found affixed to the ISS) an evaluation using a more reasonable laser should be conducted. In this case, a 6kW laser will be used as the transmitter. Based on [16], a 6kW laser will yield a maximum effective range of 1170*km* (as compared to the 883*km* from the 3kW laser in the primary mission design described in Section 3.5.1.2). The Darwin optimization as described in Section 4.3 was re-run with a minimum contact

time of 30sec and a maximum range of 1170km. The optimized orbital elements and the summaries of the access and AER reports from this third optimization simulation can be see in Tables 4.9 - 4.11. A detailed discussion on the execution of Darwin can be found in Section 4.3.

Table 4.9: Optimal Orbit with Minimum Access Time of 30sec and Maximum Range of 1170km Using a 6kW Laser

Semi-major Axis:	6770.0km
Eccentricity:	0.0086
Inclination:	50.26°
Argument of Perigee:	155.6°
Right Ascension of Ascending Node:	-30.2°
Mean Anomaly at Epoch:	218.5°

Table 4.10: Global Statistics for STK Access Report with FalconSat6 in Enhanced Orbit Using a 6kW Laser

	Access	Start Time (UTCG)	Stop Time (UTCG)	Duration (sec)
Min Duration	26	7 Mar 2010 14:25:34.753	7 Mar 2010 14:26:25.411	50.658
Max Duration	3	14 Jan 2010 01:47:27.101	14 Jan 2010 04:43:07.931	10540.830
Mean Duration				4242.134
Total Duration				156958.975

Table 4.11: Global Statistics for STK AER Report with FalconSat6 in Enhanced Orbit Using a 6kW Laser

	Access Time (UTCG)	Azimuth (deg)	Elevation (deg)	Range (km)
Min Elevation	4 Feb 2010 11:06:41.296	351.580	-4.942	1130.324898
Max Elevation	24 Jan 2010 23:11:59.887	351.900	20.000	268.230839
Mean Elevation		1.957		
Min Range	19 Jan 2010 14:46:09.530	8.496	-0.503	70.734924
Max Range	12 Mar 2010 13:04:01.156	358.057	0.200	1170.000663
Mean Range				739.268272

Similar to Table 4.8, Table 4.12 excludes argument of perigee, right ascension of ascending node, and mean anomaly as these orbital elements are concerned with phasing and launch times and therefore not as readily comparable. As expected, an increase in the maximum effective range of the laser allowed for a larger semi-major axis. As is

Table 4.12: Differences in FalconSAT6's Optimized Orbital Elements from ISS's Orbital Elements

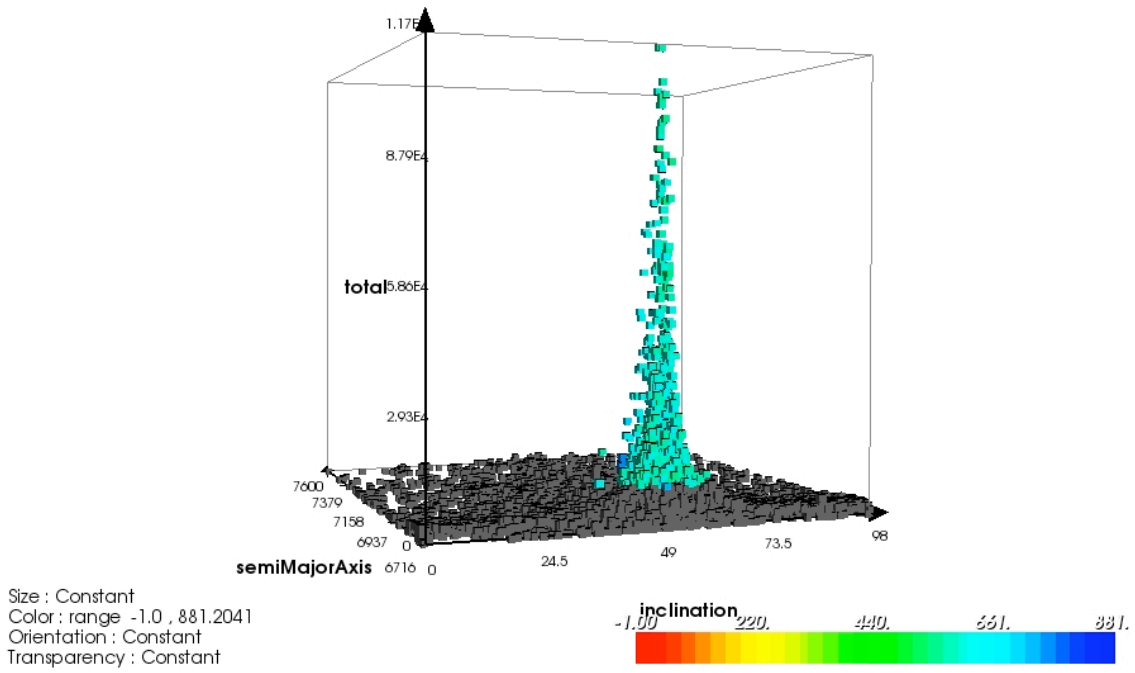
	ISS Orbital Elements	FalconSAT6 Orbital Elements (6kW Laser)	Difference
Semi-major Axis:	6716.398km	6770.0km	53.6km
Eccentricity:	0.0007655	0.0086	0.0078
Inclination:	51.6475°	50.26°	1.39°

evident from the comparison of Tables 4.8 and 4.12, it would potentially take quite a bit more power than is currently available to have a dramatic impact on other key orbital elements, such as inclination.

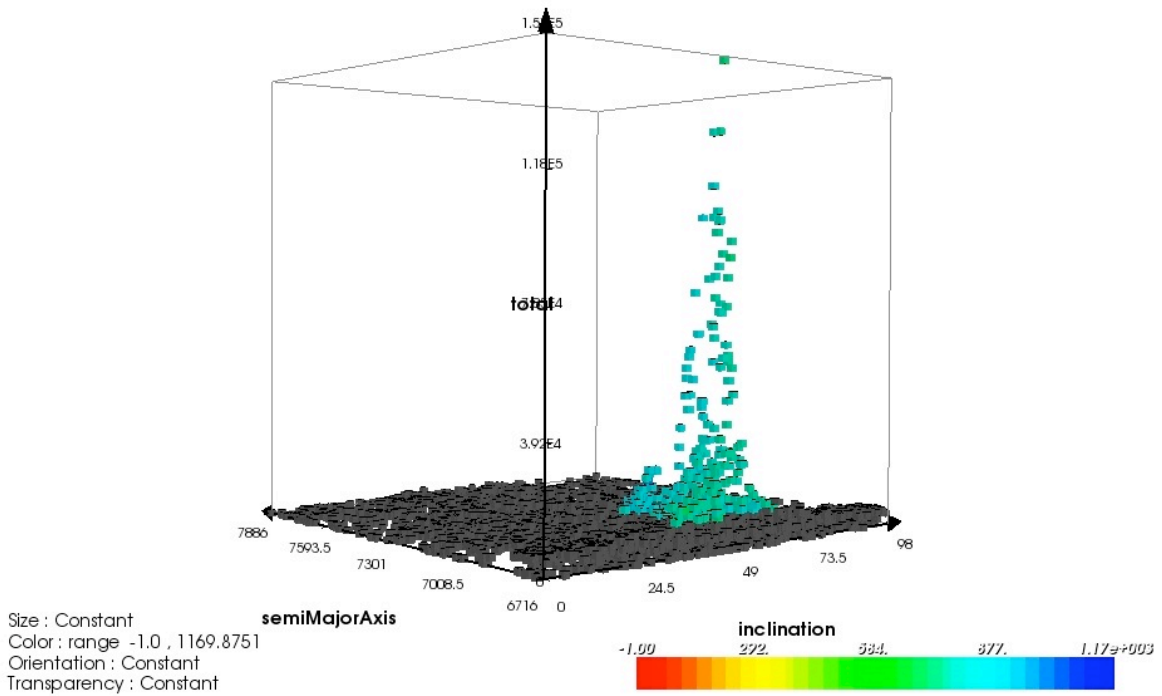
As seen in Figure 4.17, there are definitely more feasible orbits over a wider range of orbits for a 6kW laser as shown in Figure 4.17(b) than for the 3kW laser as shown in Figure 4.17(a). As discussed above, this definitely indicates that more power is required to extend the envelope of feasible orbits.

4.6 Summary

This chapter has shown the use of ModelCenter's Design of Experiments tool and Darwin, as well as STK's Obscuration tool. After evaluating the model with the design of experiments, Darwin, ModelCenter's genetic optimization tool was utilized to find the orbit for FalconSAT6 that would yield the maximum total access time while minimizing the mean range between the satellites. After evaluating the various multi-dimensional outputs from the simulation run in Darwin, the suspected optimal orbit was validated via STK's built-in Access and AER tools. These tools confirmed that the solution was not only feasible, but also met all constraints placed on the problem. A final evaluation of the suspected optimal solution using STK's Obscuration tool revealed no ill effects on the total access time as a result from an obscuration of the laser by the ISS. The chapter concluded with an analysis of what would be possible given more liberal constraints on the orbit.



(a) Feasible Orbits Using a 3kW Laser



(b) Feasible Orbits Using a 6kW Laser

Figure 4.17: Comparison of Feasible Orbits When Using a 3kW Laser and a 6kW Laser

V. Conclusions

5.1 Overview of Research Effort

This research conducted a feasibility study on NASA's proposed mission to wirelessly beam power via laser from the ISS to a target satellite (in this case a derivative of the USAFA's FalconSAT5 satellite). This study centered around the development and validation of an orbital design tool. First, a detailed orbital model of the problem was constructed in STK and then validated through the use of parametric studies and a design of experiment. Using the results from these evaluations, Darwin, ModelCenter's genetic optimizer, was utilized to find the orbit for FalconSAT6 that would yield the maximum total access time while minimizing the mean range between the satellites. After evaluating the various multi-dimensional outputs from the simulation run in Darwin, the suspected optimal orbit was validated via STK's built-in Access and AER tools. These tools confirmed that the solution was not only feasible, but also met all constraints placed on the problem resulting in approximately 4885sec of firing time for the BHT over the three month evaluation period [16]. A final evaluation of the suspected optimal solution using STK's Obscuration tool revealed no ill effects on the total access time as a result of an obscuration of the laser by the ISS. Finally, an investigation was conducted into which orbits would be possible given a more powerful laser and more rapid slew rate on the fast-steering mirror.

5.2 Conclusions

As is evident from this thesis, it is feasible to execute a wireless laser power beaming mission involving the ISS and a target satellite for the purpose of powering a payload. There are however, several limitations which result in a relatively inflexible mission profile. Ideally, one would want the ability to launch into as orbits as possible, however all of the highly feasible orbits very close to the ISS. The optimized orbit easily satisfies the requirement for this proposed mission; however, it would not expand well into other missions where some degree of flexibility is required. The geometry of the mission and the limitations on the strength of the laser are the major contributors to the lack of flexibility. As the laser must be physically attached to the ISS, there will always be a

limited field of view for the laser. The field of view must also be constrained so as to add a factor of safety to prevent striking any of the ISS's solar arrays with the laser. The slew rate on the fast-steering mirror also limits the relative rate at which the objects may pass each other. Additionally, the limitation on available power from the ISS to the laser translates into a relatively limited range that the target satellite must be within in order to transfer the appropriate amount of power to the payload. As demonstrated, any means to reduce the constraints on the problem will most certainly translate into either an increase in total access time (either through an increase in the slew rate of the fast-steering mirror and/or greater mean range through an increase in the output power of the laser). Overall, this work rigorously demonstrated that a feasible wireless laser power transfer mission between the ISS and a target satellite is possible given today's technology.

5.3 Recommendations for Future Work

Future work should focus on extending this feasibility study into a workable mission. This research should take the form of the following topics: First, an analysis into real time mission planning should be conducted. That is, plan a mission far enough in the future with enough lead time to actually execute it using the pre-planned data. This mission plan should incorporate any planned maneuvers of the ISS as well as all ISS ephemeris in STK. Incorporating these additional factors would enable planners to get a true sense of which orbit would truly be optimal. Another component of a real time mission plan would be to determine optimal launch windows and launch sites as these details are obviously critical when choosing various orbital elements. Also, an analysis of the mission profile including a target satellite in an orbit lower (closer to the Earth's surface) than the transmitter should be evaluated. As mentioned in Section 3.6, placing the target closer to the Earth's surface than the transmitter could invoke new challenges not present in a mission when the laser is fired away from the Earth. Careful consideration will need to be given to the potential consequences of striking the Earth's atmosphere or surface with the laser. Additionally, the 40km minimum range constraint would poten-

tially still be present and need to be considered in the geometry and atmospheric drag aspects of the mission.

Other significant research that can be derived from this thesis includes research into what possible orbital configurations are possible when the laser is not constrained to being attached to the ISS. This laser could possibly be its own mission on a different satellite with the ability to point in any direction through the maneuvering of the laser satellite. Also, the orbit of the laser satellite could be optimized along with that of the target satellite to satisfy a new set of constraints. Additional research could also be conducted to use similar genetic optimization techniques in a more computational manner on the Hill's Equations as shown in Section 3.3 to determine an optimal interceptor orbit.

*Appendix A. Selected Screenshots of the STK and ModelCenter
Graphical User Interface*

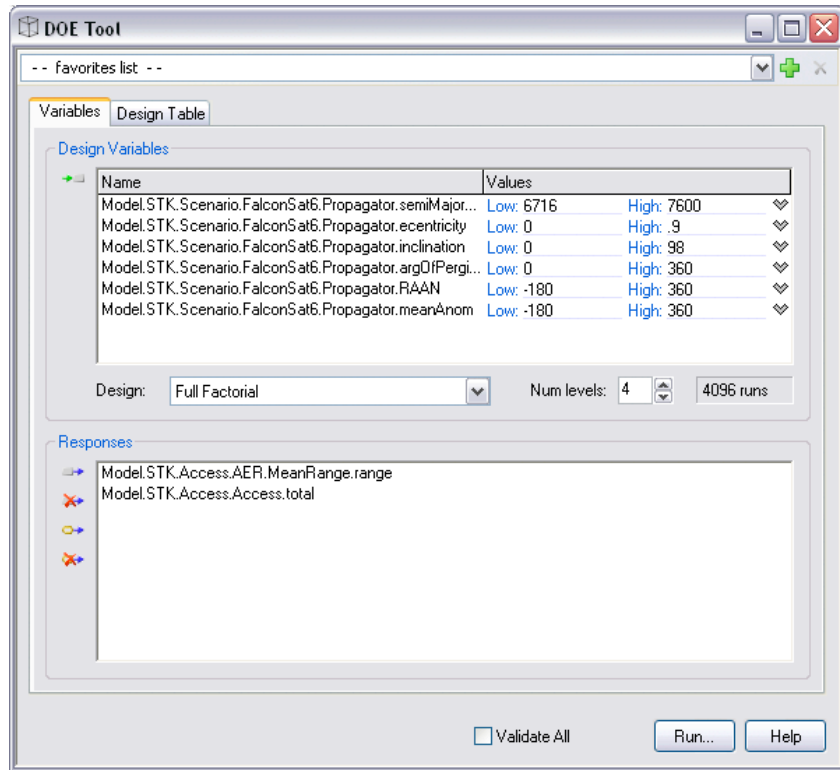


Figure A.1: ModelCenter's Design of Experiments Tool

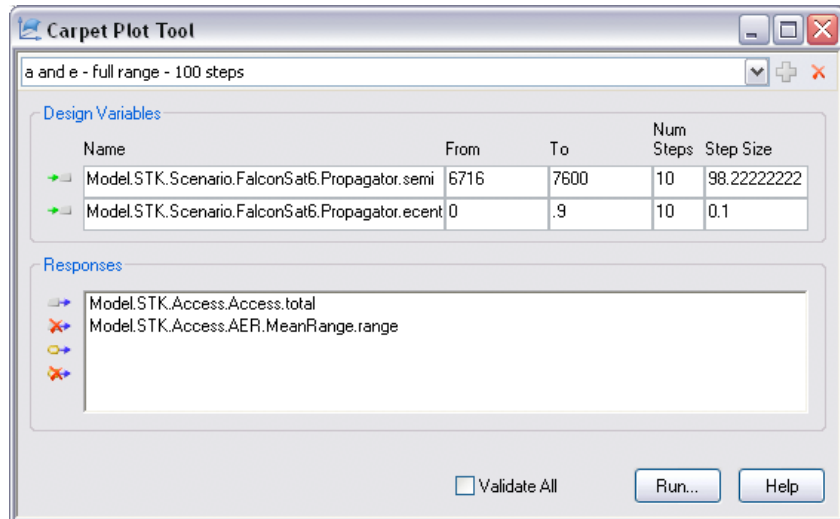


Figure A.2: ModelCenter's Carpet Plot Tool

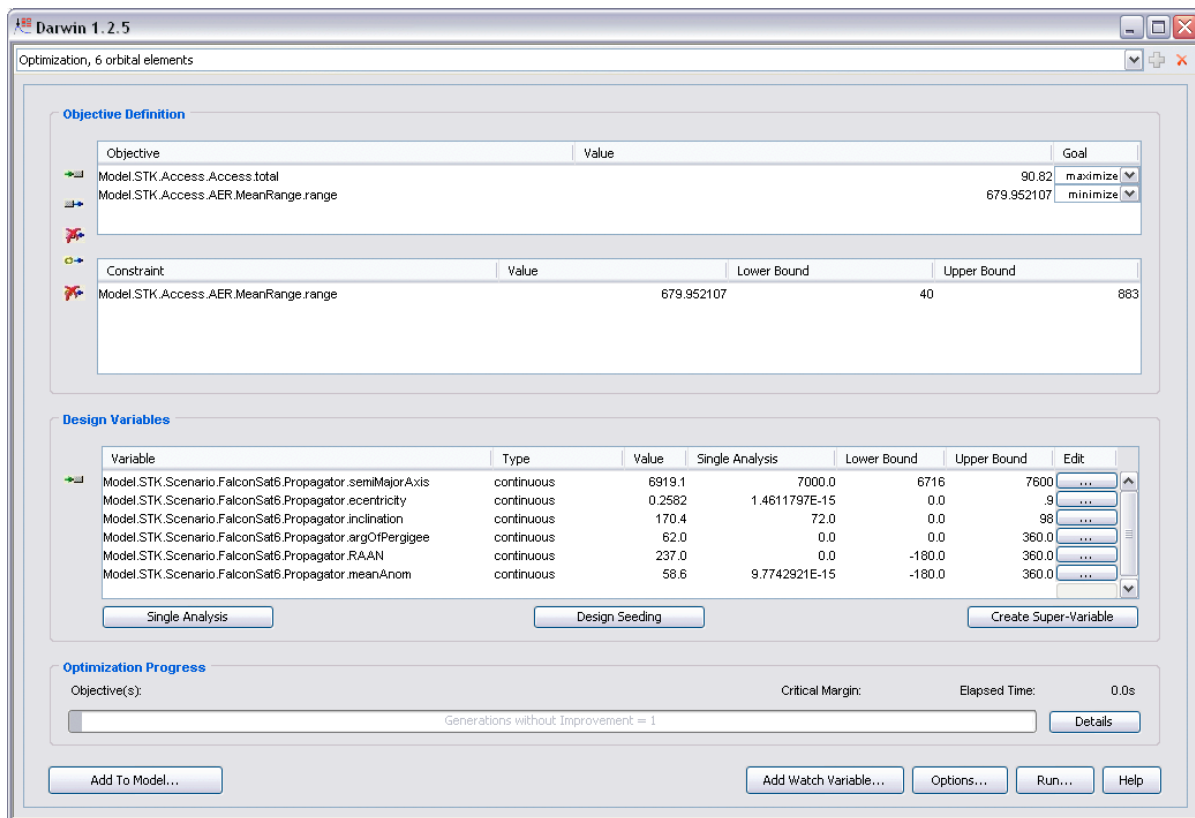
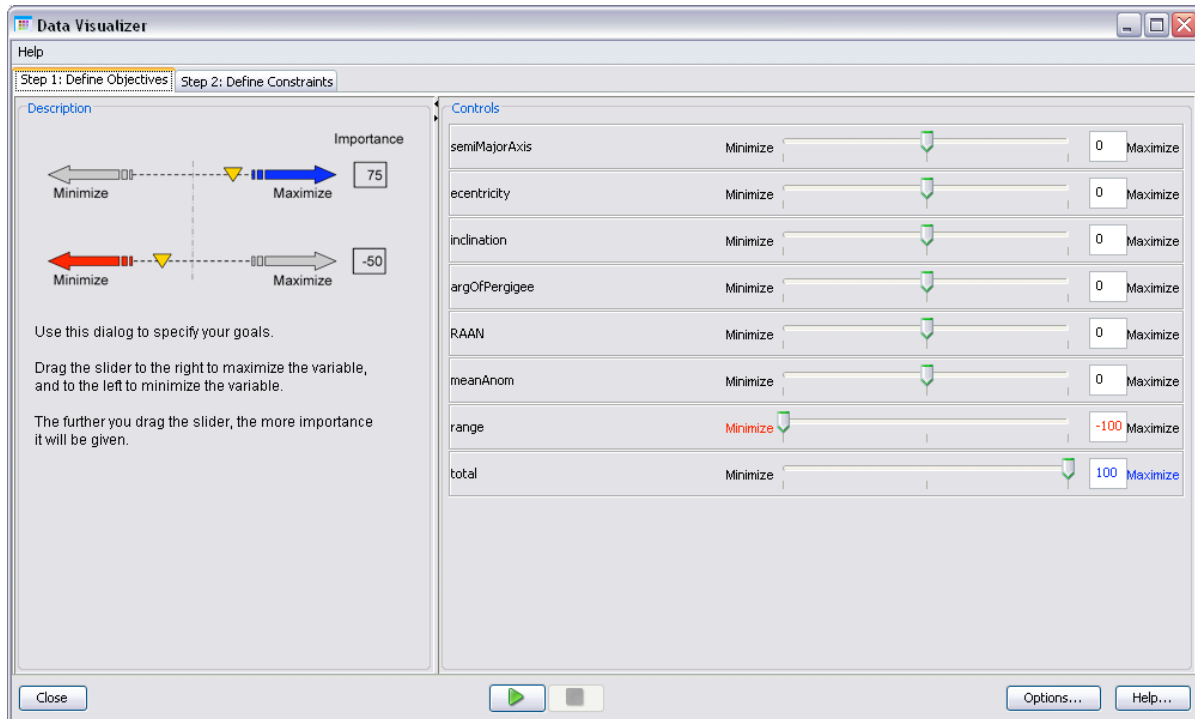
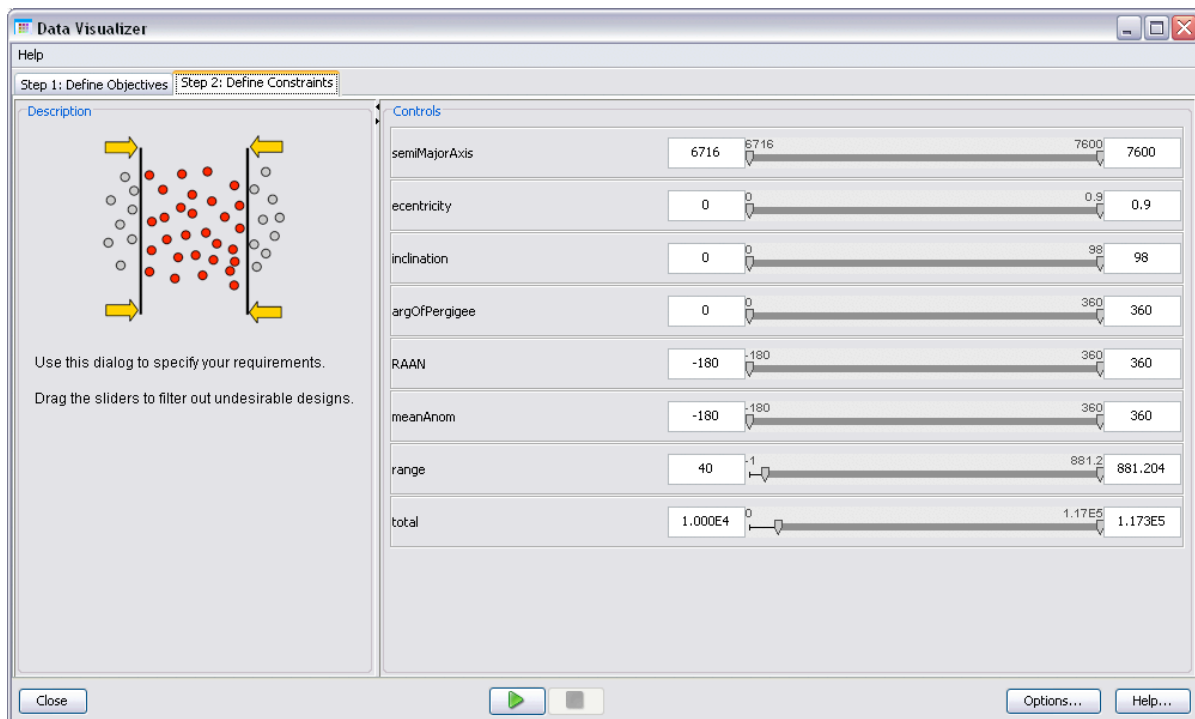


Figure A.3: ModelCenter's Genetic Optimization Tool



(a) Darwin Data Visualizer Objective Window



(b) Darwin Data Visualizer Constraint Window

Figure A.4: Darwin's Data Visualizer Configuration

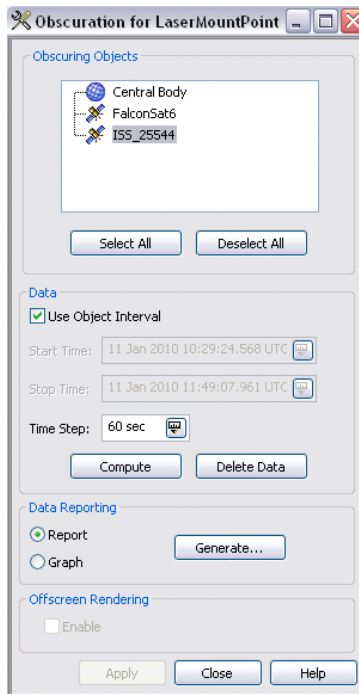


Figure A.5: STK's Access Obscuration Tool

Appendix B. Additional Multi-Dimensional Darwin Plots from ModelCenter

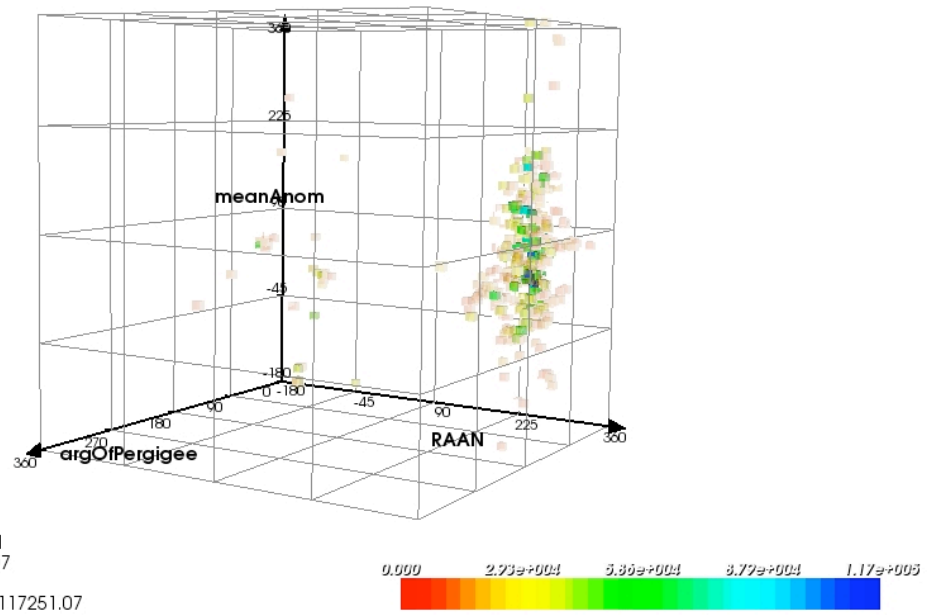
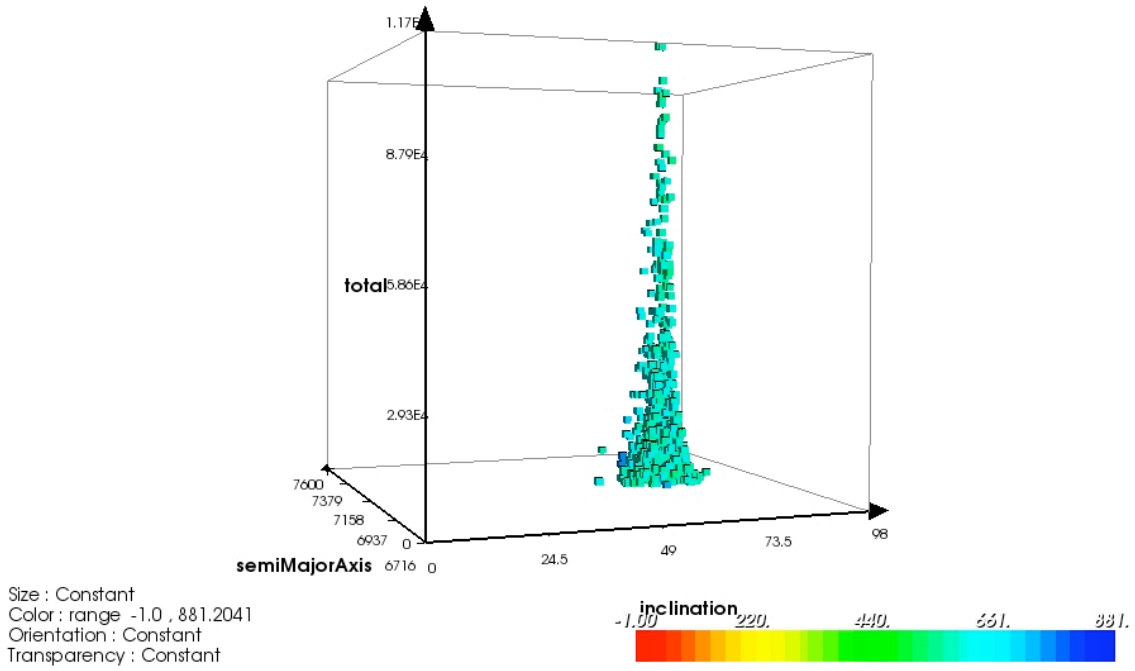
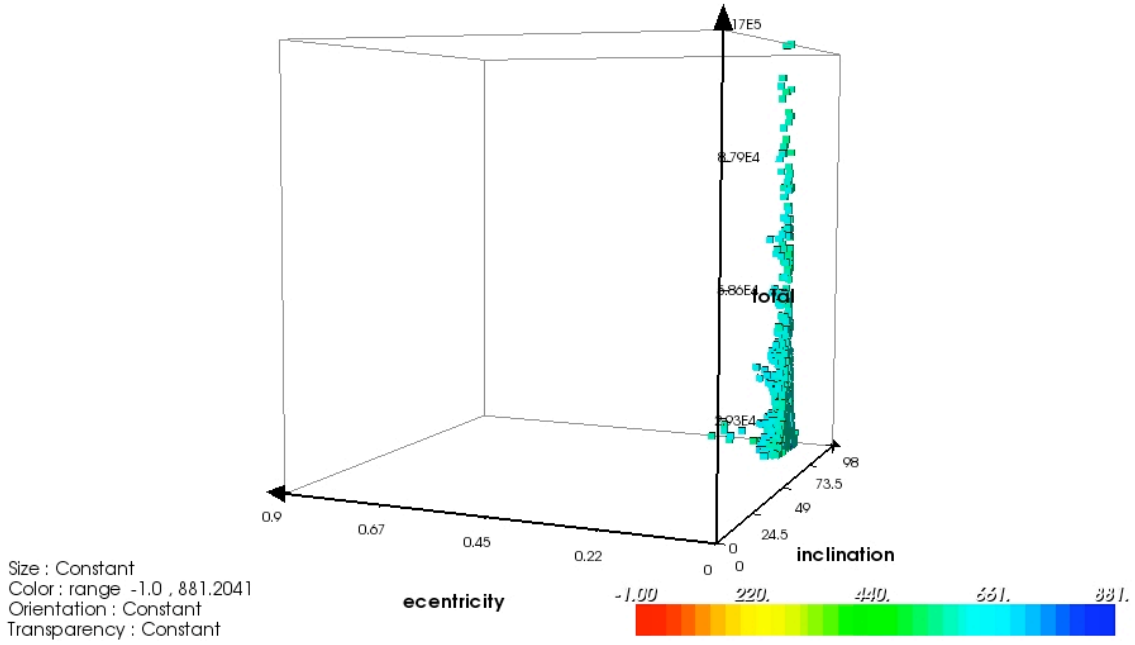


Figure B.1: 5-Dimensional Plot of Right Ascension of Ascending Node, Argument of Perigee, Mean Anomaly, Mean Range, and Total Access Time - Feasible Solutions Hi-lighted



(a) Semi-Major Axis, Inclination, Total Access Time, and Mean Range



(b) Eccentricity, Inclination, Total Access Time, and Mean Range

Figure B.2: 4-Dimensional Plots Showing the Relationship of Total Access Time and Mean Range to Inclination - Feasible Solutions Only

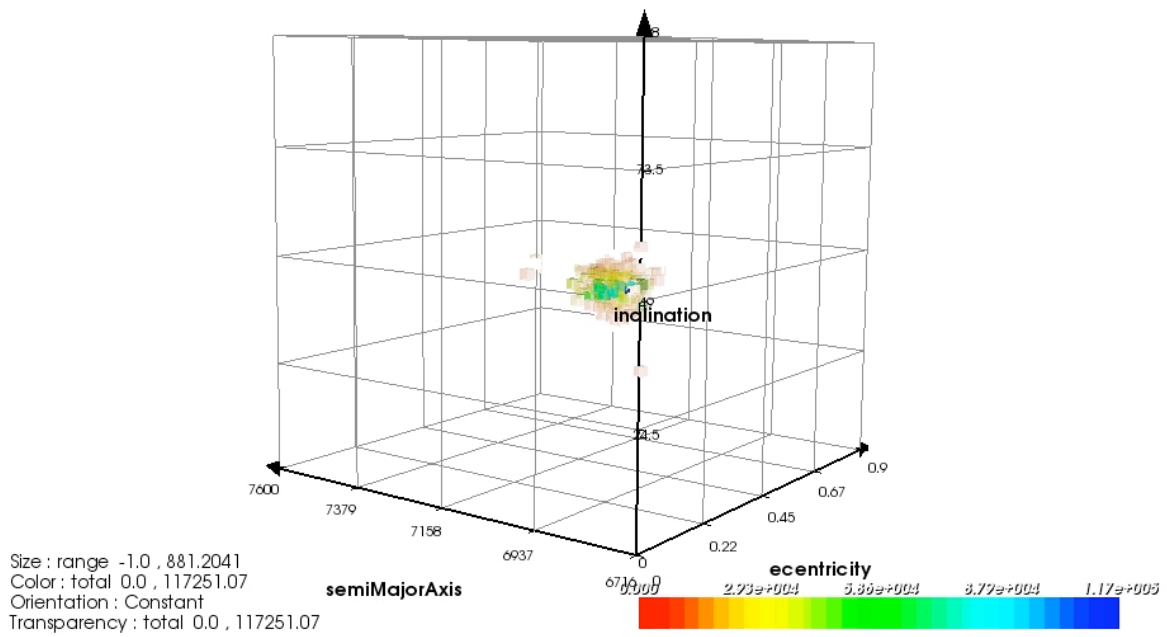


Figure B.3: 5-Dimensional Plot Showing Semi-Major Axis, Eccentricity, Inclination, Total Access Time, and Mean Range - Feasible Solutions Only

Appendix C. STK Access Report for Optimized Orbit

Shown here is the entire access report for using design 4083 as the orbital elements for FalconSat6's orbit. There is approximately an 81min contact about once per week.

Educational Use Only

31 Jan 2010 21:09:12

Satellite-ISS_25544-Sensor-LaserMountPoint-To-Satellite-FalconSat6-Receiver-TargetSolarCells:

Access Summary Report

LaserMountPoint-To-TargetSolarCells

Access	Start Time (UTCG)	Stop Time (UTCG)	Duration (sec)
1	11 Jan 2010 10:29:24.568	11 Jan 2010 11:49:07.961	4783.393
2	11 Jan 2010 12:10:13.771	11 Jan 2010 12:28:41.187	1107.416
3	17 Jan 2010 12:45:23.316	17 Jan 2010 14:29:59.001	6275.685
4	17 Jan 2010 14:57:10.477	17 Jan 2010 15:09:16.888	726.412
5	23 Jan 2010 13:50:52.688	23 Jan 2010 15:40:09.687	6556.999
6	23 Jan 2010 16:08:53.742	23 Jan 2010 16:19:50.598	656.857
7	29 Jan 2010 13:41:31.534	29 Jan 2010 15:23:08.727	6097.192
8	29 Jan 2010 15:43:05.629	29 Jan 2010 15:59:59.786	1014.157
9	4 Feb 2010 12:16:46.566	4 Feb 2010 14:12:57.641	6971.075
10	4 Feb 2010 14:37:52.562	4 Feb 2010 14:46:14.867	502.305
11	10 Feb 2010 09:43:30.177	10 Feb 2010 11:35:44.358	6734.181
12	10 Feb 2010 11:54:07.824	10 Feb 2010 12:11:38.505	1050.681

13	16 Feb 2010 06:09:58.317	16 Feb 2010 08:05:28.704	6930.387
14	22 Feb 2010 01:11:53.575	22 Feb 2010 03:09:31.557	7057.982
15	22 Feb 2010 03:30:05.685	22 Feb 2010 03:42:42.451	756.766
16	27 Feb 2010 19:17:58.880	27 Feb 2010 21:21:15.094	7396.214
17	5 Mar 2010 12:12:03.910	5 Mar 2010 14:09:07.519	7023.609
18	5 Mar 2010 14:26:28.652	5 Mar 2010 14:41:47.473	918.821
19	11 Mar 2010 04:06:30.044	11 Mar 2010 06:05:49.413	7159.370
20	16 Mar 2010 18:50:34.163	16 Mar 2010 21:07:52.963	8238.800
21	22 Mar 2010 08:35:58.448	22 Mar 2010 10:46:20.257	7821.809
22	27 Mar 2010 21:20:25.110	27 Mar 2010 23:33:43.797	7998.688
23	2 Apr 2010 09:01:35.914	2 Apr 2010 10:57:51.162	6975.248
24	7 Apr 2010 19:43:55.267	7 Apr 2010 21:32:08.143	6492.876

Global Statistics

Min Duration	4 Feb 2010 14:37:52.562	4 Feb 2010 14:46:14.867	502.305
Max Duration	16 Mar 2010 18:50:34.163	16 Mar 2010 21:07:52.963	8238.800
Mean Duration			4885.289
Total Duration			117246.924

Appendix D. Abridged STK AER Report for Optimized Orbit

Shown here is the abridged AER report for using design 4083 as the orbital elements for FalconSAT6's orbit. Each access as enumerated in Appendix C has a corresponding entry in the AER report. The azimuth, elevation, and range detail for accesses 1 and 24 are shown here with the summary data.

31 Jan 2010 21:09:59

Educational Use Only

Satellite-ISS_25544-Sensor-LaserMountPoint-To-Satellite-FalconSat6-Receiver-TargetSolarCells:

Inview Azimuth, Elevation, & Range

LaserMountPoint-To-TargetSolarCells

Time (UTCG)	Azimuth (deg)	Elevation (deg)	Range (km)
11 Jan 2010 10:29:24.568	13.161	-0.773	882.999997
11 Jan 2010 10:30:24.000	12.968	-0.743	877.764190
11 Jan 2010 10:31:24.000	12.713	-0.710	872.280535
11 Jan 2010 10:32:24.000	12.398	-0.674	866.612455
11 Jan 2010 10:33:24.000	12.022	-0.635	860.778078
11 Jan 2010 10:34:24.000	11.586	-0.593	854.799028
11 Jan 2010 10:35:24.000	11.091	-0.548	848.700086
11 Jan 2010 10:36:24.000	10.539	-0.500	842.508798
11 Jan 2010 10:37:24.000	9.930	-0.450	836.255017
11 Jan 2010 10:38:24.000	9.267	-0.397	829.970389
11 Jan 2010 10:39:24.000	8.551	-0.342	823.687793
11 Jan 2010 10:40:24.000	7.785	-0.286	817.440740

11 Jan 2010 10:41:24.000	6.971	-0.228	811.262733
11 Jan 2010 10:42:24.000	6.113	-0.170	805.186609
11 Jan 2010 10:43:24.000	5.214	-0.110	799.243867
11 Jan 2010 10:44:24.000	4.277	-0.051	793.464005
11 Jan 2010 10:45:24.000	3.306	0.008	787.873869
11 Jan 2010 10:46:24.000	2.307	0.067	782.497043
11 Jan 2010 10:47:24.000	1.284	0.124	777.353292
11 Jan 2010 10:48:24.000	0.241	0.180	772.458065
11 Jan 2010 10:49:24.000	359.184	0.234	767.822092
11 Jan 2010 10:50:24.000	358.118	0.286	763.451076
11 Jan 2010 10:51:24.000	357.049	0.336	759.345487
11 Jan 2010 10:52:24.000	355.983	0.383	755.500483
11 Jan 2010 10:53:24.000	354.925	0.427	751.905942
11 Jan 2010 10:54:24.000	353.880	0.469	748.546619
11 Jan 2010 10:55:24.000	352.855	0.509	745.402418
11 Jan 2010 10:56:24.000	351.854	0.545	742.448770
11 Jan 2010 10:57:24.000	350.883	0.580	739.657110
11 Jan 2010 10:58:24.000	349.947	0.612	736.995434
11 Jan 2010 10:59:24.000	349.050	0.642	734.428922
11 Jan 2010 11:00:24.000	348.196	0.671	731.920613
11 Jan 2010 11:01:24.000	347.390	0.698	729.432108

11 Jan 2010 11:02:24.000	346.636	0.725	726.924291
11 Jan 2010 11:03:24.000	345.935	0.751	724.358044
11 Jan 2010 11:04:24.000	345.293	0.778	721.694953
11 Jan 2010 11:05:24.000	344.711	0.805	718.897982
11 Jan 2010 11:06:24.000	344.192	0.833	715.932110
11 Jan 2010 11:07:24.000	343.738	0.863	712.764925
11 Jan 2010 11:08:24.000	343.351	0.895	709.367159
11 Jan 2010 11:09:24.000	343.033	0.929	705.713174
11 Jan 2010 11:10:24.000	342.785	0.966	701.781383
11 Jan 2010 11:11:24.000	342.609	1.007	697.554607
11 Jan 2010 11:12:24.000	342.507	1.051	693.020374
11 Jan 2010 11:13:24.000	342.479	1.100	688.171151
11 Jan 2010 11:14:24.000	342.526	1.152	683.004511
11 Jan 2010 11:15:24.000	342.650	1.209	677.523232
11 Jan 2010 11:16:24.000	342.851	1.270	671.735339
11 Jan 2010 11:17:24.000	343.130	1.337	665.654073
11 Jan 2010 11:18:24.000	343.487	1.407	659.297791
11 Jan 2010 11:19:24.000	343.924	1.483	652.689806
11 Jan 2010 11:20:24.000	344.440	1.563	645.858141
11 Jan 2010 11:21:24.000	345.036	1.647	638.835226
11 Jan 2010 11:22:24.000	345.711	1.736	631.657505

11 Jan 2010 11:23:24.000	346.465	1.828	624.364972
11 Jan 2010 11:24:24.000	347.298	1.923	617.000624
11 Jan 2010 11:25:24.000	348.207	2.020	609.609833
11 Jan 2010 11:26:24.000	349.193	2.120	602.239638
11 Jan 2010 11:27:24.000	350.252	2.221	594.937963
11 Jan 2010 11:28:24.000	351.381	2.322	587.752757
11 Jan 2010 11:29:24.000	352.578	2.423	580.731088
11 Jan 2010 11:30:24.000	353.838	2.523	573.918178
11 Jan 2010 11:31:24.000	355.157	2.620	567.356421
11 Jan 2010 11:32:24.000	356.529	2.715	561.084404
11 Jan 2010 11:33:24.000	357.948	2.805	555.135948
11 Jan 2010 11:34:24.000	359.406	2.890	549.539222
11 Jan 2010 11:35:24.000	0.896	2.970	544.315942
11 Jan 2010 11:36:24.000	2.411	3.044	539.480712
11 Jan 2010 11:37:24.000	3.940	3.111	535.040523
11 Jan 2010 11:38:24.000	5.475	3.171	530.994436
11 Jan 2010 11:39:24.000	7.007	3.223	527.333485
11 Jan 2010 11:40:24.000	8.527	3.267	524.040784
11 Jan 2010 11:41:24.000	10.025	3.304	521.091858
11 Jan 2010 11:42:24.000	11.492	3.334	518.455175
11 Jan 2010 11:43:24.000	12.921	3.357	516.092853

11 Jan 2010 11:44:24.000	14.303	3.374	513.961531
11 Jan 2010 11:45:24.000	15.630	3.385	512.013347
11 Jan 2010 11:46:24.000	16.897	3.392	510.196996
11 Jan 2010 11:47:24.000	18.096	3.396	508.458836
11 Jan 2010 11:48:24.000	19.223	3.397	506.743989
11 Jan 2010 11:49:07.961	19.999	3.396	505.470512

Min Elevation	11 Jan 2010 10:29:24.568	13.161	-0.773	882.999997
Max Elevation	11 Jan 2010 11:48:24.000	19.223	3.397	506.743989
Mean Elevation			1.242	
Min Range	11 Jan 2010 11:49:07.961	19.999	3.396	505.470512
Max Range	11 Jan 2010 10:29:24.568	13.161	-0.773	882.999997
Mean Range				685.552981

Time (UTC)	Azimuth (deg)	Elevation (deg)	Range (km)
7 Apr 2010 19:43:55.267	358.129	-0.280	883.000234
7 Apr 2010 19:44:55.000	358.722	-0.232	877.490964
7 Apr 2010 19:45:55.000	359.332	-0.185	872.012587
7 Apr 2010 19:46:55.000	359.952	-0.138	866.594919
7 Apr 2010 19:47:55.000	0.580	-0.091	861.241651
7 Apr 2010 19:48:55.000	1.213	-0.045	855.954960
7 Apr 2010 19:49:55.000	1.849	0.001	850.735446
7 Apr 2010 19:50:55.000	2.483	0.047	845.582088
7 Apr 2010 19:51:55.000	3.114	0.093	840.492237
7 Apr 2010 19:52:55.000	3.739	0.139	835.461644
7 Apr 2010 19:53:55.000	4.353	0.186	830.484518
7 Apr 2010 19:54:55.000	4.955	0.233	825.553615
7 Apr 2010 19:55:55.000	5.541	0.281	820.660363
7 Apr 2010 19:56:55.000	6.109	0.329	815.795013
7 Apr 2010 19:57:55.000	6.656	0.379	810.946811
7 Apr 2010 19:58:55.000	7.178	0.430	806.104199
7 Apr 2010 19:59:55.000	7.674	0.482	801.255028
7 Apr 2010 20:00:55.000	8.141	0.536	796.386794
7 Apr 2010 20:01:55.000	8.576	0.591	791.486868

7 Apr 2010 20:02:55.000	8.977	0.648	786.542749
7 Apr 2010 20:03:55.000	9.342	0.707	781.542306
7 Apr 2010 20:04:55.000	9.669	0.767	776.474016
7 Apr 2010 20:05:55.000	9.956	0.829	771.327202
7 Apr 2010 20:06:55.000	10.202	0.893	766.092250
7 Apr 2010 20:07:55.000	10.404	0.959	760.760817
7 Apr 2010 20:08:55.000	10.562	1.026	755.326017
7 Apr 2010 20:09:55.000	10.673	1.094	749.782584
7 Apr 2010 20:10:55.000	10.737	1.164	744.127012
7 Apr 2010 20:11:55.000	10.754	1.235	738.357670
7 Apr 2010 20:12:55.000	10.721	1.307	732.474882
7 Apr 2010 20:13:55.000	10.639	1.380	726.480983
7 Apr 2010 20:14:55.000	10.506	1.454	720.380339
7 Apr 2010 20:15:55.000	10.323	1.527	714.179339
7 Apr 2010 20:16:55.000	10.089	1.601	707.886345
7 Apr 2010 20:17:55.000	9.805	1.675	701.511614
7 Apr 2010 20:18:55.000	9.470	1.748	695.067188
7 Apr 2010 20:19:55.000	9.085	1.820	688.566748
7 Apr 2010 20:20:55.000	8.651	1.891	682.025427
7 Apr 2010 20:21:55.000	8.168	1.961	675.459611
7 Apr 2010 20:22:55.000	7.638	2.029	668.886689

7 Apr 2010 20:23:55.000	7.061	2.096	662.324789
7 Apr 2010 20:24:55.000	6.440	2.160	655.792486
7 Apr 2010 20:25:55.000	5.777	2.222	649.308490
7 Apr 2010 20:26:55.000	5.073	2.281	642.891318
7 Apr 2010 20:27:55.000	4.331	2.338	636.558955
7 Apr 2010 20:28:55.000	3.554	2.392	630.328512
7 Apr 2010 20:29:55.000	2.745	2.443	624.215886
7 Apr 2010 20:30:55.000	1.907	2.492	618.235434
7 Apr 2010 20:31:55.000	1.044	2.537	612.399655
7 Apr 2010 20:32:55.000	0.160	2.580	606.718913
7 Apr 2010 20:33:55.000	359.258	2.621	601.201180
7 Apr 2010 20:34:55.000	358.343	2.659	595.851833
7 Apr 2010 20:35:55.000	357.420	2.695	590.673489
7 Apr 2010 20:36:55.000	356.493	2.729	585.665899
7 Apr 2010 20:37:55.000	355.566	2.762	580.825907
7 Apr 2010 20:38:55.000	354.646	2.794	576.147457
7 Apr 2010 20:39:55.000	353.735	2.825	571.621671
7 Apr 2010 20:40:55.000	352.840	2.856	567.236989
7 Apr 2010 20:41:55.000	351.965	2.888	562.979360
7 Apr 2010 20:42:55.000	351.115	2.920	558.832491
7 Apr 2010 20:43:55.000	350.293	2.953	554.778142

7 Apr 2010 20:44:55.000	349.505	2.989	550.796461
7 Apr 2010 20:45:55.000	348.754	3.027	546.866345
7 Apr 2010 20:46:55.000	348.044	3.067	542.965833
7 Apr 2010 20:47:55.000	347.379	3.111	539.072502
7 Apr 2010 20:48:55.000	346.763	3.158	535.163869
7 Apr 2010 20:49:55.000	346.198	3.210	531.217800
7 Apr 2010 20:50:55.000	345.688	3.266	527.212887
7 Apr 2010 20:51:55.000	345.235	3.326	523.128831
7 Apr 2010 20:52:55.000	344.842	3.392	518.946777
7 Apr 2010 20:53:55.000	344.510	3.463	514.649641
7 Apr 2010 20:54:55.000	344.243	3.539	510.222391
7 Apr 2010 20:55:55.000	344.042	3.620	505.652301
7 Apr 2010 20:56:55.000	343.909	3.707	500.929160
7 Apr 2010 20:57:55.000	343.845	3.800	496.045452
7 Apr 2010 20:58:55.000	343.852	3.899	490.996486
7 Apr 2010 20:59:55.000	343.931	4.003	485.780497
7 Apr 2010 21:00:55.000	344.083	4.112	480.398694
7 Apr 2010 21:01:55.000	344.310	4.227	474.855280
7 Apr 2010 21:02:55.000	344.612	4.348	469.157422
7 Apr 2010 21:03:55.000	344.990	4.473	463.315184
7 Apr 2010 21:04:55.000	345.445	4.603	457.341417

7 Apr 2010 21:05:55.000	345.977	4.738	451.251609
7 Apr 2010 21:06:55.000	346.586	4.877	445.063694
7 Apr 2010 21:07:55.000	347.273	5.020	438.797815
7 Apr 2010 21:08:55.000	348.037	5.166	432.476047
7 Apr 2010 21:09:55.000	348.878	5.316	426.122075
7 Apr 2010 21:10:55.000	349.795	5.468	419.760832
7 Apr 2010 21:11:55.000	350.787	5.623	413.418097
7 Apr 2010 21:12:55.000	351.851	5.779	407.120048
7 Apr 2010 21:13:55.000	352.987	5.937	400.892789
7 Apr 2010 21:14:55.000	354.190	6.095	394.761845
7 Apr 2010 21:15:55.000	355.458	6.254	388.751629
7 Apr 2010 21:16:55.000	356.787	6.412	382.884909
7 Apr 2010 21:17:55.000	358.173	6.570	377.182265
7 Apr 2010 21:18:55.000	359.609	6.727	371.661570
7 Apr 2010 21:19:55.000	1.091	6.882	366.337496
7 Apr 2010 21:20:55.000	2.611	7.035	361.221072
7 Apr 2010 21:21:55.000	4.164	7.187	356.319303
7 Apr 2010 21:22:55.000	5.740	7.336	351.634880
7 Apr 2010 21:23:55.000	7.334	7.484	347.165979
7 Apr 2010 21:24:55.000	8.935	7.629	342.906172
7 Apr 2010 21:25:55.000	10.537	7.773	338.844450

7 Apr 2010 21:26:55.000	12.130	7.915	334.965373
7 Apr 2010 21:27:55.000	13.707	8.057	331.249320
7 Apr 2010 21:28:55.000	15.259	8.199	327.672858
7 Apr 2010 21:29:55.000	16.779	8.342	324.209193
7 Apr 2010 21:30:55.000	18.259	8.487	320.828707
7 Apr 2010 21:31:55.000	19.692	8.635	317.499541
7 Apr 2010 21:32:08.143	20.000	8.668	316.773866
Min Elevation	358.129	-0.280	883.000234
Max Elevation	20.000	8.668	316.773866
Mean Elevation		3.188	
Min Range	20.000	8.668	316.773866
Max Range	358.129	-0.280	883.000234
Mean Range			591.523357

Global Statistics

Min Elevation	29 Jan 2010 13:41:31.534	355.655	-0.999	883.000128
Max Elevation	5 Mar 2010 14:41:47.473	12.590	19.999	145.177607
Mean Elevation			3.658	
Min Range	5 Mar 2010 14:41:47.473	12.590	19.999	145.177607
Max Range	22 Feb 2010 01:11:53.575	5.037	-0.272	883.000659
Mean Range				566.871968

Bibliography

1. "Busek." <http://www.busek.com/halleffect.html>, cited 01 Feb 10.
2. "The Hall Effect." <http://www.eeel.nist.gov/812/effe.htm>, cited 02 Feb 10.
3. "Japanese Experiment Module - Exposed Facility." http://www.nasa.gov/multimedia/imagegallery/image_feature_1430.html, cited 02 Feb 2010.
4. "NASA Image." http://www.nasa.gov/images/content/160328main_s129e009327_small.jpg, cited 08 Feb 2010.
5. "Schriever Air Force Base." <http://www.schriever.af.mil/photos/mediagallery.asp?galleryID=1442>, cited 08 Feb 2010.
6. "JAXA Exposed Facility Website." <http://kibo.jaxa.jp/en/about/kibo/jef/>, cited 09 Feb 2010.
7. "JAXA Website." http://www.jaxa.jp/projects/iss_human/kibo/index_e.html, cited 09 Feb 2010.
8. "Kirtland Air Force Base." <http://www.kirtland.af.mil/>, cited 09 Feb 2010.
9. "Los Angeles Air Force Base - SMC." <http://www.losangeles.af.mil/>, cited 09 Feb 2010.
10. "Calsky." <http://www.calsky.com/cs.cgi>, cited 17 Jan 2010.
11. "FalconSAT Program Fact Sheet." <http://www.usafa.af.mil/information/factsheets/factsheet.asp?id=14314>, cited 17 Jan 2010.
12. "STK User Resources." <http://www.stk.com/resources/>, cited Tuesday, January 26, 2010.
13. Abraham, Douglas S., et al. *A Demonstration Plan for Laser-Beamer Power*. Technical Report 2014/34883, Jet Propulsion Laboratory, February 1993.
14. Aldrich, Lisa J. *Nikola Tesla and the Taming of Electricity* (1st Edition). Morgan Reynolds Publishing, 2005.
15. Bate, Roger R., et al. *Fundamentals of Astrodynamics* (1st Edition). Dover Publications, Inc., 1971.
16. Bellows, Charlie. *Minimizing Losses in a Space Power Beaming Experiment*. MS thesis, Air Force Institute of Technology, Wright Patterson Air Force Base, OH, March 2010.
17. Campbell, Bruce A. and Jr. Samuel Walter McCandless. *Introduction to Space Sciences and Spacecraft Applications* (1st Edition). Gulf Publishing Company, 1996.
18. Dickinson, R. and J. Grey. *Lasers for Wireless Power Transmission*. Technical Report 2014/16855, Jet Propulsion Laboratory and AIAA, February 1999.
19. Frisbee, R.H., et al. "Laser Propulsion for the Orbital Transfer Mission." *AIAA/SAE/ASME/ASEE 21st Joint Propulsion Conference*. Number AIAA-85-1224. American Institute of Aeronautics and Astronautics, July 1985.

20. Griffiths, David J. *Introduction to Electrodynamics* (3rd Edition). Prentice Hall, 1998.
21. Hall, Stephen S. *Inventors and Discoverers Changing Our World* (1st Edition), chapter 3, 44–79. National Geographic Society, 1988.
22. Helvajian, Henry and Siegfried W. Janson, editors. *Small Satellites: Past, Present, and Future* (1st Edition). Aerospace Press, 2009.
23. Kaplan, Marshall H. *Modern Spacecraft Dynamics and Control* (1st Edition). John Wiley and Sons, 1976.
24. Kelso, T.S. “Validation of SGP4 and IS-GPS-200D Against GPS Precision Ephemerides.” Number AAS 07-127. January 2007.
25. Landis, Geoffrey A. “Solar Power for the Lunar Night.” *Space Manufacturing 7: Space Resources to Improve Life on Earth*. 290–296. May 1989.
26. Pakhomov, Andrew V., editor. *Fifth International Symposium on Beamed Energy Propulsion, 997*, Suite 1NO1, 2 Huntington Quadrangle, Melville, NY, 11747-4502: AIP Conference Proceedings, November 2007.
27. Phoenix Integration, Blacksburg, VA. *ModelCenter 8.0*, 2009.
28. Rather, John D.G. “Ground to Space Laser Power Beaming: Missions, Technologies, and Economic Advantages.” *BEAMED ENERGY PROPULSION: First International Symposium on Beamed Energy Propulsion 664*. 37–48. May 2003.
29. Rogers, Mark E. *Lasers in Space - Technological Options for Enhancing US Military Capabilities*. Technical Report Occasional Paper No. 2, Air War College, November 1997.
30. Sellers, Jerry Jon. *Understanding Space - An Introduction to Astronautics* (2nd Edition). McGraw Hill, 2000.
31. Simmons, Joseph R. *Aeroelastic Optimization of Sounding Rocket Fins*. MS thesis, Air Force Institute of Technology, Wright Patterson Air Force Base, OH, June 2009.
32. Tesla, Nikola. “The Transmission of Electrical Energy without Wires,” *Electrical World and Engineer* (March 1904).
33. Tribble, Alan C. *The Space Environment - Implications for Spacecraft Design* (1st Edition). Princeton University Press, 1995.
34. Vallado, David A. *Fundamentals of Astrodynamics and Applications* (2nd Edition). Microcosm Press, 2001.
35. Wertz, James R. and Wiley J. Larson, editors. *Space Mission Analysis and Design* (3rd Edition). Microcosm Press, 1999.
36. Wiesel, William E. *Spaceflight Dynamics* (2nd Edition). Irwin/McGraw Hill, 1997.
37. Wiesel, William E. *Modern Orbit Determination* (1st Edition). Aphelion Press, 2003.
38. Zuev, V. E. *Laser-light transmission through the atmosphere, 14*. Springer Berlin / Heidelberg, 1976.

REPORT DOCUMENTATION PAGE			<i>Form Approved</i> <i>OMB No. 0704-0188</i>	
The public reporting burden for this collection of information is estimated to average 1 hour per response, including the time for reviewing instructions, searching existing data sources, gathering and maintaining the data needed, and completing and reviewing the collection of information. Send comments regarding this burden estimate or any other aspect of this collection of information, including suggestions for reducing this burden to Department of Defense, Washington Headquarters Services, Directorate for Information Operations and Reports (0704-0188), 1215 Jefferson Davis Highway, Suite 1204, Arlington, VA 22202-4302. Respondents should be aware that notwithstanding any other provision of law, no person shall be subject to any penalty for failing to comply with a collection of information if it does not display a currently valid OMB control number. PLEASE DO NOT RETURN YOUR FORM TO THE ABOVE ADDRESS.				
1. REPORT DATE (DD-MM-YYYY) 25-03-2010		2. REPORT TYPE Master's Thesis	3. DATES COVERED (From - To) Aug 2009 - Mar 2010	
4. TITLE AND SUBTITLE Mission Analysis and Design for Space Based Inter-Satellite Laser Power Beaming			5a. CONTRACT NUMBER	
			5b. GRANT NUMBER	
			5c. PROGRAM ELEMENT NUMBER	
6. AUTHOR(S) Keller, Nicholas M., LT, USN			5d. PROJECT NUMBER	
			5e. TASK NUMBER	
			5f. WORK UNIT NUMBER	
7. PERFORMING ORGANIZATION NAME(S) AND ADDRESS(ES) Air Force Institute of Technology Graduate School of Engineering and Management (AFIT/ENY) 2950 Hobson Way WPAFB OH 45433-7765			8. PERFORMING ORGANIZATION REPORT NUMBER AFIT/GA/ENY/10-M05	
9. SPONSORING / MONITORING AGENCY NAME(S) AND ADDRESS(ES) Dr. Raymond F. Beach National Aeronautics and Space Administration Glenn Research Center 21000 Brookpark Road Cleveland, OH, 44135 (216) 433-5320 raymond.f.beach@nasa.gov			10. SPONSOR/MONITOR'S ACRONYM(S) NASA	
			11. SPONSOR/MONITOR'S REPORT NUMBER(S)	
12. DISTRIBUTION / AVAILABILITY STATEMENT APPROVED FOR PUBLIC RELEASE; DISTRIBUTION UNLIMITED				
13. SUPPLEMENTARY NOTES				
14. ABSTRACT This research effort develops an interdisciplinary design tool to optimize an orbit for the purpose of wirelessly beaming power from the International Space Station's (ISS) Japanese Experimental Module Exposed Facility (JEM/EF) to a target satellite. For the purpose of this initiative, the target satellite will be referred to as FalconSAT6, a reference to the proposed follow-on satellite to the U.S. Air Force Academy's (USAFA) FalconSAT5 program. The USAFA FalconSAT program provides cadets an opportunity to design, analyze, build, test and operate small satellites to conduct Department of Defense (DoD) space missions. The tool developed for this research is designed to find an optimal solution balancing the need to maximize the amount of access time between the ISS and FalconSAT6 while minimizing the range between the spacecraft. This tool places mathematical rigor to the problem and determines realistic solutions using current technology. Using this tool allows mission planners to economically and accurately predict the outcome of a proposed wireless power beaming mission.				
15. SUBJECT TERMS Laser Power Beaming, International Space Station, FalconSAT				
16. SECURITY CLASSIFICATION OF:			17. LIMITATION OF ABSTRACT UU	18. NUMBER OF PAGES 119
a. REPORT U	b. ABSTRACT U	c. THIS PAGE U		
			19b. TELEPHONE NUMBER (Include Area Code) (937) 255-3636, ext 4578	

Standard Form 298 (Rev. 8-98)
Prescribed by ANSI Std. Z39.18